Institute for Cardiovascular Prevention

Ludwig Maximilian University of Munich

A dissertation submitted for the degree of

Doctor of Philosophy (Ph.D.)

at the Faculty of Medicine

Ludwig Maximilian University of Munich

Individualized rupture risk assessment and analysis of mechanotransduction in the abdominal aortic aneurysm

by

Susanne Elke Metschl

Burglengenfeld, Germany

2023

With approval of the Faculty of Medicine

Ludwig Maximilian University of Munich

First supervisor:	Priv.-Doz. Dr. rer. nat. Jaroslav Pelisek
Second supervisor:	Univ.-Prof. Dr. Dr. med. Oliver Söhnlein
Third supervisor:	Univ.-Prof. Dr. rer. nat. Sabine Steffens

Dean: Prof. Dr. med. Thomas Gudermann

Date of defence:
January 11th, 2023

Table of contents

Abstract

Background and aim of the study: Abdominal aortic aneurysms (AAA) are local dilatations of the infrarenal aorta, which are holding the risk of acute rupture and life-threatening aortic bleeding. Surgical or endovascular treatment based on the aortic diameter (≥ 5.5 cm) are currently the only therapeutic options for AAA patients. As AAAs are still among the major causes of death in elderly patients, the identification of biomarkers for AAA development and rupture remains a key challenge. The aim of this study was to investigate structural, biological and mechanical properties of the aortic wall in order to contribute to an individualized rupture risk assessment and to improve surgical decision-making.

Methods: The structural composition of aortic tissue from patients with ruptured AAAs (rAAAs; n=29) and electively repaired AAAs (eAAAs; n=78) was compared to healthy aortas (n=8) using quantitative protein analysis. Load-bearing extracellular matrix (ECM) components, especially collagens and proteoglycans, as well as inflammatory parameters were determined and mechanical properties of the aortic specimen were evaluated using tensile testing. Corresponding serum samples from the AAA patients were analyzed regarding structural and inflammatory parameters in order to assess their potential as serological biomarkers for AAA development. This was complemented by a histological evaluation and semiquantitative scoring of ECM components as well as gene expression analysis and patients clinical and demographic data. Correlation analyses with biological parameters from tissue and serum samples as well as mechanical and clinical data were applied to evaluate possible associations. Moreover, the activation of underlying mechanotransduction pathways was examined via protein kinase phosphorylation assays.

Results: In AAA tissue, collagen type I (Col1) was increased in both eAAA and rAAA samples compared to controls ($p = 0.0001$ and $p = 0.003$, respectively) and collagen type III (Col3) was

elevated in eAAA ($p = 0.016$). Chondroitin sulfate (CS) proteoglycans were increased in eAAA and rAAA subcohorts ($p = 0.002$ and $p = 0.004$, respectively) and also in rAAA compared to eAAA ($p = 0.020$). A similar pattern was found for dermatan sulfate (DS) proteoglycans (eAAA and rAAA compared to controls: $p = 0.011$ and $p < 0.0001$, respectively; rAAA compared to eAAA: $p < 0.0001$). The amounts of endocan, a soluble circulating proteoglycan, were higher in rAAA compared to controls and eAAA ($p = 0.014$ and $p = 0.0003$, respectively) while inflammatory parameters (CXCR4 and CXCL12) did not change. In corresponding AAA serum, Col1 was increased in both subcohorts compared to controls ($p = 0.009$ and $p = 0.0008$, respectively) and also in rAAA compared to eAAA ($p < 0.0001$). Serum endocan showed a similar pattern (eAAA and rAAA samples compared to controls: $p = 0.014$ and $p = 0.028$, respectively; rAAA compared to eAAA: $p = 0.021$). DS amounts, by contrast, were decreased in eAAA and rAAA serum compared to controls ($p = 0.0008$ and $p = 0.042$, respectively) and also in rAAA compared to eAAA ($p = 0.042$). CXCR4 was higher in rAAA serum compared to eAAA ($p = 0.003$) while CXCL12 was increased in both subgroups compared to controls ($p = 0.036$ and $p = 0.047$, respectively). Histological evaluation showed characteristics of vessel wall degeneration and inflammatory infiltration along with glycosaminoglycan accumulation in AAA samples. Increased glycosaminoglycan amounts could also be confirmed via semiquantitative scoring. ECM-producing vascular smooth muscle cells (VSMCs) were found to be diminished in AAA tissue. Regarding the mechanical tissue properties, β stiffness was higher in rAAA tissue compared to eAAA ($p = 0.022$). Serum Col1 as well as tissue endocan correlated positively with α stiffness ($r = 0.239$, $p = 0.07$ and $r = 0.311$, $p = 0.02$, respectively). Similar positive correlations were found for serum Col1 and tissue endocan with the maximum tensile force ($r = 0.448$, $p < 0.01$ and $r = 0.274$, $p = 0.06$, respectively). Within the tissue and serum amounts, tissue endocan correlated positively with tissue CS and DS ($r = 0.235$, $p = 0.04$

and r = 0.291, $p < 0.01$, respectively) as well as with serum Col1 (r = 0.388, $p < 0.01$). Moreover, serum endocan correlated positively with serum CS and Col3 (r = 0.327, $p < 0.01$ and r = 0.268, p = 0.02, respectively). Regarding the activation of underlying signaling pathways, particularly proteins associated to ECM synthesis and VSMC proliferation were found to be involved. Especially Src family kinases as well as platelet-derived growth factor- and epidermal growth factor-related factors seem to be activated in AAA tissue.

Conclusion: The current study confirms that, next to other ECM components, proteoglycans play a key role for the mechanical stability of the aortic wall and are associated with the changing mechanical loads during AAA pathogenesis. Changes in ECM composition seem to be reflected to a certain degree in patient serum and could serve as potential biomarkers of disease progression or increased rupture risk. Especially Col1 and endocan seem to be related to the mechanical wall properties and could be associated to ECM degradation processes during AAA development. Due to its biological characteristics, particularly endocan might be a promising candidate for AAA risk stratification. Further studies, including also patient follow-up data and clinical outcome, will be needed to assess the diagnostic value of such biomarkers.

List of figures

List of tables

List of abbreviations

AAA	Abdominal aortic aneurysm
ACE	Angiotensin converting enzyme
Akt 1/2/3	Ak-strain transforming protein kinase 1/2/3
Ang-II	Angiotensin II
BCA	Bicinchoninic acid assay
BMP	Bone morphogenic protein
CD45	Cluster of differentiation 45
CD68	Cluster of differentiation 68
cDNA	Complementary DNA
Chk-2	Checkpoint kinase 2
c-Jun	Junana oncogenic transcription factor
CKD	Chronic kidney disease
Col1	Collagen type I
Col3	Collagen type III
Co-SMAD	Common partner SMAD
CREB	CAMP response element-binding protein
CS	Chondroitin sulfate
Ct	Cycle threshold
CT	Computed tomography
CXCL12	CXC motif chemokine 12
CXCR4	Chemokine receptor 4
DNA	Desoxyribonucleic acid
DS	Dermatan sulfate
eAAA	electively excised AAA
ECM	Extracellular matrix
EGFR	Epidermal growth factor receptor
ELISA	Enzyme-linked immunosorbent assay
eNOS	Endothelial nitric oxide synthase
ERK1/2	Extracellular signal-regulated kinase 1/2
ESM-1	Endothelial cell-specific molecule 1
EVAR	Endovascular aneurysm repair
EvG	Elastica van Gieson
FAM	Fluorescein amidites
FFPE	Formalin-fixed paraffin-embedded
Fgr	Gardner-Rasheed feline sarcoma oncogene homolog
GAG	Glycosaminoglycan
GFR	Glomerular filtration rate
GSK-3	Glycogen synthase kinase 3
HE	Hematoxylin-eosin
HRP	Horseradish peroxidase
HS	Heparan sulfate
hsCRP	high-sensitivity C-reactive protein
HSP27	Heat shock protein 27
HSP60	Heat shock protein 60
IHC	Immunohistochemistry
JNK	c-Jun N-terminal kinase
JNK1/2/3	c-Jun N-terminal kinase 1/2/3
KS	Keratan sulfate
Lck	Lymphocyte-specific protein tyrosine kinase

Lyn	Lck/Yes novel tyrosine kinase
MAPK	Mitogen-activated protein kinase
MMP2/9	Matrix metalloproteinase 2/9
MRI	Magnetic resonance imaging
mRNA	Messenger RNA
MSK1/2	Mitogen- and stress-activated protein kinase 1/2
mTOR	Mammalina target of rapamycin
OD	Optical density
p38a	Proline 38 replaced with alanine mitogen-activated protein kinase
p53	Phophoprotein p53
p70 S6 kinase	Ribosomal protein S6 kinase
PBS	Phosphate-buffered saline
PDGFRb	Platelet-derived growth factor receptor beta
PI3K	Phosphoinositide 3-kinase
PLC-y1	Phospholipase C y1
PRAS40	Proline-rich AKT substrate of 40 kDa
PYK2	Protein tyrosine kinase 2
qPCR	Quantitative polymerase chain reaction
rAAA	Ruptured AAA
RNA	Ribonucleic acid
ROUT	Robust regression and outlier removal
RPLP0	Ribosomal protein lateral stalk subunit P0
RSK1/2/3	Ribosomal protein S6 kinase 1/2/3
R-SMAD	Receptor-regulated SMAD
RT	Reverse transcription
RT-PCR	Reverse transcription PCR
SLRP	Small leucin-rich proteoglycan
SMA	Smooth muscle alpha actin
SMAD	Acronym from Caenorhabditis elegans SMA genes and Drosophila MAD family genes
Src	Cellular sarcoma tyrosine-protein kinase
STAT1/2/3/5/6	Signal transducer and activator of transcription 1/2/3/5/6
TGFB1/2	Transforming growth factor beta 1/2
TGFBR1/2	Transforming growth factor receptor beta receptor 1/2
TGF-β	Transforming growth factor beta
TMB	Tetramethylbenzidine
VSMC	Vascular smooth muscle cell
WNK1	With no lysine/K protein kinase 1
Yes	Yamaguchi sarcoma proto-oncogene tyrosine protein kinase

1. Background and research questions

1.1. Disease etiology and state of the art

An aneurysm is defined as a pathological and irreversible dilatation of a vessel, involving all three layers of the vessel wall. Abdominal aortic aneurysms (AAA) are local dilatations of the infrarenal aorta with an aortic diameter greater than 30 mm or enlarged at least 1.5-fold compared to the initial diameter.[1, 2] AAA development is a complex and multifactorial process with many still unknown variables. Well-known risk factors include a history of smoking, male sex, positive family history and age (> 65 years in men).[2] In ultrasound screening studies, 1-2.6% of 65-year-old men and 0.5% of 70-year-old women have been diagnosed with AAA.[2]

Acute AAA rupture poses a life-threatening condition to patients and is related to intra-abdominal bleeding. If untreated, AAA rupture carries an overall mortality of >80% and is among the major causes of death in western countries.[3] It represents one of the leading causes of death especially for elderly men, who are most frequently affected by AAA disease.[4] As the risk of AAA rupture increases with increasing diameter [5], current medical guidelines recommend surveillance imaging for medium-sized aneurysms (e.g. 12-month interval for patients with 40-49 mm diameter; 6-month interval for patients with 50-54 mm diameter).[6] For AAAs ≥ 5.5 cm in diameter, elective aneurysm repair is recommended. As female patients tend to have ruptures at smaller diameters, AAA repair in women is suggested already with a 50-54 mm diameter.[6]

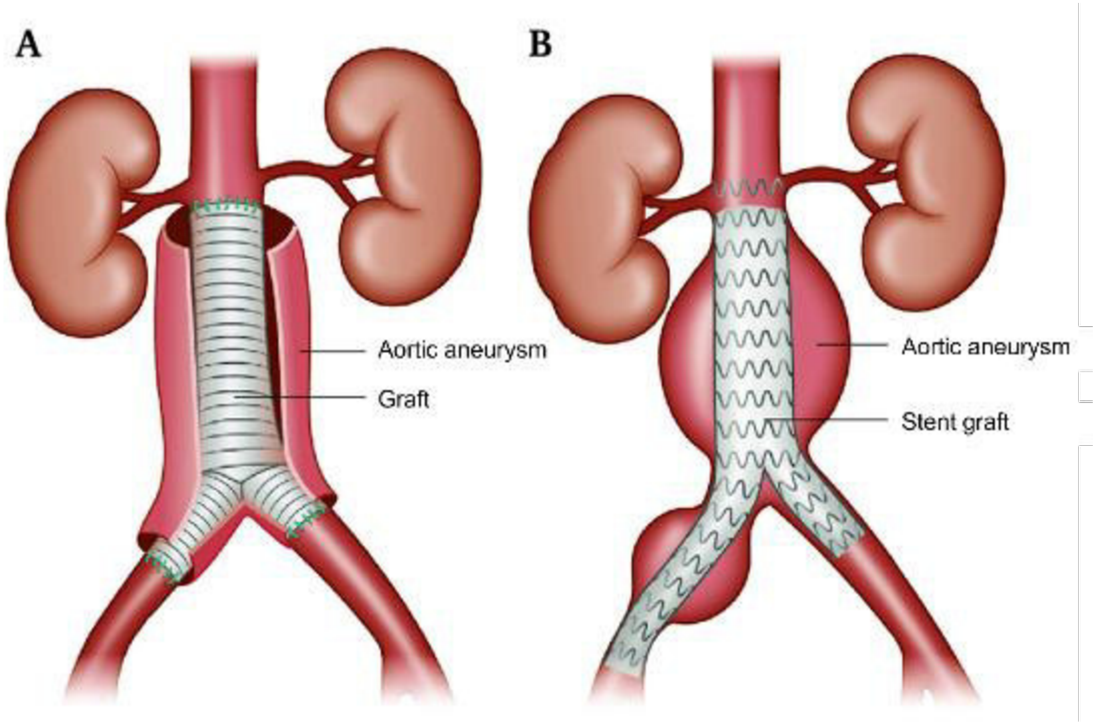

Figure 1: Surgical AAA repair. A) Open AAA repair. The aneurysmatic segment is replaced by a synthetic graft. B) Endovascular AAA repair. A stent graft is placed within the aneurysm. Modified from: Wanhainen, A., et al., European Society for Vascular Surgery (ESVS) 2019 Clinical Practice Guidelines on the Management of Abdominal Aorto-iliac Artery Aneurysms. Eur J Vasc Endovasc Surg, 2019. 57(1): p. 8–93.

AAA repair (Fig. 1) is currently either done by endovascular aneurysm repair (EVAR) or by an open aneurysm excision. An EVAR procedure involves the minimally-invasive placement of a stent graft within the aneurysm in order to stabilize the aneurysmatic section and to reduce pressure onto the vessel wall. During open aneurysm repair, a graft is directly sutured into the aneurysmatic aorta via a larger abdominal incision. This synthetic graft then replaces the aneurysmatic section. Both procedures are associated with a certain operation risk, which is further increased by e.g. patient's age and underlying diseases. As there is still no pharmacological treatment to limit AAA development and thus prevent rupture, the operation risk of a surgical intervention needs to be weighed against the risk of AAA rupture for each individual patient. The decision for or against surgical repair depends to a large extent on the aortic diameter as the most important diagnostic parameter of AAA growth.[6] However,

limitations of this diameter criterion must be taken into consideration: aneurysms with smaller diameters might rupture unexpectedly, while those with larger diameters may remain stable for a long time. A more differentiated and individualized approach could help to predict AAA rupture risk and to reduce unnecessary risks for patients.[7, 8] The identification and evaluation of biomarkers for AAA development therefore remains a major challenge and could help to improve decision-making for or against AAA repair.[9, 10]

1.2. Composition and function of the ECM

The structural composition of the aortic wall (Fig. 2) is primarily determined by its physiological function to supply the body with oxygenated blood while maintaining physiological blood pressure. Its elastic properties account for constant blood flow towards peripheral vessels and help to even out the pulsatile flow from the heart. These structural features are represented by extracellular matrix (ECM) proteins, consisting of 60% fibrous proteins. These fibrous proteins are mainly collagen and elastin, forming a large part of the aortic middle layer.[11] Up to 5% of the ECM consist of glycosaminoglycans (GAGs), which have been shown to be equally decisive for the aortic structural integrity despite their relatively small proportion.[12] The overall ECM composition is determined to a great extent by vascular smooth muscle cells (VSMCs), which synthesize and organize ECM components and thereby define the mechanical properties of the vessel wall.[11] While initial triggers of aneurysm formation are not yet fully understood, some central mechanisms of AAA development with regard ECM composition are well described. During early AAA development, reduced vessel wall stability and integrity are caused to a large extent by alterations in VSMCs and fibroblasts. Alterations in the phenotypic state of VSMCs together with enhanced apoptosis in the long term lead to loss of stability of the aortic wall. Also the increased proteolytic degradation of ECM components impairs aortic

wall structures and increases the rupture risk over time.[13, 14] Local forces upon the aneurysm wall play a crucial role, as AAAs rupture as soon as mechanical stress derived from blood pressure exceeds the local vessel wall strength. AAA rupture thereby follows the fundamental principles of material failure, meaning that rupture occurs as soon as a mechanical failure criterion is met.[2, 15] Wall strength, in the vascular context defined as the resistance to maximum load upon the vessel wall, is closely associated with its structural composition.[11, 12]

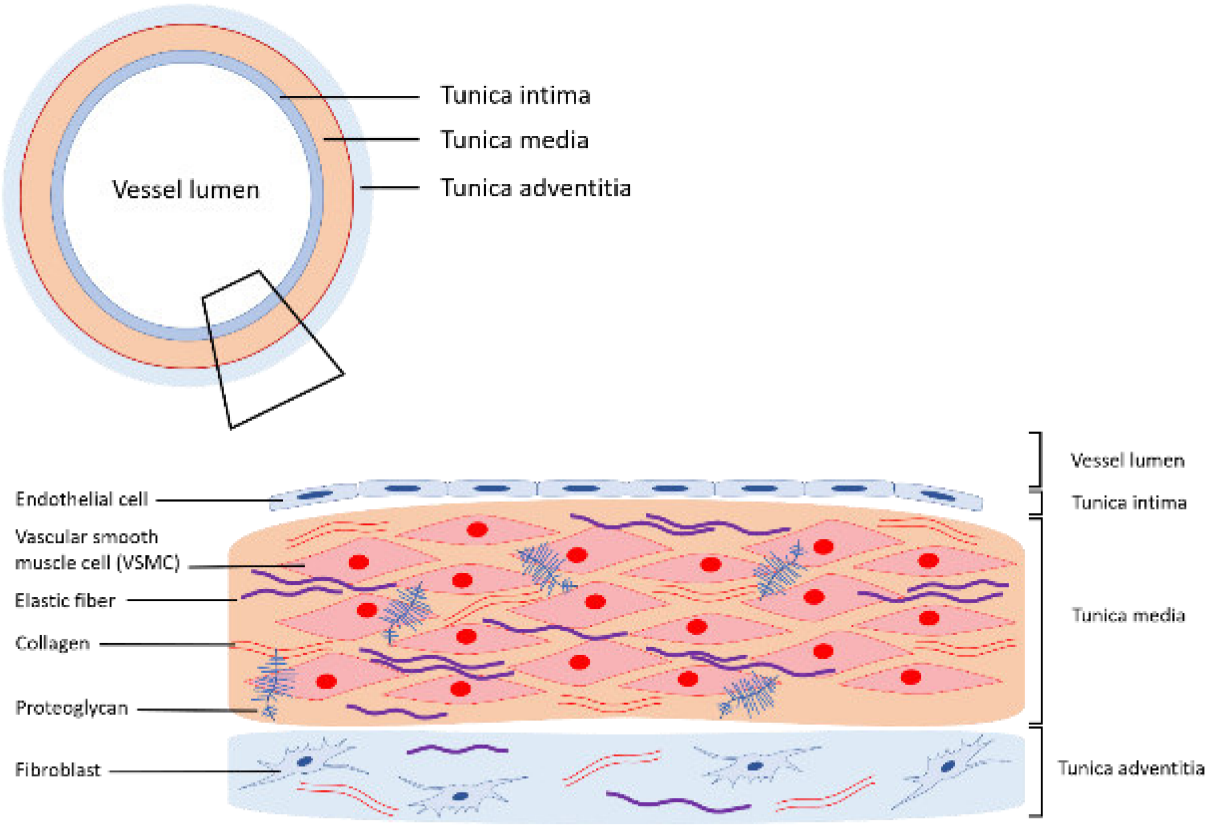

Figure 2: Schematic composition of the aortic wall. Overview of wall layers and localization of collagen, elastic fibers and proteoglycans within the vessel layers. Illustration was created using www.motifolio.com.

1.3. Role and localization of collagen and elastin

Collagen and elastin fibers have decisive roles for the mechanical properties of a vessel wall and both types of fibers are found in abundance particularly in the medial layer.[11] They are both oriented in a circumferential manner and are structurally interconnected with VSMCs, especially in regions with cumulated layers of VSMCs.[16, 17] From the 28 known types of collagen, collagen type I and III (Col1 and Col3) are the most abundant ones in the human vessel wall. Both are fibril-forming and are predominantly responsible for wall strength.[11] The close association between collagens and vascular stability is underlined by the fact that mutations in human collagen genes result in diseases like the Ehlers-Danlos syndrome, which is characterized by vessel instability and high susceptibility to vessel rupture.[18, 19] Elastin provides elasticity to a variety of organs including lung, skin and vasculature. Elastic fibers in the vessel wall are arranged as elastic lamellae (more than 29 in the mammalian media) and are characterized by inter-lamellar connections for the transmission of mechanical strain.[11] Besides the medial layers, larger amounts of collagen and smaller quantities of elastic fibers can also be found in the adjacent tunica adventitia of a vessel. This layer moreover contains vasa vasorum as an essential component for medial nutrition.[20]

1.4. Role and localization of proteoglycans

Besides collagen and elastin, glycosylated proteins play an important role for the mechanical properties of a vessel wall. These proteoglycans typically consist of a central core protein and covalently attached GAG side chains. Hyaluronic acid, also classified as a GAG, serves as a central ‘anchor’ for other non-covalently attached proteoglycans within the ECM. (Fig. 3)

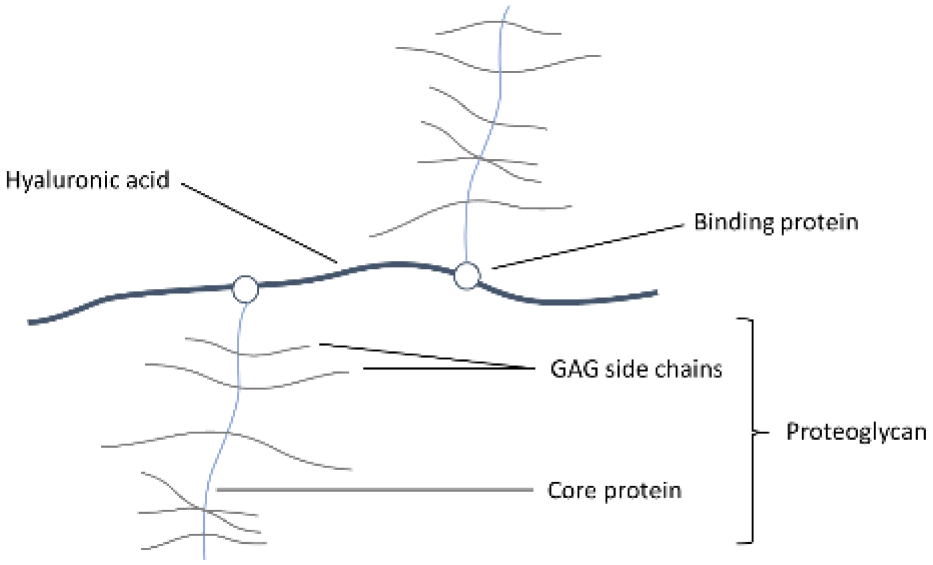

Figure 3: Schematic structure and composition of ECM proteoglycans. Proteoglycans consist of a core protein and covalently attached GAG chains. Various proteoglycans are non-covalently bound to a central hyaluronic acid via binding proteins. Illustration was created using www.motifolio.com.

The type and number of GAG side chains defines a specific proteoglycan. GAG chains can be characterized as follows: chondroitin sulfate (CS) and dermatan sulfate (DS) consist of galactosamine-disaccharides with glucuronic or iduronic acid; heparan sulfate (HS) consists of a glucosamine-disaccharide with glucuronic or iduronic acid; keratan sulfate (KS) consists of a disaccharide of glucosamine and galactose.[11] Proteoglycans can be further classified into large, aggregating and small, leucin-rich proteoglycans (SLRPs). SLRPs in turn are secreted proteoglycans that can bind other ECM molecules such as collagen.[11] Proteoglycans are synthesized by a variety of mammalian cells, including VSMCs and vascular endothelial cells. They are either directly secreted into the ECM, integrated into plasma membranes or stored in secretory granules.[21, 22] Various types of proteoglycans can be associated with certain cellular localizations. HS proteoglycans can be found predominantly in direct proximity of the cell. This can be either as a transmembrane proteoglycan on the cell surface (e.g. syndecan, betaglycan) or pericellular as component of the basement membrane (e.g. perlecan). By contrast, CS and DS proteoglycans are mainly associated to extracellular structures and

matrices.[23] As these extracellular structures are providing mechanical stability to the vessel wall, the focus of this study was placed on CS and DS proteoglycans. Both groups of proteoglycans are known to be structurally related to collagens and to strongly interact with Col1. CS and DS can also be incorporated into Col1 precipitates, when present during fibril formation. Large CS proteoglycans like aggrecan can bind to collagen and form large, strongly connected aggregates.[21, 24] SLRPs also have this binding capacity, but besides that can regulate collagen fibrillogenesis and influence biological activity by binding to signaling molecules like transforming growth factor beta (TGF-β) and bone morphogenetic proteins (BMPs).[23] Endocan or endothelial cell-specific molecule 1 (ESM-1) is a soluble DS proteoglycan mainly synthetized by vascular endothelial cells. Endocan is of particular interest in as a large part of it was found to be circulating in the human bloodstream.[25] This makes endocan a potential candidate for biomarkers of AAA growth that can be determined noninvasively in patient serum.

1.5. Inflammatory parameters during AAA development

Destabilizing processes within the aortic wall are closely linked to inflammatory processes and the recruitment of inflammatory cells seems to be one of the initial steps of degeneration. Pro-inflammatory mediators and matrix-degrading enzymes are released mainly by lymphocytes, macrophages and plasmas cells, and contribute to the progressive weakening of the aortic wall.[26] Associations between inflammatory serum markers, structure proteins and characteristics of aneurysm development have been described earlier.[27, 28] Among the involved inflammatory factors, chemokine receptor 4 (CXCR4) and the CXC motif chemokine 12 (CXCL12) have been shown to have a special role in the development of vascular diseases.

The receptor-ligand-complex CXCR4/CXCL12 was described as a relatively specific marker of inflammation during AAA development and was found to be overexpressed in AAA tissue in a previous study.[29] Furthermore, blocking CXCR4 with an antagonist suppressed AAA formation and progression in rodent models.[26] However, it has not been evaluated so far if CXCR4 and CXCL12 could be used as serum biomarkers and to what extent they may reflect the stage of aortic wall degeneration.

1.6. Biomechanical interactions in the AAA wall

The mechanical properties of a vessel wall are closely connected to its physiological function and different matrix components are expressed and regulated in adaption to hemodynamic factors. With low blood pressure, elastic properties of the vessel wall prevail and collagen fibers only contribute little to the elastic recoil. With higher blood pressure, however, the vital characteristic of collagen fibers to counteract the mechanical load becomes more important. Such elevated and unphysiological blood pressure levels usually occur within aneurysmatic regions and could also determine increasing wall stiffness.[11] A previous study showed that changing biomechanical conditions within an aneurysm are linked to an increase in ECM components.[30] This study also demonstrated that proteoglycans correlate with mechanical parameters similar to collagens and equally contribute to the vessel wall stability.[30] These circumstances emphasize the ability of vessel wall proteins to counteract the local stress and strain and thus their capacity of vascular remodeling.

1.7. Mechanical properties of the AAA wall

From a physical point of view, rupture risk assessment using the diameter criterion is based on the Law of Laplace. It describes the linear correlation between diameter and wall stress with a constant wall thickness and pressure upon the wall. As this law assumes a cylindrical AAA geometry, risk assessment only by diameter criterion can lead to undifferentiated risk prediction and unexpected ruptures.[31] Furthermore, it does not take into consideration highly relevant AAA factors like individual aneurysm morphology, material properties of the vessel wall, calcification and the resulting individual wall stability. This emphasizes the importance of a more differentiated and individualized approach.

Material properties of AAA tissue samples can be derived from tensile testing, where specific forces are applied to the tissue samples. Elastic properties (expressed as alpha and beta stiffness) as well as so-called failure measures (wall strength and failure tension) are evaluated. Further parameters (like wall stress and wall strain) can then be derived from computer assisted calculations. Physiological ranges of these properties have been determined earlier, however, individual variations have been taken less into account regarding risk stratification of AAA rupture. For a more patient-specific prediction, a combined evaluation of individual AAA wall properties and load-bearing ECM components is essential.

1.8. Mechanotransduction and regulation of ECM synthesis

Processes of constant matrix remodeling and turnover aim to maintain mechanical stability and homeostasis of the aortic wall. These remodeling processes are initiated by vascular mechanosensing, whereby transmembrane integrins and subsequent actomyosin contractility play a key role (Fig. 4).

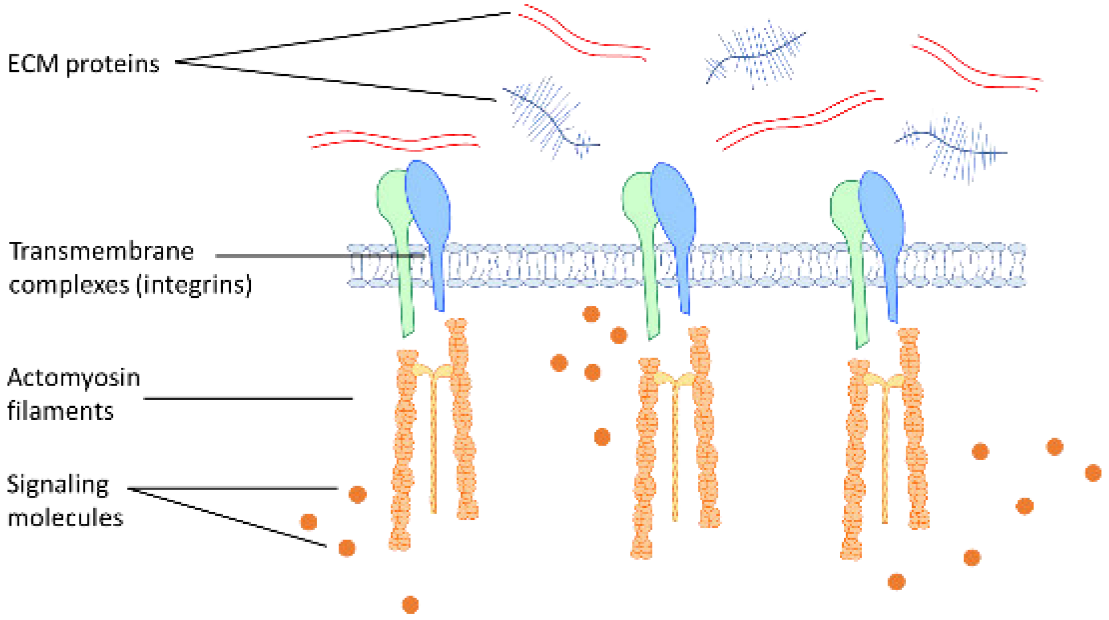

Figure 4: Central components of vascular mechanosensing and mechanotransduction. Mechanical forces are detected by transmembrane integrins, and signals are further transmitted by actomyosin contractility and intracellular signaling molecules. Modified from: Humphrey, J.D., et al., Role of mechanotransduction in vascular biology: focus on thoracic aortic aneurysms and dissections. Circ Res, 2015. 116(8): p. 1448-61. Illustration was created using www.motifolio.com.

Mechanical signals are further mediated by signaling molecules and pathways of mechanotransduction.[12] Those signals can then alter the synthesis of ECM proteins by VSMCs, responding to alternating mechanical loading.[32] This direct connection between mechanical strain and ECM composition of the aortic wall is an important prerequisite in the context of aneurysm rupture.

Both angiotensin II (Ang-II) signaling and the central TGF-ß signaling pathway have been shown to be important mediators of this corresponding VSMC response. TGF-ß signaling is initiated by the binding of a TGF-ß superfamily ligand (e.g. TGF-ß 1-3, BMPs) to a TGF-ß type II receptor. This receptor kinase phosphorylates and activates the type I receptor kinase. In the next step, the type I receptor kinase in turn phosphorylates a cytoplasmic receptor-regulated SMAD (R-SMAD; SMAD as an acronym from *Caenorhabditis elegans* SMA genes and *Drosophila* MAD family genes). Phosphorylation of SMADs enables complex formation with the common partner SMAD (Co-SMAD; SMAD4) and translocation to the cell nucleus. These R-SMAD/Co-SMAD complexes serve as transcription factors and modulate the expression of different effector genes of ECM synthesis and degradation. In addition to this so-called canonical signaling, TGF-ß signaling can also be mediated by SMAD-independent signaling molecules. The mitogen-activated protein kinase (MAPK) family with the downstream extracellular-regulated kinases (ERK1/2), c-Jun N-terminal kinases (JNKs) and p38 MAPK is referred to as non-canonical signaling pathway. The phosphoinositide 3-kinase (PI3K) axis is a third TGF-ß-regulated signaling pathway. Activation of PI3K initiates phosphorylation of protein kinase B (Akt), which in turn activates downstream effectors like the mammalian target of rapamycin (mTOR). An overview of TGF-ß-related signaling pathways is summarized in Figure 5, without any claim to completeness of the involved effectors.

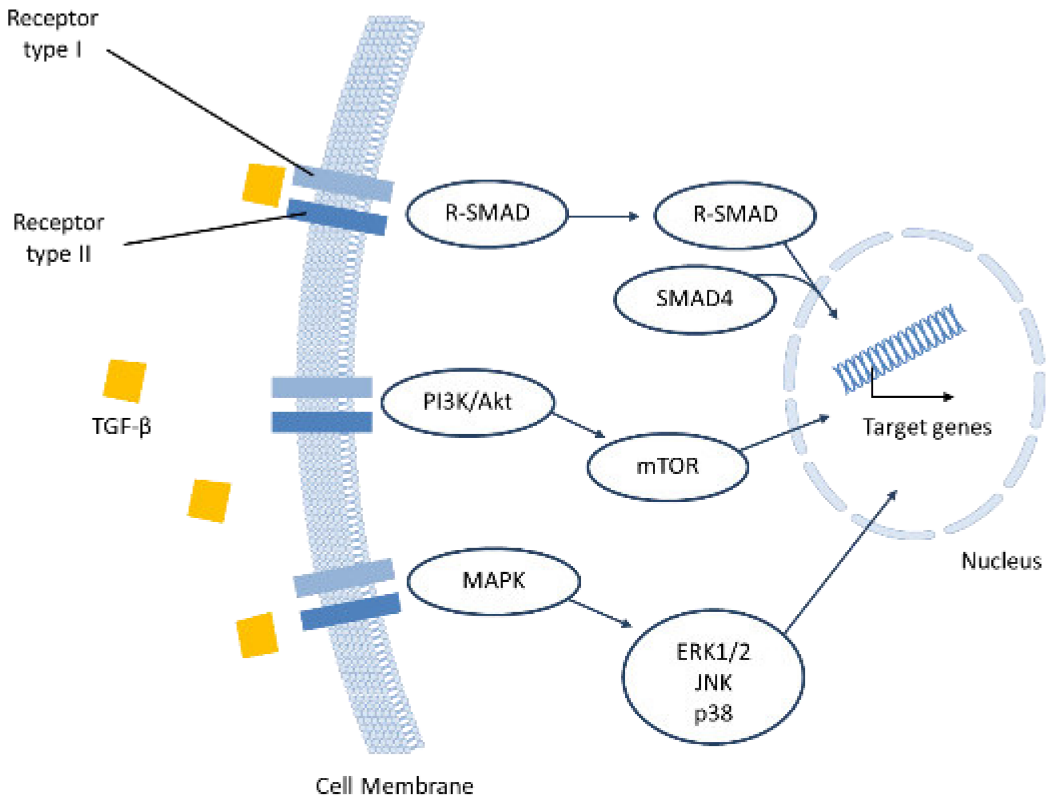

Figure 5: TGF-ß-related signaling pathways involved in vascular mechanotransduction. TGF-ß ligands bind to TGF-ß type II receptors, followed by activation of TGF-ß type I receptors. Signal transduction via the SMAD pathway (= canonical signaling), the PI3K/Akt/mTOR pathway or the MAPK/ERK pathway (= non-canonical signaling). Modulation of ECM-related target genes. The illustration represents a schematic overview of some of the potentially involved pathways and does not make a claim for completeness. Modified from: Humphrey, J.D., et al., Role of mechanotransduction in vascular biology: focus on thoracic aortic aneurysms and dissections. Circ Res, 2015. 116(8): p. 1448-61. Illustration was created using www.motifolio.com.

Mechanical stimuli can activate both the associated MAPK and SMAD pathways, which are connected to TGF-β via extensive cross-talk.[12] The role of TGF-β activation in the development AAA disease remains controversial, as both pathogenic and protective roles are discussed.[14] Previous studies tend to stress the protective effects of TGF-β on Ang-II mediated aneurysm formation, and also on AAA growth and rupture via decreased ECM degradation.[33, 34] Underlying mechanisms of load-dependent receptor activation, signal transduction and degrading processes are still unclear and play a decisive role for the evaluation of surrogate parameters.

1.9. Aim of the study and research questions

The overall aim of this study was to evaluate and validate structural, biological and mechano-biological properties as well as mechanotransduction processes of the AAA wall. These findings can contribute to the development and improvement of an individualized rupture risk stratification model in the context of personalized vascular medicine. Based on the results of previous studies [29-31], the objective of the study was a predictive classification of small- to medium-sized AAAs, where decision for or against surgical intervention is inconclusive using the current clinical methods. The following scientific questions were pursued:

- Which structural and biological factors play a critical role in the pathophysiological processes of a AAA wall, especially regarding its mechanical properties?
- How far are histological and biological findings correlating with the material properties of the aortic wall?
- Are surrogate parameters of AAA tissue and blood samples correlating with material properties of the aortic wall?
- Which mechanotransduction processes influence the biological and mechanical properties of the AAA wall?

To explore the above outlined research questions, especially two decisive aspects of AAA development were addressed: the composition and changes in structural and load-bearing proteins of the ECM, and the mechanical characteristics of these ECM components. Furthermore, inflammatory markers contributing to aortic wall degeneration were assessed. Both structural and inflammatory parameters were then evaluated regarding their potential to serve as possible serological surrogate parameters reflecting the biological state of the

aneurysm wall. Moreover, the mechano-biological interactions and involved mechanotransduction pathways were examined.

To evaluate the biological and structural composition of the aortic wall, protein levels of ECM components and inflammatory factors were analyzed. In addition, mRNA expression levels of these components along with central parameters of ECM composition were measured. Tissue and corresponding serum samples from patients with ruptured AAA (rAAA) and patients who underwent elective surgery (eAAA) were compared to samples from healthy individuals to determine changes during AAA pathogenesis. Tissue morphology and degeneration as well as distribution of collagens and proteoglycans were also assessed on the histological level. In parallel, mechanical characteristics of vessel wall specimen were evaluated using tensile testing. Elastic wall properties were quantified and subsequent destructive testing was applied to measure failure loads. In the next step, correlation analyses of biological parameters were performed to assess potential relationships between tissue and serum levels. Correlations between biological and mechanical properties were also evaluated for tissue, serum and histology. Finally, the activation of regulatory pathways for ECM components was determined in the tissue samples.

2. Material and methods

2.1. Study cohorts and samples

2.1.1. Munich Vascular Biobank

All samples used for analysis were part of the Munich Vascular Biobank. The samples were collected from patients treated in the Department of Vascular and Endovascular Surgery at Klinikum rechts der Isar (TU Munich). This existing database was maintained and continuously expanded during the duration of the study, focusing on blood and tissue samples from AAA patients. For every patient, corresponding patient data like medical history, comorbidities, medication or blood parameters were recorded and routine aortic wall characterization was carried out. The collection of human specimens was approved by the ethics committee of the university hospital Klinikum rechts der Isar (2799/10, Ethikkommission der Fakultät für Medizin der Technischen Universität München, Munich, Germany) and the study was performed in accordance with the World Medical Association Declaration of Helsinki. Written informed consent was obtained from all patients.

2.1.2. Sample collection and processing

Aortic tissue samples (total n=115) were collected during open AAA repair (Fig. 1). Before vascular graft interposition the samples were excised from the anterior or lateral parts of the aortic aneurysm, ensuring that enough aortic tissue remained to fully cover the graft after excision. N=29 of these samples were excised from patients who had been diagnosed with a ruptured AAA, where AAA repair represents an emergency surgery. The remaining n=78 samples were collected during elective aneurysm repair, implying that the aneurysm was unruptured and patients underwent a planned surgery. Healthy aortic samples (n=8) served

as control tissue and were obtained from adult kidney donors during transplantation in the Department of Trauma Surgery at Klinikum rechts der Isar (TU Munich).

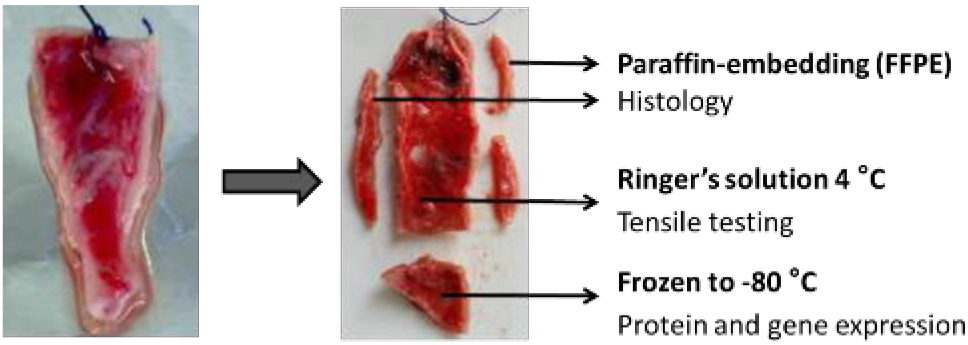

Figure 6: Tissue processing after excision. FFPE: formalin-fixed, paraffin-embedded. Modified from: Reeps, C., et al., Measuring and modeling patient-specific distributions of material properties in abdominal aortic aneurysm wall. Biomech Model Mechanobiol, 2013. 12(4): p. 717-33.

Tissue samples were processed as fast as possible after excision, mostly within a few hours. The tissue was then divided according to further use (Fig. 6). The central and largest part was used for mechanical testing, as a rectangular-shaped specimen is required for the testing machine. The specimens were stored in lactated Ringer's solution (130 mmol/L sodium chloride, 5 mmol/L potassium chloride, 2 mmol/L calcium chloride, 3 mmol/L sodium lactate) at 4 degrees until testing was performed (normally within 24 h after surgery). Smaller, adjacent pieces of tissue were used for protein and gene expression analysis and were immediately frozen down to -80 degrees and stored for later use. For histological analyses, other adjacent pieces were fixed with 4% formalin and subsequently embedded in paraffin (FFPE).

Corresponding serum samples from these patients were collected where possible (n=13 for rAAA, n=72 for eAAA). Whole blood samples were obtained prior to surgery during routine blood collection and were centrifuged for 15 minutes for serum separation. The supernatant

was immediately transferred to new polypropylene tubes (Eppendorf AG, Hamburg, Germany) and frozen down to -80 degrees. For serum controls, whole blood was taken from n=5 healthy adult individuals and processed in the same way.

Furthermore, the following blood parameters were determined during routine blood analysis and were transferred from clinical chemistry records: hsCRP (high-sensitivity C-reactive protein; to determine the inflammatory status and evaluate the risk of cardiovascular disease and atherosclerosis), creatinine (to evaluate the filtration of this waste product from blood and thereby assess kidney function), urea (to determine the amount of urea nitrogen in blood and evaluate urea clearance), GFR (glomerular filtration rate; the estimated Chronic Kidney Disease Epidemiology Collaboration (CKD-EPI) rate has been used to evaluate the filtration of creatinine per minute, based on blood creatinine and patient age, sex and skin type), erythrocytes (to measure the number of red blood cells), hemoglobin (to evaluate red blood cells and oxygen transport), thrombocytes (to determine the number of platelets in blood and assess blood clotting), leucocytes (to measure the number of white blood cells and thereby evaluate the immune status). These parameters were only available for AAA patients and could not be obtained from healthy controls.

2.2. Quantitative protein analysis

2.2.1. Protein extraction and concentration measurement

For total protein extraction, approximately 50 mg of tissue were weighed from the dedicated parts (Fig. 6) using a precision scale (Kern & Sohn GmbH, Balingen, Germany) and then cut into smaller pieces using a scalpel. The tissue samples were stored on ice and 200 µl lysis buffer (Tissue Extraction Reagent I, Thermo Fisher Scientific, Waltham, MA, USA) were added. Before homogenization, the samples were snap frozen in liquid nitrogen. The samples were then

homogenized with a tissue homogenizer (Bio-Gen PRO200 with Multi-Gen 7XL probes, PRO Scientific, Oxford, CT, USA) for approximately 30-60 seconds, depending on tissue quality and extent of calcification. The homogenate was centrifuged for 20 minutes at 4 degrees and the supernatant (= protein lysate) was used for determination of protein concentration. A bicinchoninic acid assay (Pierce BCA Protein-Assay Kit, Thermo Fisher Scientific, Waltham, MA, USA) was used to quantify protein concentration according to the manufacturer's instructions. In this assay, the total protein concentration can be determined by color change of the sample solutions proportional to their protein concentration. This color change is caused by the protein-dependent reduction of Cu^{2+} to Cu^{1+} and the chelation of Cu^{1+} with BCA molecules. The formed complexes absorb light at 562 nm and can be detected colorimetrically with a plate reader (Epoch Microplate Spectrophotometer, BioTek, Winooski, VT, USA). Following determination of protein concentration, all samples were diluted to a concentration of 1 µg/µl with lysis buffer (Tissue Extraction Reagent I, Thermo Fisher Scientific, Waltham, MA, USA).

2.2.2. Protein quantification via enzyme-linked immunosorbent assay (ELISA)

Enzyme-linked immunosorbent assays (ELISAs) were used for quantitative protein analyses of both tissue and serum samples. For the evaluation of inflammatory factors, CXCR4 (ELISA Kit for Human CXCR4, Cloud-Clone Corp., Katy, TX, USA) and its ligand CXCL12 (Quantikine ELISA for Human CXCL12, R&D Systems, Minneapolis, MN, USA) were measured. To evaluate the collagenous components of the vessel wall, firstly hydroxyproline (HYP; Human Hydroxyproline ELISA Kit, BlueGene Biotech, Shanghai, China) as the major component of all types of fibrillar collagen was determined. To further evaluate the most abundant vascular collagens, collagen type I (Col1; ELISA Kit for Human Collagen Type I, Cloud-Clone Corp., Katy, TX, USA) and type III (Col3; Human Collagen Type III ELISA Kit, Abbexa Ltd., Cambridge, UK)

were measured. These types of collagen are also described as being predominantly responsible for force transmission within the vessel wall.[11] Proteoglycans, the second important group of ECM components related to mechanical properties, were assessed by the total amount of GAG chains (Human Glycosaminoglycans ELISA Kit, BlueGene Biotech, Shanghai, China). CS (Chondroitin Sulfate ELISA Kit, Abbexa Ltd., Cambridge, UK) and DS (Human Dermatan Sulfate ELISA Kit, Elabscience Biotechnology Inc., Wuhan, China) were quantified to further investigate the proteoglycan composition of tissue and serum samples. CS and DS proteoglycans are those subgroups mainly associated to extracellular structures. In contrast to that, the amount of HS (Human Heparan Sulfate Proteoglycan ELISA Kit, Abbexa Ltd., Cambridge, UK) was determined as the subgroup that is associated to cell surfaces and basement membranes. Moreover, to specifically evaluate a potential serum biomarker, endocan (Human ESM1 ELISA Kit (Endocan), Abcam, Cambridge, UK) levels were measured.

Prior to all ELISA assays, protein concentration of the samples was compared to the given detection range of each assay. Where necessary, samples were diluted with phosphate buffered saline (pH 7.4, Gibco, Thermo Fisher Scientific, Waltham, MA, USA) appropriately to be within the respective detection range. All samples were measured in duplicates. The quantitative determination of all proteins was based on standard sandwich ELISA technology. The respective monoclonal antibodies (specific for each measured protein) were pre-coated onto 96-well plates. Protein standards were included in each kit and were used to prepare defined serial dilutions of known concentration, which were then used as standard curves. After adding standards and samples to the plates, biotinylated detection antibodies (specific for each measured protein) were added. After washing with the respective assay buffers, an avidin-biotin-peroxidase complex was added. Unbound conjugates were removed with a further washing step. Next, an enzymatic reaction is used to generate a detectable color

product. Tetramethylbenzidine (TMB) is used as a substrate for horseradish peroxidase (HRP), and by TMB catalyzation a detectable color change (blue) is induced. After incubation with TMB, an acidic stop solution for stopping the enzymatic reaction was added. The stop solution induced another color change (yellow) and the color density was proportional to the amount of measured protein on the plate. Color density was detected as optical density (OD) of each well and was measured with a plate reader at a wavelength of 450 nm. An OD standard curve was plotted using the known concentrations of the protein standards and the unknown sample concentrations were derived by comparison with this standard curve. Sample concentrations were calculated by interpolation and using the slope formula (y = mx + b) of each standard curve, with y being the sample OD and x the sample concentration.

2.3. Gene expression analysis

2.3.1. RNA extraction

For gene expression analysis, total RNA was extracted from the dedicated parts of the aortic tissue samples (Fig. 6). From all available tissue samples, n=8 rAAA, n=10 eAAA and n=4 controls were selected for gene expression analysis based on amount and macroscopic quality. Approximately 50 mg of tissue (including all visible layers of vessel wall) were cut from each tissue sample using a precision scale (Kern & Sohn GmbH, Balingen, Germany) and were placed in microcentrifuge tubes (2 ml, Eppendorf AG, Hamburg, Germany). The sections were then stored on ice. Before homogenization, 700 µl of QIAzol (a phenol and guanidine thiocyanate solution; Qiagen, Hilden, Germany) were added for tissue lysis and removal of DNA and proteins, and the sections were subsequently frozen in liquid nitrogen. The samples were then homogenized for 30-60 seconds (depending on the extent of calcification) using a

Bio-Gen PRO200 Homogenizer and Multi-Gen 7XL Probes (PRO Scientific, Oxford, CT, USA). Extraction and silica membrane-based purification of total RNA was performed using the miRNeasy Mini Kit (Qiagen, Hilden, Germany) according to the manufacturer's instructions. Following homogenization, samples were incubated for 5 min on the benchtop and 140 µl chloroform (Chloroform ≥ 99.8%, Carl Roth, Karlsruhe, Germany) was added to each sample. After another short incubation (3 min), samples were centrifuged for 15 min at 12 000 x g in a pre-cooled centrifuge (4 degrees). The samples separated into three phases during centrifugation (upper, aqueous phase; white middle phase; lower, reddish phase containing tissue debris). The upper phase (containing RNA) was transferred to a provided collection tube and was mixed with 525 µl 100% ethanol (Ethanol ≥ 99,5%, extra pure, Carl Roth, Karlsruhe, Germany). The mixture was transferred to a provided spin column (placed in another 2 ml tube) and was centrifuged for 15 sec at 8 000 x g. The resulting flow-through was discarded. 700 µl of provided buffer (RWT) was added to the spin column, followed by another centrifugation step (15 sec). Two times 500 µl of another provided buffer (RPE) were added subsequently and the samples were centrifuged two more times (15 sec and 2 min), with the flow-through always being discarded. In the last step, the remaining spin column was placed in a new 1.5 ml tube and 50 µl of provided RNase-free water were added onto the column for RNA elution. Tubes were centrifuged for 1 min at 8 000 x g and the eluted RNA was collected in the tube. Following elution, RNA concentration was determined via the NanoDrop 2000c (Thermo Fisher Scientific, Waltham, MA, USA) spectrometer. RNA samples were stored at -80 degrees.

2.3.2. cDNA synthesis and real-time qPCR

Based on the previously measured RNA concentration, all samples were diluted to an initial concentration of 300 ng/µl total RNA before reverse transcription (RT). The High Capacity RNA-to-cDNA Kit (Thermo Fisher Scientific, Waltham, MA, USA) was used to synthesize cDNA from the total RNA. 300 ng total RNA of each sample were used for the RT reaction and were mixed with 10µl of the provided buffer mix and 1µl of the provided enzyme mix. The respective amount of provided nuclease-free water was added for a total reaction volume of 20µl. All components were prepared in microcentrifuge tubes (0.2 ml Tube strips, Eppendorf AG, Hamburg, Germany) and were placed on ice until the RT reaction. The RT program (incubation for 60 min at 37 degrees, heating to 95 degrees for 5 min to stop the reaction, holding at 4 degrees) was performed in a thermal cycler (Mastercycler Nexus Gradient, Eppendorf AG, Hamburg, Germany).

The mRNA expression of ECM collagens (Col1A1 and Col3A1; representing the main components of type I and III collagen) as well as the expression of elastin- and collagen-degrading matrix metalloproteinases (MMP2 and MMP9; representing important vascular metalloproteinases) was determined. TGF-ß-dependent signaling was evaluated based on the expression levels of the two effector molecules and cytokine isoforms TGFB1 and TGFB2. Furthermore, the expression of their corresponding TGF-ß receptors (TGFBR1 and TGFBR2) was evaluated. The mRNA levels of the related downstream effectors and transcription factors (SMAD2, SMAD3, SMAD4) were quantified to gain a complete overview of the signaling pathway. The respective assays (all manufactured by Thermo Fisher Scientific, Waltham, MA, USA) are listed below (Table 1).

Assay/target	Assay reference
Col1A1	HS00164004_M1
Col3A1	HS00943809_M1
MMP2	HS01548727_M1
MMP9	HS00957562_M1
TGFB1	HS00998133_M1
TGFB2	HS00234244_M1
TGFBR1	HS00610320_M1
TGFBR2	HS00234253_M1
SMAD2	HS00998187_M1
SMAD3	HS00969210_M1
SMAD4	HS00929647_M1
RPLP0	HS00420895_gH

Table 1: TaqMan gene expression assays. Target names and respective assay references.

mRNA expression levels were measured via real-time quantitative polymerase chain reaction (qPCR) using TaqMan (derived from *Thermus aquaticus* polymerase and the game PacMan) probes. These probes are labelled with fluorescein amidites (FAM) as a fluorescent dye and also carry a non-fluorescent quencher molecule that decreases and suppresses the fluorescent signal. The probe principle is based on the detection of a specific, amplified PCR product with these fluorescent probes. In the first step of the qPCR, the synthesized and double-stranded cDNA is denatured by temperature while the fluorescent signal of the probe is still quenched. Next, the temperature is lowered and the primers as well as the probe can anneal to the respective target sequences. A new DNA strand is then synthesized by the Taq

polymerase and the fluorescent dye of the probe is separated from the quenching molecule by nuclease activity of the polymerase. This degradation of the probe abolishes the quenching effect and the fluorescent signal can be detected. The fluorescent signal increases with every PCR cycle and corresponds to the amount of synthesized target sequence.

Prior to qPCR, the previously synthesized cDNA was diluted at a ratio 1:3 with nuclease-free water (RT-PCR Grade Water, Thermo Fisher Scientific, Waltham, MA, USA) in a separate microcentrifuge tube (Eppendorf AG, Hamburg, Germany). All reagents were thawed on ice and were prepared in 96-well reaction plates (MicroAmp Optical 96-Well Reaction Plate, Thermo Fisher Scientific, Waltham, MA, USA). The following reagents were added to each well: 8.5µl TaqMan mix (TaqMan Universal Master Mix II, no UNG, Thermo Fisher Scientific, Waltham, MA, USA), 5.65µl nuclease-free water, 0.85µl of the respective assay (see Table 1) and 2µl of the pre-diluted cDNA. All samples on each plate were measured in duplicates and negative controls (also in duplicates) for each assay were included. For the negative controls, the abovementioned reagents were added to the wells with 2µl nuclease-free water instead of cDNA. Ribosomal protein lateral stalk subunit P0 (RPLP0) served as a reference (or housekeeping) gene in order to normalize sample gene expression and was measured in duplicates for each sample on each plate. After adding all reagents, the plates were sealed with adhesive foil (ABsolute qPCR Plate Seals, Thermo Fisher Scientific, Waltham, MA, USA) and were placed in a QuantStudio 3 PCR System (Thermo Fisher Scientific, Waltham, MA, USA). Real-time target amplification was performed for 40 cycles using the following reaction stages: heating to 95 degrees for 5 min, 10 sec at 95 degrees, 30 sec at 60 degrees, 10 sec at 72 degrees. Relative expression of the target genes was then calculated using the ΔΔCt method. The cycle threshold (Ct) represents the amplification cycle number where the fluorescent signal exceeded the level of background noise and was measured for each well.

As Ct levels are based on the initial amount of target sequence in each well that has been amplified, the cycle values are inversely proportional to the initial amounts (i.e. low Ct values correspond to high initial amounts). Firstly, the Ct values of all sample duplicates were averaged. The delta Ct (ΔCt) was calculated by subtracting the Ct values of the reference gene (RPLP0) from those of the target genes. Next, the average ΔCt from all control samples on the respective plate was calculated. This control average was then subtracted from the ΔCt values of the AAA (eAAA + rAAA) samples in order to generate the ΔΔCt values. The expression results are therefore always calculated as gene expression relative to the control samples. In a last step, the fold gene expressions were calculated as 2^-(ΔΔCt) for each sample and are displayed as fold change compared to control samples.

2.4. Histological analyses

2.4.1. Tissue fixation, embedding and sectioning

Histological analyses were performed for most of the aortic samples (n=93). However, due to limited size of the collected tissue specimens, for some samples all tissue needed to be used for protein analyses and no remaining tissue could be used for histology. For histological tissue processing, smaller aortic tissue pieces (Fig. 6) were placed in 4% formalin (Morphisto, Frankfurt am Main, Germany) immediately after tissue collection. The tissue was then fixed for at least 24h and was placed in embedding cassettes (Universal, Medite, Burgdorf, Germany). These cassettes were stored in 70% ethanol (Carl Roth, Karlsruhe, Germany) and were further dehydrated overnight. Immediately after dehydration, the tissue was embedded with paraffin (Paraffin extra pure, Carl Roth, Karlsruhe, Germany).

For histological staining, 2-3µm sections were cut from the paraffin-embedded tissue blocks. The blocks were placed on a cold plate (EG1150 C, Leica, Wetzlar, Germany) and were sectioned using a rotary microtome (RM2255, Leica, Wetzlar, Germany). For overview and alcian blue staining, sections were mounted onto SuperFrost glass slides (Thermo Fisher Scientific, Waltham, MA, USA). For immunohistochemistry (IHC), SuperFrost Plus glass slides (Thermo Fisher Scientific, Waltham, MA, USA) were pre-coated with 0.1% poly-L-lysine (Sigma-Aldrich, St. Louis, MO, USA) and were then used for mounting. The slides were dried overnight in a drying cabinet (Heratherm General Protocol Oven, Thermo Fisher Scientific, Waltham, MA, USA) at 56 degrees and the following staining protocols were used for evaluation of different tissue components.

2.4.2. Overview staining (HE and EvG)

A standard hematoxylin-eosin (HE) staining was used for basic evaluation of the tissue structure, focusing on cellular composition of the aortic wall and inflammatory infiltration. Hematoxylin serves as a nuclear staining while eosin is used as a cytoplasmic dye and to differentiate between cytoplasmic and nuclear components. In a first step, xylene (2 x 10 min; Xylene (isomers), Carl Roth, Karlsruhe, Germany) was used for deparaffinization of the sections and was subsequently removed with isopropyl (2 x 5 min; 2-Propanol 70%, Carl Roth, Karlsruhe, Germany). The sections were then hydrated with 96% ethanol (2 x 5 min; Ethanol ≥ 96%, Carl Roth, Karlsruhe, Germany) and 70% ethanol (2 x 5 min) until finally distilled water (1 x 5 min) is used. The slides were placed in hematoxylin solution (Mayer's hematoxylin, Carl Roth, Karlsruhe, Germany) for 10 min, rinsed with running tap water for approx. 5 min and then placed in eosin solution (Eosin 1%, alcoholic, Morphisto, Frankfurt am Main, Germany) for 2 min. For dehydration, the slides were placed in 96% ethanol (30 sec) and isopropyl (30

sec) again. In a final clearing step ethanol was replaced with xylene (2 x 2 min) before mounting medium (Eukitt, Sigma-Aldrich, St. Louis, MO, USA) and glass coverslips (24 x 50 mm, Menzel, Thermo Fisher Scientific, Waltham, MA, USA) were applied.

Elastica van Gieson (EvG) staining was used to evaluate connective tissue components, especially collagen and elastic fibers. The initial deparaffinization and hydration steps were performed as described above for HE. Following hydration, the slides were placed in a resorcin-fuchsin solution (Romeis 16, Hospital pharmacy Klinikum rechts der Isar, Munich, Germany) for 25 min. After washing with 96% ethanol (2 x 1,5 min), the slides were stained in an iron hematoxylin solution (Weigert's solution – part I + II, Romeis 15, Hospital pharmacy Klinikum rechts der Isar, Munich, Germany) for 15 min. The slides were rinsed with running tap water for approx. 5 min and then placed in a picrofuchsin solution (Romeis 16, Hospital pharmacy Klinikum rechts der Isar, Munich, Germany) for 2 min. Dehydration, clearing and mounting was performed as described above for HE.

2.4.3. Alcian blue staining*

Alcian blue staining was used to evaluate acidic glycosaminoglycans and polysaccharides. With regard to vessel wall components, it was used to determine the amount and distribution of proteoglycans. The staining has been performed by Katharina Jakob as part of her master's thesis. The initial deparaffinization and hydration steps were again performed as described above for HE. The slides were placed in 3% acetic acid (diluted in distilled water, Sigma-Aldrich, St. Louis, MO, USA) for 2 min and were subsequently placed in alcian blue dye (Alcian blue 8GX, Merck, Darmstadt, Germany) dissolved in 3% acetic acid for 10 min. After rinsing the slides with running tap water for 1-2 min they were then placed in aluminium sulphate

* The staining described in this section has been performed by Katharina Jakob.

solution (Nuclear fast red aluminium sulphate solution, Carl Roth, Karlsruhe, Germany) for 8 min. After another rinsing with tap water the slides were dehydrated, cleared and mounted as described above for HE.

2.4.4. Immunohistochemistry

Following histo-morphological characterization (based on the respective HE and EvG staining), representative samples from all groups were selected based on tissue quality and extent of relevant tissue characteristics. These samples were used for further immunohistochemical (IHC) evaluation and were stained with the following markers: SM-α actin (SMA, smooth muscle cells), CD68 (macrophages), CD45 (leucocytes), CXCR4 (chemokine receptor 4), ESM1 (endocan). Both the abundance of these markers and their cellular localization were assessed via IHC. SMA staining was used to evaluate mainly the distribution SMCs, which synthesize ECM components and determine vessel wall properties. The cellular context and distribution of inflammatory markers, especially CXCR4, were evaluated using consecutive IHC staining. For this, sequential 2-3 µm sections were cut from the respective tissue blocks and were stained with the respective markers always in the same order (CXCR4 – CD68 – CD45 – SMA). The first section of each sequence was used for a standard HE staining and served as a histological reference and orientation. ESM1 staining was performed to assess the localization and abundance of endocan in relation to other vessel wall components.

The initial deparaffinization and hydration steps were again the same as for HE, EvG and alcian blue. This was followed by an antigen retrieval step, where the slides were boiled in 10nM citrate acid monohydrate (Merck, Darmstadt, Germany) diluted in distilled water (pH 6.0) in a pressure cooker for 7 min. For blocking of endogenous peroxidase activity, 3% hydrogen peroxide (diluted in distilled water; Hydrogen peroxide 30%, Merck, Darmstadt, Germany) was

applied to the slides for 15 min. The samples were incubated for 1 hour with the following primary antibodies, previously diluted with REAL Antibody Diluent (Dako, Glostrup, Denmark): anti-SM-α actin (M0635, clone HHF35, Dako, Glostrup, Denmark; dilution 1:200), anti-CD68 (M0814, clone KP1, Dako, Glostrup, Denmark; dilution 1:2000), anti-CD45 (M0701, clones 2B11 + PD7126, Dako, Glostrup, Denmark; dilution 1:500), anti-CXCR4 (ab124824, Abcam, Cambridge, UK; dilution 1:300) and anti-ESM1/endocan (ab224591, Abcam, Cambridge, UK, dilution 1:1000).

The slides were then incubated with a biotinylated secondary antibody (REAL Detection System Peroxidase/DAB+, Dako, Glostrup, Denmark) for 25 min and peroxidase conjugated streptavidin (REALTM Detection System Peroxidase/DAB+, Dako, Glostrup, Denmark) for 25 min. The reaction was visualized with a DAB chromogen (REALTM Detection System Peroxidase/DAB+, Dako, Glostrup, Denmark) that was applied to the slides for 3-5 min, depending on the intensity of color development. For nuclear counterstaining, the slides were placed in Mayer's hematoxylin (Carl Roth, Karlsruhe, Germany) for 20 sec. For dehydration, the slides were placed in 70% ethanol (3 min), 96% ethanol (3 min) and isopropyl (3 min) before replacing ethanol with xylene (3 min). Mounting was performed as described above for HE. Corresponding control slides were included for every marker. Human tonsil tissue samples served as positive controls for the markers and were sectioned, prepared and stained in the same way as the aortic samples. For primary antibody control, slides were incubated without the respective primary antibody and the diluent alone was applied. The following steps (secondary antibody incubation and detection) were the same as for the other samples.

2.4.5. Semiquantitative scoring

To evaluate histological tissue characteristics and then compare between AAA groups, a semiquantitative scoring method was applied. Systematic scoring was performed via light microscopy (DM4000 B, Leica, Wetzlar, Germany) for HE, EvG and alcian blue staining. The general scoring range for tissue characteristics was "-" for 0% incidence of the specific characteristic to "++++" for 100% incidence, with scoring examples for each tissue characteristic given below. Also intermediate scoring points (such as "+/++") were used. Scoring was performed by persons who were trained and experienced in vessel wall histopathology and were blinded to AAA groups. The following histological characteristics were evaluated for each aortic sample:

- **Histological quality:** the overall tissue quality and completeness was evaluated. Also the quality of the performed staining was included, especially regarding visibility of important tissue characteristics. Poor quality was scored as "-" while a particularly suitable sample was scored as "++++". The suitability of individual samples for further immunohistochemical evaluation was based on the overall histological quality.
- **Cellularity**: the amount of cells within the vessel wall was scored, taking into account also cell density and cell distribution. Cell nuclei were stained purple-blue in the HE staining and SMCs (spindle-shaped) could be differentiated from inflammatory cells (round-shaped). Acellular tissue was scored as "-" while very cell-rich tissue was scored as "++++".
- **Infiltrates**: inflammatory cell infiltration within the vessel wall was scored, meaning the accumulation of mainly white blood cells (neutrophils, lymphocytes, monocytes). No infiltration was scored as "-" while several large regions of infiltration were scored

as “++++”. The extent of infiltration was closely connected to tissue cellularity, as pronounced infiltration is based on increased tissue cellularity. A tissue could therefore not be scored as strongly infiltrated when the cellularity was scored low, while a tissue could be scored high in cellularity without showing increased infiltration.

- **Neovessels**: the extent of neovascularization was scored based on the presence and amount of neovessel sprouts, mainly being associated with inflammatory infiltration. A neovessel is characterized by a continuous monolayer of endothelial cells forming a small vessel lumen within the aortic wall. No neovessels were scored as “-“ while pronounced neovascularization was scored as “++++”.
- **Total collagen**: the total amount of collagen fibers in within the vessel wall was scored. In the EvG staining, collagen fibers are red and typically arranged in even, wavy bundles. Complete rarefication of collagen fibers was scored as “-“ while increased occurrence of collagen was scored as “++++”.
- **Total elastin**: the extent of elastic fibers was scored, based on dark blue to black fibers in the EvG staining. These fibers are typically arranged in a regular fiber network together with collagen fibers and are increasingly fragmented with age and ECM degradation. Complete loss and fragmentation of elastic fibers was scored as “-“ while elastin abundancy was scored as “++++”.
- **Calcification**: the extent of calcification was evaluated in the HE staining, based on dark blue to purple areas that were often ripped apart during tissue sectioning due to their fragile structure. Cholesterol crystals were evaluated as preliminary stages of calcification. Samples without calcification were scored as “-“ while areas of extensive calcification were scored as “++++”.

- **Hemorrhage**: intramural bleeding was scored as the extent of clear red areas in the HE staining. Microbleedings derive from sectioned neovessels or vasa vasorum and can be identified by areas of red blood cells. No hemorrhage was scored as "-" while areas of extensive bleeding were scored as "++++".
- **Adventitia**: adventitial characteristics were scored based on adventitial thickening and an increased adventitial vasa vasorum. Both are closely connected to increased neovascularization towards the medial and intimal layers. An unaltered adventitia was scored as "-" while extensive changes were scored as "++++".
- **Atherosclerosis:** the overall extent of atherosclerotic characteristics was scored. Several histopathological characteristics (inflammatory infiltration, foam cells, neovascularization, medial degeneration, elastin degradation, cholesterol crystals and calcification) were taken into account for a combined evaluation. Unaltered histology was scored as "-" while extensive atherosclerosis was scored as "++++".
- **Alcian blue (total):** the overall extent of proteoglycans was scored in the alcian blue staining, focusing on the distribution over the entire sample area. Unstained samples were scored as "-" while extensive staining was scored as "++++".
- **Alcian blue (selective):** the focal accumulation of proteoglycans was scored, focusing here on the extent of local proteoglycan "hotspots" (areas with intense blue coloring). Selective staining was closely connected to the total extent of proteoglycans and samples could not be scored higher in focal accumulation than they were scored in the total staining. Samples without local "hotspots" and with an even distribution of proteoglycans were scored as "-" while samples with extensive focal accumulation were scored as "++++".

The scoring range was then transferred to numerical values (0 to 4, in steps of 0.5) for further analysis.

2.5. Mechanical testing*

2.5.1. Sample preparation

To evaluate material properties of aortic tissue samples with regard to aneurysm progression and risk stratification, tensile testing was used. The experiments described below were performed by members of the Mechanics and High Performance Computing Group (TU Munich).

As biological tissue samples are anisotropic materials (i.e. materials with properties that are direction dependent and are not identical in all directions as for isotropic materials), uniaxial tensile testing would not provide sufficient information about material parameters. A biaxial testing approach was therefore required for adequate testing of aortic tissue. The respective central tissue parts (Fig. 6) of the excised samples were used. N=64 of all collected AAA samples were suitable for mechanical testing, based on tissue integrity and available sample size. Control tissue was not used for tensile testing, as these samples are presumed to have strongly differing material properties and conclusive comparison with diseased tissue would thus not be possible.

The central tissue parts were further cut into rectangular-shaped specimens with a length of approximately 20-30 mm and a width of approximately 8-10 mm to meet the requirements of the tensile test machine. Prior to tensile testing, the specimen thickness of each sample was determined at five measuring points using a digital thickness gauge (Quick-Mini Series 700,

* Mechanical testing of aortic tissue samples has been performed by the Mechanics and High Performance Computing Group (TU Munich) led by Prof. Gee.

Mitutoyo, Kawasaki, Japan) and was averaged for further analyses. For the following measurements (elastic and destructive testing), a Zwick/Roell mediX 0.1 (Messphysik Materials Testing, Fürstenried, Austria) biaxial testing machine was used (Fig. 7). The specimens were clamped into the test machine on all four sides so that force could be applied in all directions. The force range of the transducers was ± 100 N with a resolution of 0.6 mN and clamp distance was measured with a resolution of 0.1 µm. Tensile testing was performed according to previously described testing protocols.[30, 31]

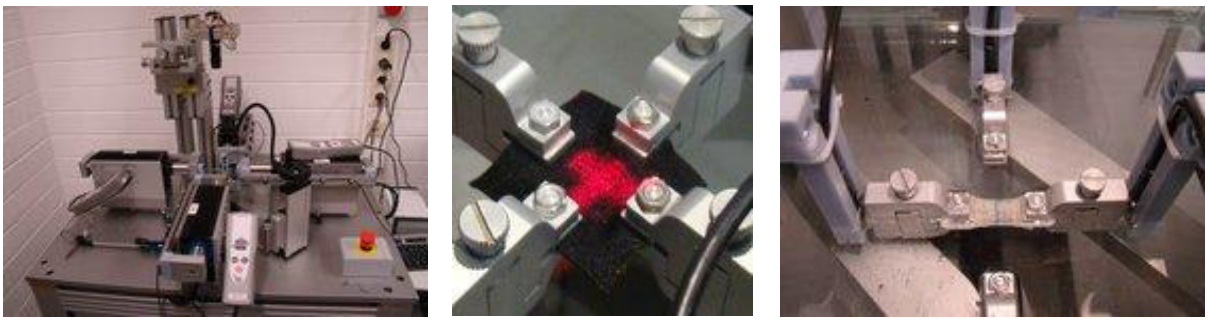

Figure 7: Biaxial tensile testing machine. Left: Zwick/Roell mediX 0.1 testing machine with four independent linear actuators for force transduction. Middle: detailed view of clamps with laser for optical strain measurement. Right: tissue sample clamped into testing machine. Modified from: https://www.epc.ed.tum.de/lnm/research/methods/expunibiax/; Institute for Computational Mechanics (TU Munich).

2.5.2. Cyclic testing

Firstly, elastic tissue properties were determined in a cyclic test. The specimens were exposed to cyclic loading and a pre-conditioning phase of 19 cycles was applied. The final (20th) cycle was then used for data collection and the applied force as well as clamp displacement were continuously measured during this cycle. The elastic tissue properties were described as α and β stiffness. As aortic tissue shows a non-linear stretch-stress behavior during loading (increasing material stiffening with loading), α stiffness is used to describe the initial, load-free

material stiffness while β stiffness describes material stiffness with higher stretch. Stretch (λ) was calculated by means of clamp displacement (Δx) and the initial clamp distance (l_0):

$$\lambda = \frac{\Delta x + l_0}{l_0}$$

Stress was calculated as the first Piola-Kirchhoff stress (P), with F as the measured applied force and A_0 as the initial cross-sectional specimen area:

$$P = \frac{F}{A_0}$$

The stretch-stress curves from cyclic testing were fitted to a hyperelastic material model [35] to take into account the non-linear material behavior. α and β stiffness were then derived from the loading curve of the 20th cycle using the Levenberg-Marquardt curve fitting algorithm.[36]

2.5.3. Destructive testing

Destructive testing was used to determine the failure load of the specimens and was carried out directly after elastic testing, with the specimens still being clamped into the machine. The clamps were moved apart at a constant speed until maximum clamp displacement was reached. The maximum applied force (F_{max}, expressed as N) and clamp displacement were measured, and from this maximum measured force two failure parameters were derived. The maximum stress (P_{max}, also described as wall strength) was calculated as F_{max} per initial cross-sectional specimen area (A_0):

$$P_{max} = \frac{F_{max}}{A_0}$$

P_{max} is therefore expressed as N/mm^2. The maximum failure tension (T_{max}) was calculated as F_{max} per intial undeformed specimen width (b_0):

$$T_{max} = \frac{F_{max}}{b_0}$$

T_{max} is expressed as N/mm and is used to describe the resistance of an aortic specimen against rupture. In contrast to wall strength, failure tension T_{max} can be calculated independent from the wall thickness (expressed as the cross-sectional specimen area A_0). This is particularly important for clinical practice and applicability, as wall thickness cannot be obtained from routine CT or MRI imaging and failure tension can be calculated without wall thickness estimations.

2.6. Protein kinase phosphorylation array

Mechano-biological interactions were evaluated based on the activation profiles of potentially involved mechanotransduction pathways. Mechanical stimuli are associated with the activation of several MAP kinases and SMAD pathways, which are further connected to the central TGF-β signaling. To gain a broad overview of the phosphorylation levels of a variety of kinases, a membrane-based sandwich immunoassay (Proteome Profiler Human Phospho-Kinase Array Kit, R&D Systems, Minneapolis, MN, USA) was used. This array provided a simultaneous detection of the phosphorylation levels from different kinases and reference proteins (Table 2) and a thus a profiling of potentially involved kinases and a comparison between AAA groups and controls. Representative samples from all groups (n=4 rAAA, n=4 eAAA, n=3 healthy aortas) were selected based on tissue quality, sufficient previously measured protein concentration (see 2.2.1.) and the remaining amounts of tissue.

CREB	Akt 1/2/3_T308
EGF R	Akt 1/2/3_S473
eNOS	Chk-2
ERK1/2	c-Jun
Fgr	p53_S15
GSK-3a/b	p53_S46
GSK-3b	p53_S392
HSP27	p70 S6 Kinase_T389
JNK1/2/3	p70 S6 Kinase_T421/S424
Lck	PRAS40
Lyn	PYK2
MSK1/2	RSK1/2
p38a	RSK1/2/3
PDGF Rb	STAT1
PLC-y1	STAT3_Y705
Src	STAT3_S727
STAT2	STAT6
STAT5a/b	Beta-Catenin (reference protein)
WNK1	HSP60 (reference protein)
Yes	

Table 2: Membrane-based sandwich immunoassay. Measured kinases and reference proteins. Phosphorylation sites are given after the underscore.

Following determination of the sample protein concentration, 500 µg of each sample lysate were diluted with the provided array buffer (Proteome Profiler Human Phospho-Kinase Array

Kit, R&D Systems, Minneapolis, MN, USA) to an initial volume of 2000 µl. Capture antibodies for the respective kinases and for two reference proteins were pre-spotted in duplicate onto nitrocellulose membranes, divided in two corresponding membrane parts (part A + part B) for each sample. In an initial blocking step, each membrane part was incubated with the provided array buffer for 1h on a rocking platform (VXR basic Vibrax shaker with VX7 attachment, IKA, Staufen im Breisgau, Germany). The diluted sample lysates were added to the membrane parts (1000 µl to part A and 1000 µl to part B) and were incubated overnight at 4 degrees on a rocking platform. Following a washing step with the provided wash buffer, detection antibody cocktail for membrane parts A and B were added and the membranes were incubated for 2h on a rocking platform. After another washing step, 1000 µl infrared-dye labeled streptavidin (IRDye 800CW Streptavidin, LI-COR Biosciences, Lincoln, NE, USA) was added to each membrane part and was incubated for 30min on a rocking platform. The membranes were washed again and 1000µl detection mixture (hydrogen peroxide and luminol) were applied to each membrane set for signal detection. The fluorescent signal corresponds to the amount of phosphorylated protein at each spot and was subsequently detected using a digital imager (Azure c600, Azure Biosystems, Dublin, CA, USA) and an exposure time of 2min. Representative membrane images are shown below (Fig. 8).

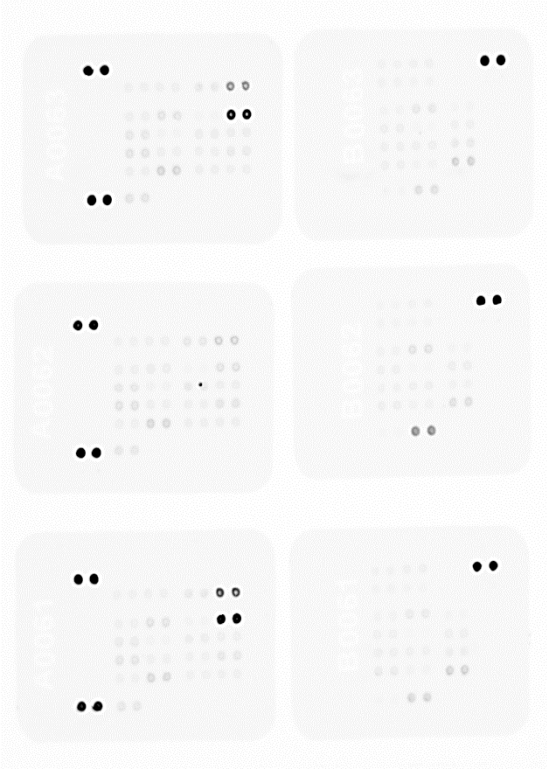

Figure 8: Representative membrane images of the sandwich immunoassay. Corresponding membrane parts (part A: left column; part B: right column) of a healthy control (upper row), eAAA (middle row) and rAAA (lower row) sample. Exposure time 2min. Reference spots (two pairs on the left edge of part A membranes; one pair on the right edge of part B membranes) were used to align the membranes with the template overlay and as a positive control for streptavidin incubation.

The location of positive signals was identified using the provided template overlay and aligning the corresponding reference spots on each membrane. For image analysis, the pixel densities of each pair of spots (representing each kinase) were determined using the Fiji software [37] and were averaged. Background signal (determined from unstained areas of the membrane) was subtracted from the averaged spots and the values were normalized to the given reference proteins on each membrane part. To evaluate the relative activation levels of AAA samples, eAAA and rAAA values were further normalized to those of the healthy controls.

2.7. Statistical analyses

All statistical analyses have been performed with the GraphPad Prism software (Version 8.4.2 for Windows, GraphPad Software, San Diego, CA, USA) and all graphs have been created with the same software. Normality testing (using the D'Agostino-Pearson, Anderson-Darling and Shapiro-Wilk test) has been applied to the data sets to evaluate if a normal (Gaussian) distribution can be assumed. As the data sets deviated from a normal distribution in all three tests in almost all cases, a non-normal distribution was assumed and the respective nonparametric tests have been applied. Possible outliers within the data sets have been detected using the respective calculation tool (ROUT method, Q = 0.1%, GraphPad Prism software) and were checked for possible reasons (measurement errors, bad sample quality etc.) in the raw data sets. If applicable, outliers have been excluded manually.

Patient clinical data (comorbidities, previous diseases and medication) were tested for independence from AAA groups using the Fisher's exact test. Data from protein analysis (ELISA), gene expression analysis, histological scoring, mechanical testing and phosphorylation data were analyzed based on group comparison (rAAA vs. eAAA, rAAA vs. Ctrl, eAAA vs. Ctrl). The nonparametric Mann-Whitney test was used (comparison of unpaired groups). For correlation analysis of all biological and mechanical data, the nonparametric Spearman correlation was applied (correlation coefficient r; P value). All tests were performed two-sided and a P value of ≤ 0.05 was regarded as statistically significant.

3. Results

3.1. Patient characteristics

3.1.1. Demographic and clinical data*

The study cohorts were characterized regarding patient demographic and clinical data, based on the routinely collected patient records. For the demographic evaluation, patient age and sex were recorded. Patient clinical data included the initial AAA diameter (maximum measured value prior to surgery, measured via CT imaging), relevant comorbidities and previous diseases (chronic kidney disease, hypertension, diabetes, coronary heart disease, smoking status, peripheral artery disease and hyperlipidemia) as well as current medication (aspirin/clopidogrel, beta-blockers, statins, ACE inhibitors, diuretics, antihypertensives and antidiabetics). Table 3 and 4 give an overview of patient demographic and clinical data.[38]

* The results in this section are included in the manuscript: Metschl, S., et al., *Changes in Endocan and Dermatan Sulfate Are Associated with Biomechanical Properties of Abdominal Aortic Wall during Aneurysm Expansion and Rupture*. Thromb Haemost, 2022. 122(9): p. 1513-1523. The underlying data in this section were partly used in the manuscript: Reutersberg, B., et al., *CXCR4 - a possible serum marker for risk stratification of abdominal aortic aneurysms.* Vasa, 2022. Epub ahead of print.

AAA patients (total n=107)	
Sex (male)	94
Age (y)	69.1 +/- 8.7
Max AAA diameter (mm)	67.2 +/- 19.1
Ruptured AAA (n=29)	
Sex (male)	27
Age (y)	72.3 +/- 10.5
Max AAA diameter (mm)	83.9 +/- 20.2
Elective AAA (n=78)	
Sex (male)	67
Age (y)	67.9 +/- 10.4
Max AAA diameter (mm)	61.4 +/- 19.5

Table 3: Patient demographic data and AAA diameter by groups. Patient sex (n male patients of total n), age (years) and maximum measured AAA diameter (mm, measured via CT imaging). Values given as mean with standard deviation.

N=94 of all AAA patients were male, the mean age was 69.1 (+/- 8.7) years and the mean AAA diameter was 67.2 (+/- 19.1) mm. Among the rAAA patients, n=27 were male and the mean age was 72.3 (+/- 10.5) years. The mean diameter was 83.9 (+/- 20.2) mm. In the eAAA group, n=67 patients were male and the mean age was 67.9 (+/- 10.4) years. The mean diameter was 61.4 (+/- 19.5) mm (Table 3).[38]

Control patients (healthy kidney donors, n=8) are not included in Table 3. In accordance with the respective data protection guidelines for kidney donors, only demographic data could be obtained from these individuals. N=5 of the kidney donors were male and the mean age was 65.3 (+/- 6.1) years. No initial aortic diameter was available from these individuals as they did not undergo routine CT imaging.

Comorbidities (n / % of patients)		p-value
Chronic kidney disease	29 / 27.1%	0,003
Hypertension	79 / 73.8%	1,000
Diabetes mellitus	11 / 10.3%	1,008
Coronary heart disease	35 / 32.7%	0,643
Smoking	65 / 60.7%	0,819
Peripheral artery disease	13 / 12.1%	1,000
Hyperlipidemia	53 / 49.5%	0,509
Medication (n / % of patients)		**p-value**
Aspirin/Clopidogrel	61 / 57.0%	0,792
Beta-blocker	47 / 43.9%	0,615
Statins	54 / 50.5%	0,296
ACE inhibitors	38 / 35.5%	0,609
Diuretics	33 / 30.8%	0,295
Antihypertensives	65 / 60.7%	0,151
Antidiabetics	5 / 4.7%	0,580

Table 4: Patient comorbidities, previous diseases and medication. Numbers of patients with the respective condition or medication and percentage of all patients are given. P-values were calculated to test for independence of condition or medication from the AAA groups using the Fisher's exact test. ACE = Angiotensin converting enzyme.

The proportion of patients with the respective disease condition or medication was calculated (Table 4).[38] Patients were excluded when clinical data were missing. The most prevalent disease conditions were hypertension (73.8%) and a history of smoking (60.7%), reflecting common risk factors of AAA disease. Accordingly, the most common medication were antihypertensive drugs (60.7%) followed by anticoagulants (aspirin/clopidogrel, 57.0%).

The Fisher's exact test was used to test for independence of variables and to evaluate if the respective condition or medication was different depending on the AAA group. All conditions or medications were independent from the AAA status except from chronic kidney disease ($p = 0.003$). 48.3% of all rAAA patients (n=14) and 19.2% of all eAAA patients (n=15) had chronic kidney disease.

3.1.2. Blood parameters*

Hematological parameters from routine blood collection (prior to surgery) were obtained from the Department of Clinical Chemistry at Klinikum rechts der Isar (TU Munich) and were recorded for further characterization. Blood parameters from both AAA groups were compared and the results are shown as box plots (middle line representing the median; whiskers representing the 5 and 95 percentile) (Fig. 9-10).

HsCRP (normal reference range < 5 mg/l), representing both the inflammatory status and the atherosclerotic risk, was elevated in rAAA patients compared to eAAA ($p = 0.001$). The median of both groups was within the reference range (0.6 mg/l for eAAA, 1.6 mg/l for rAAA). The blood levels of creatinine (reference range 0.7-1.3 mg/dl) and urea (reference range 7-18 mg/dl) were elevated in rAAA patients ($p = 0.002$ and $p = 0.0004$, respectively) while the estimated GFR (reference range > 90 ml/min) was lower in rAAA patients ($p = 0.008$). The median of creatinine was within the reference range (1.0 mg/dl for eAAA, 1.3 mg/dl for rAAA) while the median urea of rAAA patients was above the normal range (17.0 mg/dl for eAAA, 21.0 mg/dl for rAAA). The median estimated GFR was below the normal range in both AAA groups (74.9 ml/min for eAAA, 53.8 ml/min for rAAA). The results are shown in Figure 9.

* The underlying data in this section were partly used in the manuscript: Reutersberg, B., et al., *CXCR4 - a possible serum marker for risk stratification of abdominal aortic aneurysms.* Vasa, 2022. Epub ahead of print.

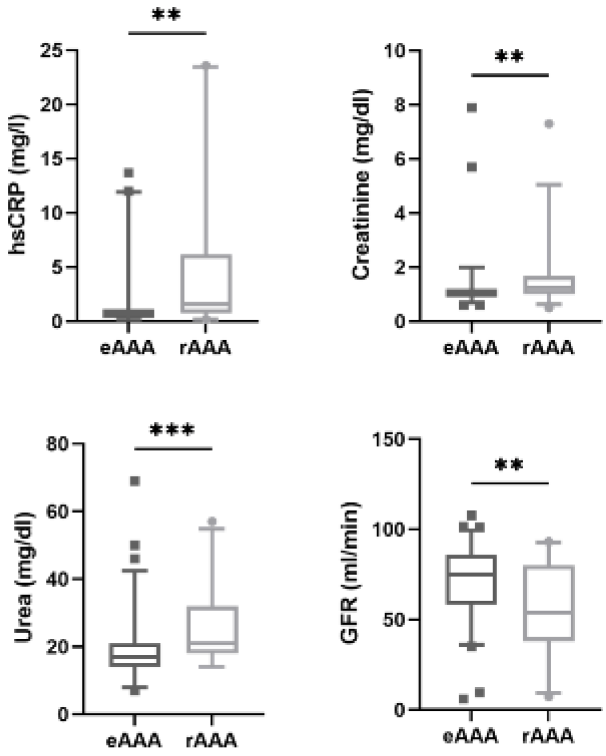

Figure 9: Routine blood parameters in eAAA and rAAA patients. Upper row: high-sensitivity C-reactive protein (hsCRP) and creatinine; lower row: urea and estimated glomerular filtration rate (GFR). $p \leq 0.05$ summarized as *, $p \leq 0.01$ summarized as **, $p \leq 0.001$ summarized as ***, $p \leq 0.0001$ summarized as ****.

Both erythrocytes (reference range 4-6 Mio/µl) and hemoglobin (reference range 14-18 g/dl) were decreased in rAAA patients ($p < 0.0001$ and $p < 0.0001$, respectively). The median erythrocyte count of rAAA patients was just below the normal range (4.6 Mio/µl for eAAA, 3.5 Mio/µl for rAAA) and also the median hemoglobin was below the reference range (14.2 g/dl for eAAA, 10.9 g/dl for rAAA). The number of thrombocytes (reference range 150-450 x 10^3/µl) was not different in eAAA and rAAA patients while the leucocyte count (reference range 4-9 x 10^9/l) was higher in rAAA patients ($p < 0.0001$). Median levels of thrombocytes were within the normal range for both groups (212.0 x 10^3/µl for eAAA, 189.0 x 10^3/µl for rAAA). In contrast to that, the median leucocyte count of rAAA patients was clearly above the normal range (7.7 x 10^9/l for eAAA, 14.0 x 10^9/l for rAAA). The results are summarized in Figure 10.

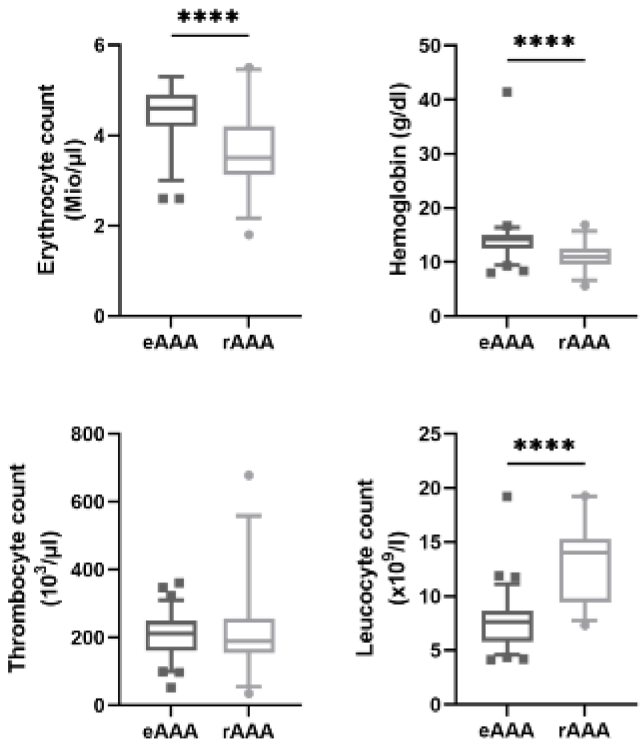

Figure 10: Routine blood parameters in eAAA and rAAA patients. Upper row: erythrocyte count and hemoglobin; lower row: thrombocyte and leucocyte count. $p \leq 0.05$ summarized as *, $p \leq 0.01$ summarized as **, $p \leq 0.001$ summarized as ***, $p \leq 0.0001$ summarized as ****.

3.2. ELISA

3.2.1. Total protein amounts in aortic tissue

Quantitative protein analysis via ELISA was used to determine the amounts of structural proteins, proteoglycans and inflammatory factors in tissue specimens. In a first step, the abundance of load-bearing structures (structural proteins and proteoglycans) was compared between healthy and diseased tissue. Structural proteins and proteoglycans from all AAA samples (eAAA and rAAA samples taken together) were compared with those from healthy tissue to get an overview of the structural composition and changes within the aortic wall during AAA development. The results are shown as median values in AAA and healthy tissue (Fig. 11).

The total amounts of hydroxyproline (as the main component of fibrillary collagen) as well as Col1 and Col3 were higher in AAA tissue compared to healthy aortic tissue (median amounts in AAA tissue: 39.1 ng/ml, 106.3 ng/ml and 11.7 ng/ml, respectively; median amounts in healthy tissue: 9.5 ng/ml, 32.2 ng/ml and 3.7 ng/ml, respectively). The overall ratio of Col1 being more prevalent than Col3, however, did not change. Regarding proteoglycans, the amounts of CS and DS were both higher in AAA tissue compared to healthy tissue (median amounts in AAA tissue: 113 ng/ml and 383.5 ng/ml, respectively; median amounts in healthy tissue: 89.7 ng/ml and 7.28 ng/ml, respectively). While CS was the most abundant subgroup in healthy tissue, DS was more prevalent in diseased tissue. The amounts of HS and endocan were much lower compared to the other proteins and proteoglycans but were also increased in AAA compared to healthy tissue (median amounts in AAA tissue: 0.63 ng/ml and 0.72 ng/ml, respectively; median amounts in healthy tissue: 0.57 ng/ml and 0.58 ng/ml, respectively). All results are shown in Figure 11.

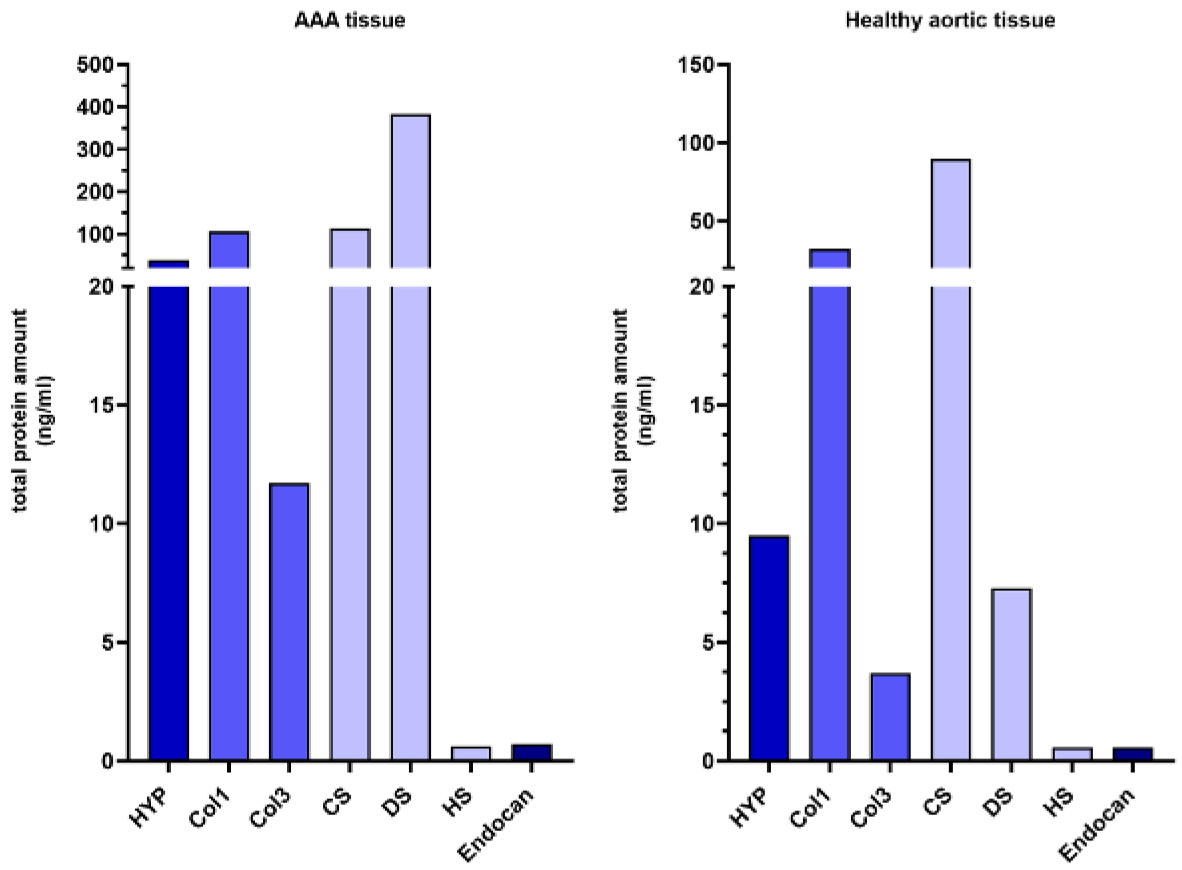

Figure 11: Total protein amounts in AAA and healthy aortic tissue. Hydroxyproline (HYP), collagen type I/III (Col1/Col3), chondroitin/dermatan/heparan sulfate (CS/DS/HS) and endocan.

It must be noted that the total amounts of GAG chains should also be determined via ELISA. However, GAG chains could be detected in none of the samples with the assay used in this study (null values for all samples; data not shown). It remains unclear whether the respective kits were defective or GAG chains were not measurable in the sample material. Total GAG chains are therefore not included in all following data (tissue and serum measurements) and the focus was placed on proteoglycan subgroups.

3.2.2. Total protein amounts in serum

Quantitative protein analysis was also used to determine the respective amounts of load-bearing structures (structural proteins and proteoglycans) in healthy versus diseased serum samples. The amounts from all AAA serum samples (eAAA and rAAA samples taken together) were compared to healthy serum samples to evaluate to what extent these proteins and proteoglycans are detectable in the patient's serum and if their composition changes along with disease progression. The results are shown as median values in AAA and healthy serum samples (Fig. 12).

The amount of hydroxyproline was slightly increased in AAA serum compared to healthy controls (median amount in AAA serum: 43.5 ng/ml; median amount in healthy serum: 48.6 ng/ml). Both types of collagen (Col1 and Col3) showed higher amounts in AAA serum (median amounts in AAA serum: 324.5 ng/ml and 0.68 ng/ml, respectively; median amounts in healthy serum: 86.2 ng/ml and 0.45 ng/ml, respectively). Similar to tissue, Col1 was much more prevalent than Col3 in both healthy and diseased serum. The amount of CS remained stable in AAA compared to healthy serum, while DS amounts decreased and HS amounts also remained constant (median amounts in AAA serum: 1.0 ng/ml, 10.9 ng/ml and 2.5 ng/ml, respectively; median amounts in healthy serum: 1.0 ng/ml, 27.1 ng/ml and 2.4 ng/ml, respectively). DS was the most prevalent proteoglycan subgroup in both AAA and healthy serum while the other groups showed markedly lower amounts. Endocan amounts were considerably lower compared to all other components but were also increased in serum of AAA patients (median amount in AAA serum: 0.06 ng/ml; median amount in healthy serum: 0.01 ng/ml). The results are presented in Figure 12.

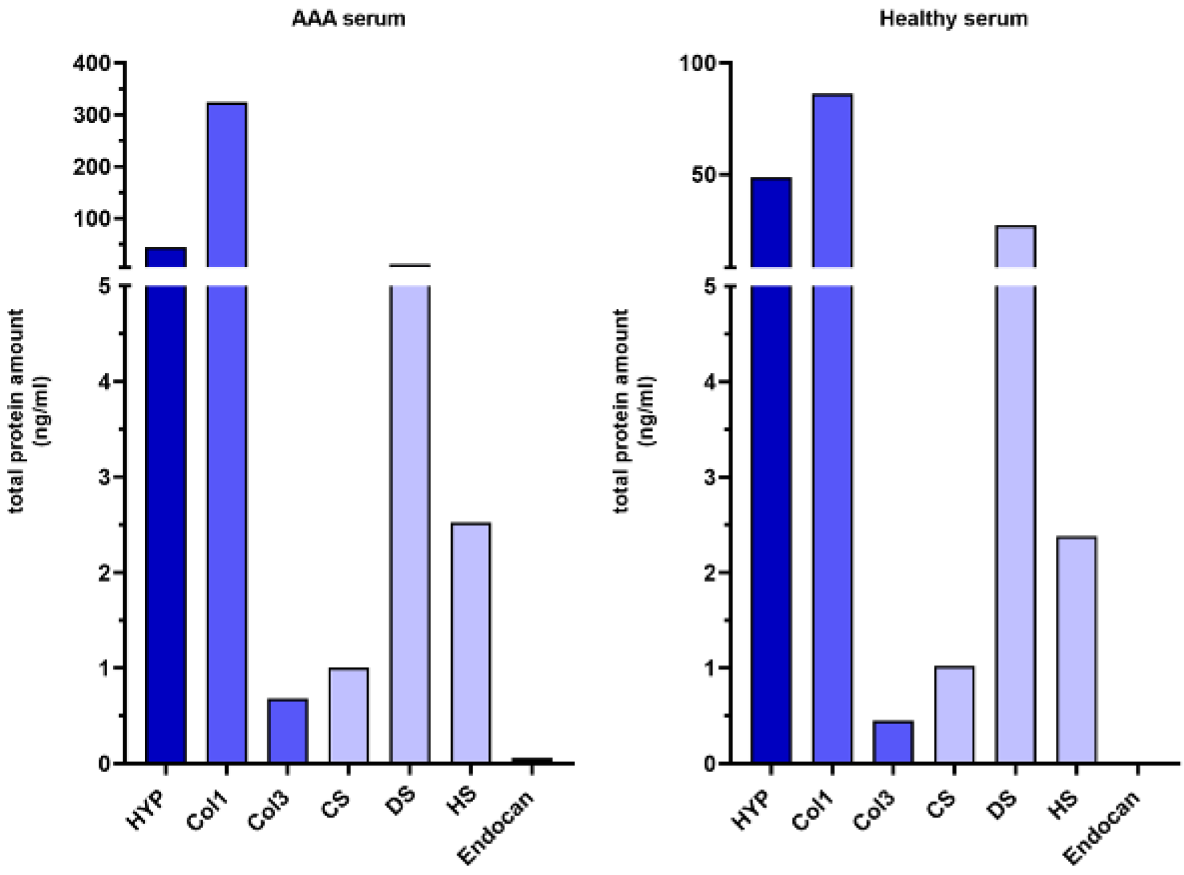

Figure 12: Total protein amounts in AAA and healthy serum. Hydroxyproline (HYP), collagen type I/III (Col1/Col3), chondroitin/dermatan/heparan sulfate (CS/DS/HS) and endocan.

3.2.3. Protein amounts in aortic tissue of AAA subcohorts*

In the next step, protein amounts in the AAA subcohorts were examined. The amounts in unruptured, electively excised AAA tissue (eAAAs) were compared to those in ruptured AAA tissue (rAAAs) and both groups were compared to healthy controls. Changes during AAA development can be evaluated by comparing the less advanced, stable eAAAs with already ruptured rAAAs. Mann-Whitney tests were used to determine differences between eAAA,

* The results in this section are included in the manuscript: Metschl, S., et al., *Changes in Endocan and Dermatan Sulfate Are Associated with Biomechanical Properties of Abdominal Aortic Wall during Aneurysm Expansion and Rupture*. Thromb Haemost, 2022. 122(9): p. 1513-1523. The underlying data in this section were partly used in the manuscript: Reutersberg, B., et al., *CXCR4 - a possible serum marker for risk stratification of abdominal aortic aneurysms.* Vasa, 2022. Epub ahead of print.

rAAA and control groups and the results are presented as box plots (middle line representing the median; whiskers representing the 5 and 95 percentile) (Fig. 13-15).

The amounts of inflammatory factors did not show significant differences between the groups. CXCR4 amounts were on a similar level in AAA and control tissue, while its ligand CXCL12 displayed a trend towards decrease in both AAA groups compared to controls (Fig. 13).

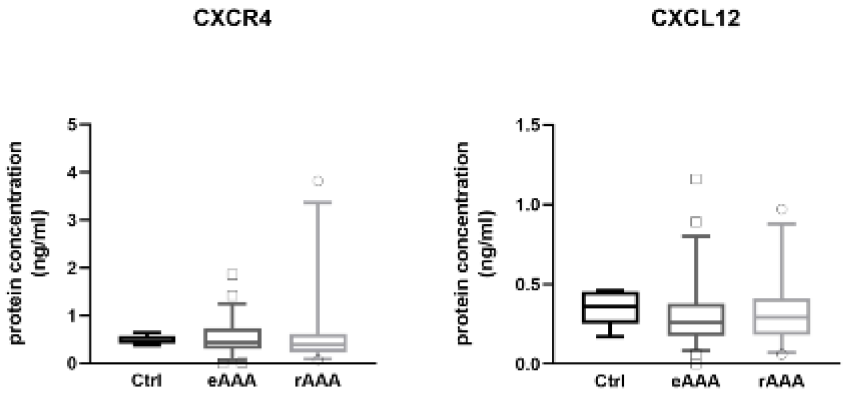

Figure 13: Protein amounts in eAAA, rAAA and control (Ctrl) tissue. $p \leq 0.05$ summarized as *, $p \leq 0.01$ summarized as **, $p \leq 0.001$ summarized as ***, $p \leq 0.0001$ summarized as ****.

Hydroxyproline amounts were increased in eAAA and rAAA samples compared to controls ($p < 0.0001$ and $p < 0.0001$, respectively) and were further increased in rAAA compared to eAAA samples ($p = 0.002$). Col1 amounts were higher in eAAA and rAAA tissue compared to controls ($p = 0.0001$ and $p = 0.003$, respectively). Col3 amounts were elevated in eAAA samples ($p = 0.016$). The results are presented in Figure 14.[38]

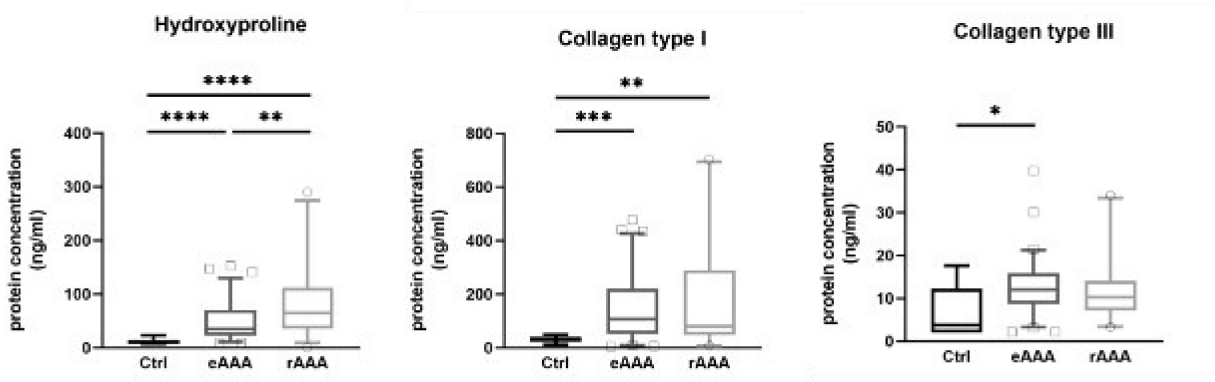

Figure 14: Protein amounts in eAAA, rAAA and control (Ctrl) tissue. $p \leq 0.05$ summarized as *, $p \leq 0.01$ summarized as **, $p \leq 0.001$ summarized as ***, $p \leq 0.0001$ summarized as ****.

Regarding proteoglycan components, CS was increased in both eAAA and rAAA samples compared to controls ($p = 0.002$ and $p = 0.004$, respectively) and was also increased in rAAA compared to eAAA ($p = 0.020$). DS amounts were also elevated in eAAA and rAAA tissue compared to controls ($p = 0.011$ and $p < 0.0001$, respectively) and were higher in rAAA compared to eAAA ($p < 0.0001$). The amounts of HS showed no significant differences between the groups. Endocan levels were increased in rAAA tissue compared to controls ($p = 0.014$) and eAAA tissue ($p = 0.0003$) (Fig. 15).[38]

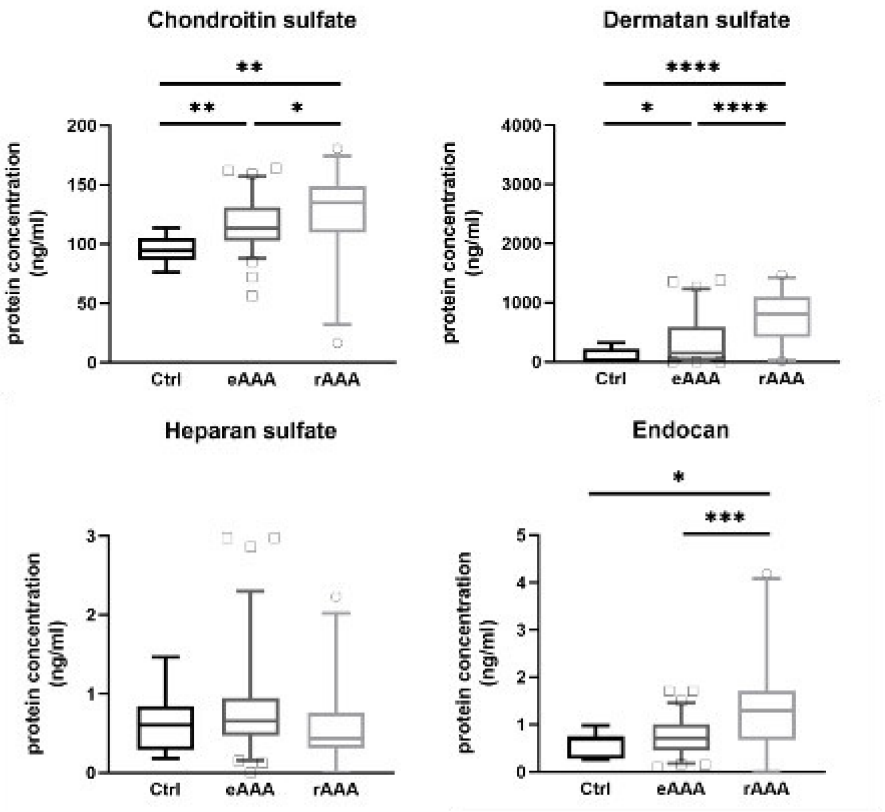

Figure 15: Protein amounts in eAAA, rAAA and control (Ctrl) tissue. $p \leq 0.05$ summarized as *, $p \leq 0.01$ summarized as **, $p \leq 0.001$ summarized as ***, $p \leq 0.0001$ summarized as ****.

3.2.4. Protein amounts in serum of AAA subcohorts*

Protein amounts in the eAAA and rAAA subcohorts were also examined in serum samples. As for tissue amounts, serum amounts were compared between eAAA, rAAA and controls in order to analyze changes with disease progression. Mann-Whitney tests were used to determine differences between the groups and the results are presented as box plots (middle line representing the median; whiskers representing the 5 and 95 percentile) (Fig. 16-18).

* The results in this section are included in the manuscript: Metschl, S., et al., *Changes in Endocan and Dermatan Sulfate Are Associated with Biomechanical Properties of Abdominal Aortic Wall during Aneurysm Expansion and Rupture*. Thromb Haemost, 2022. 122(9): p. 1513-1523. The underlying data in this section were partly used in the manuscript: Reutersberg, B., et al., *CXCR4 - a possible serum marker for risk stratification of abdominal aortic aneurysms.* Vasa, 2022. Epub ahead of print.

CXCR4 amounts were elevated in rAAA serum compared to eAAA (p = 0.003). CXCL12 was increased in both eAAA and rAAA compared to healthy serum (p = 0.036 and p = 0.047, respectively) (Fig. 16).

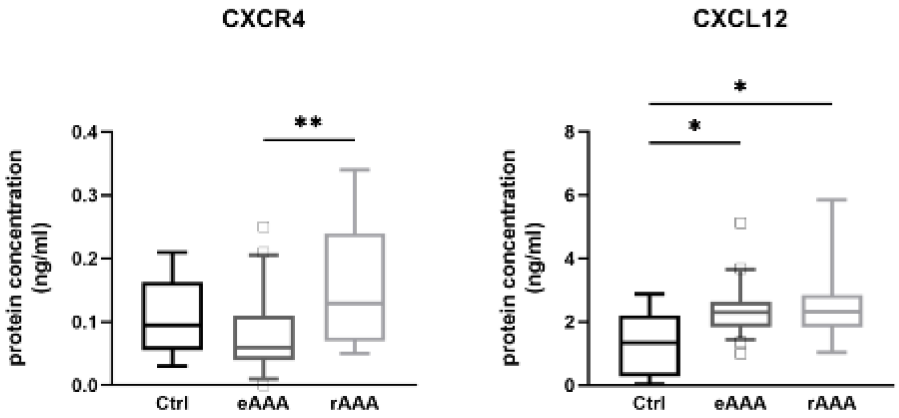

Figure 16: Protein amounts in eAAA, rAAA and control (Ctrl) serum. p ≤ 0.05 summarized as *, p ≤ 0.01 summarized as **, p ≤ 0.001 summarized as ***, p ≤ 0.0001 summarized as ****.

Hydroxyproline amounts in serum showed no significant changes between the groups. Col1 amounts showed a strong increase in both eAAA and rAAA compared to controls (p = 0.009 and p = 0.0008, respectively), while rAAA amounts were much higher compared to eAAA (p < 0.0001). Col3 amounts also showed a trend towards increase with disease progression but did not reach statistical significance. The results are summarized in Figure 17.[38]

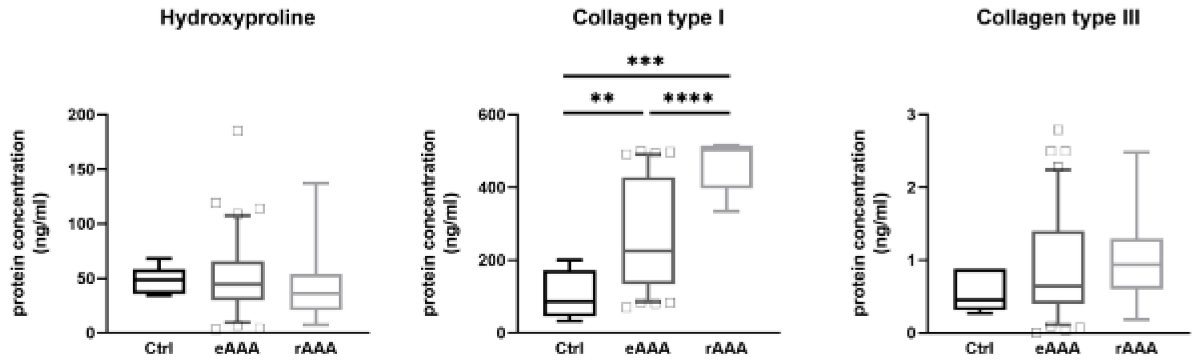

Figure 17: Protein amounts in eAAA, rAAA and control (Ctrl) serum. $p \leq 0.05$ summarized as *, $p \leq 0.01$ summarized as **, $p \leq 0.001$ summarized as ***, $p \leq 0.0001$ summarized as ****.

CS subgroup amounts did not change significantly between the groups. DS amounts showed a strong decrease in both eAAA and rAAA serum compared to controls ($p = 0.0008$ and $p = 0.042$, respectively). DS in rAAA samples was further decreased compared to eAAA ($p = 0.042$). The amounts of HS were on a similar level in all groups while endocan increased in eAAA and rAAA samples compared to controls ($p = 0.014$ and $p = 0.028$, respectively). Endocan was also

higher in rAAA serum compared to eAAA (p = 0.021). The results are presented in Figure 18.[38]

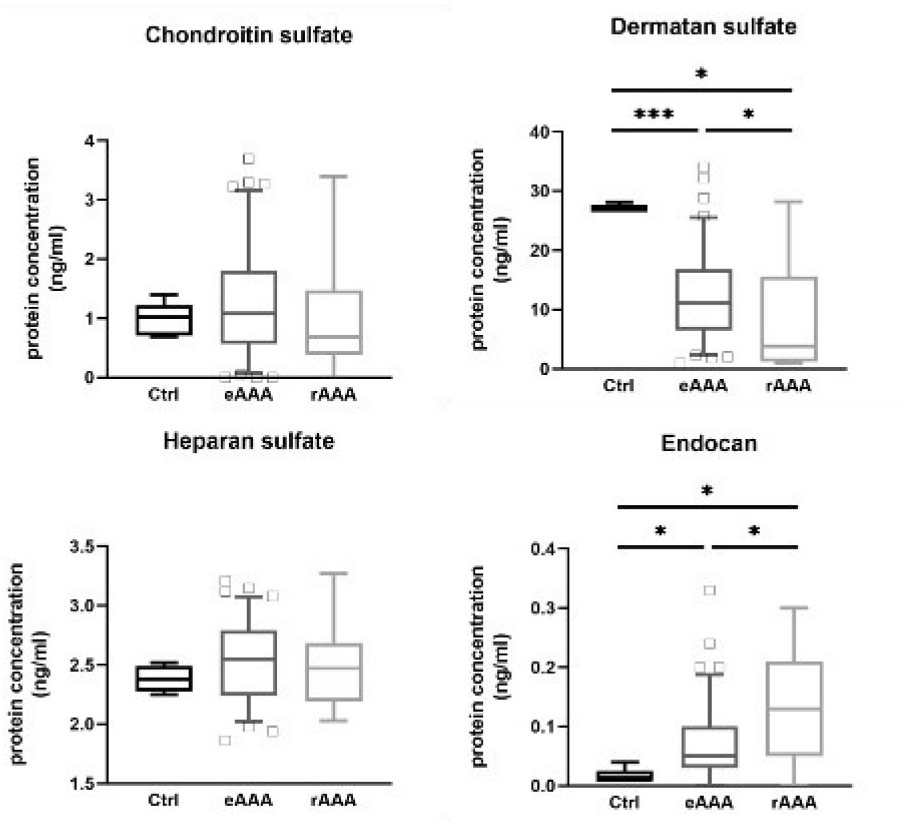

Figure 18: Protein amounts in eAAA, rAAA and control (Ctrl) serum. p ≤ 0.05 summarized as *, p ≤ 0.01 summarized as **, p ≤ 0.001 summarized as ***, p ≤ 0.0001 summarized as ****.

3.3. mRNA expression in aortic tissue

To compare mRNA expression between AAA groups and controls, expression results were calculated relative to control samples and are given as fold changes. The Mann-Whitney test was used to determine significant differences between the groups and the results are shown as box plots (middle line representing the median; whiskers representing the 5 and 95 percentile). A p-value ≤ 0.05 is marked by an asterisk (*) (Fig. 19-21).

The mRNA expression levels of both Col1A1 and Col3A1 were increased in AAA compared to controls but did not reach statistical significance. For both collagens, the expression levels in eAAA samples were higher than in rAAA samples. The expression levels of the two matrix metalloproteinases showed large differences: while the expression of MMP2 was decreased in AAA samples (with p = 0.017 for rAAA samples), the expression of MMP9 was increased in AAA samples (without, however, reaching statistical significance). The results are summarized in Figure 19.

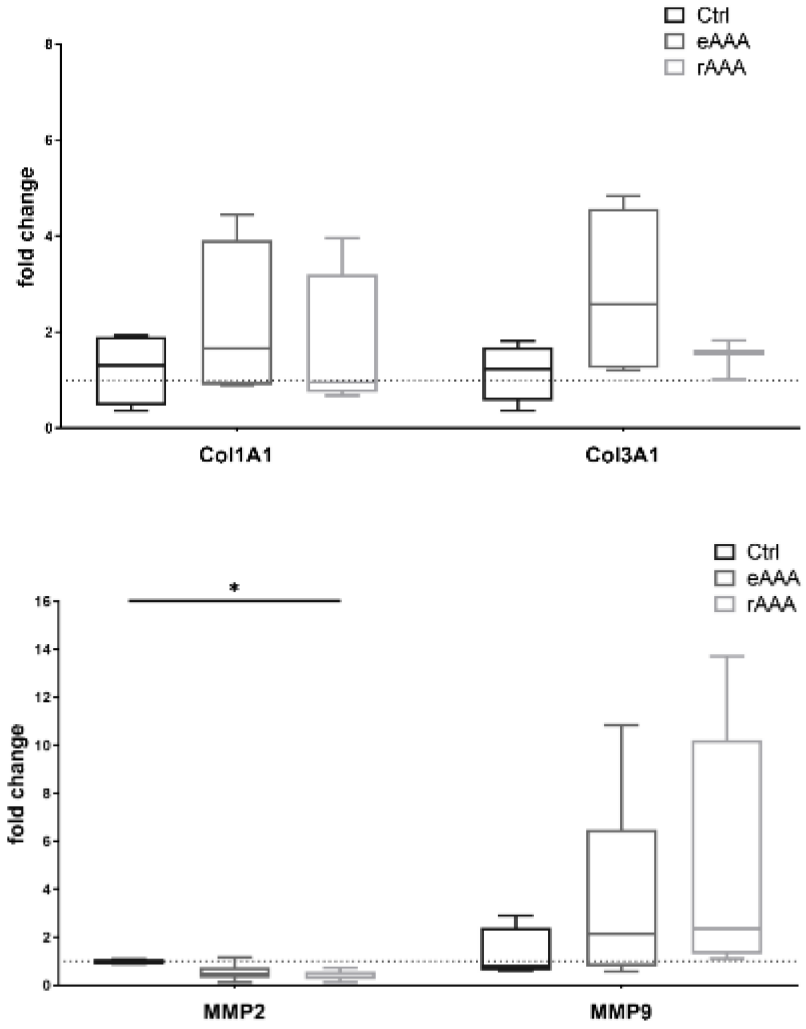

Figure 19: Relative mRNA expression of collagens and matrix metalloproteinases. Upper graph: Collagen type I and III (Col1A1 and Col3A1); lower graph: matrix metalloproteinases 2 and 9 (MMP2 and MMP9). $p \leq 0.05$ summarized as *.

Expression levels of the cytokine effector TGFB1 were increased in AAA samples and showed a significant upregulation for rAAA samples (p = 0.048). The expression of the second cytokine (TGFB2) showed a similar trend. However, due to the broad scattering of eAAA and control values, these results require a very cautious interpretation. The expression levels of the two corresponding TGF-ß receptors (TGFBR1 and TGFBR2) were decreased in AAA samples without reaching statistical significance. For both receptors, expression in rAAA samples was lower compared to eAAA samples. The results are shown in Figure 20.

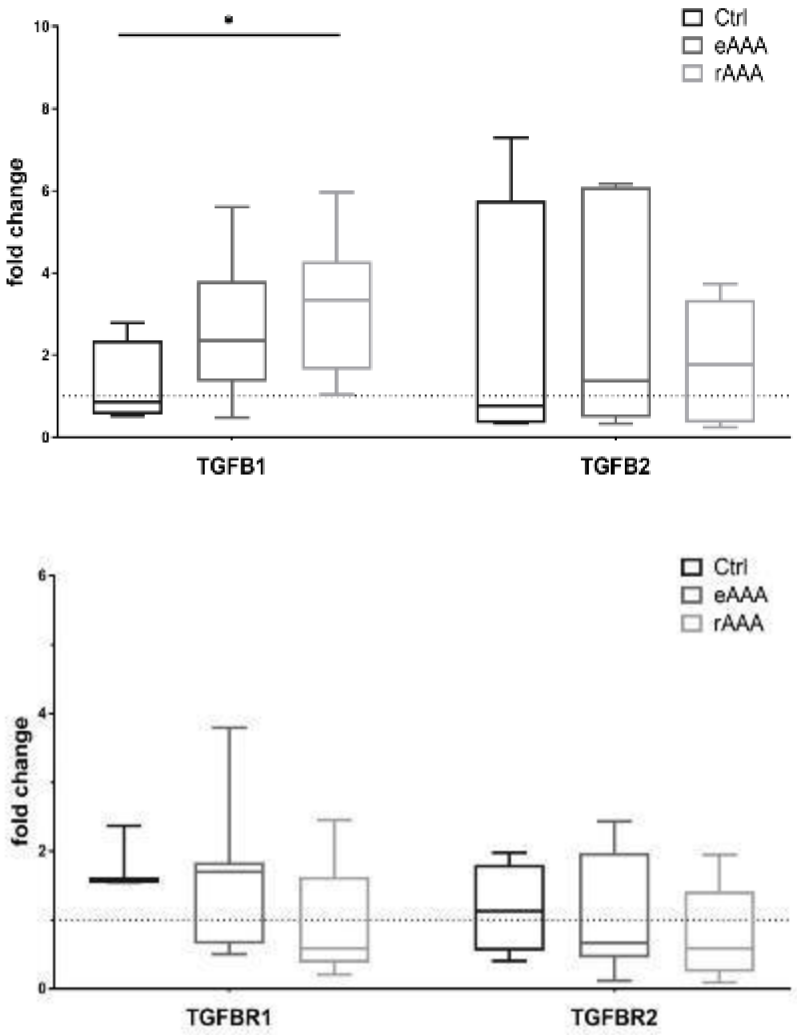

Figure 20: Relative mRNA expression of TGF-ß-related signaling molecules. Upper graph: effector cytokines transforming growth factor beta 1 and 2 (TGFB1 and TGFB2); lower graph: TGF-ß receptor type 1 and type 2 subunits (TGFBR1 and TGFBR2). p ≤ 0.05 summarized as *.

The mRNA expression of the downstream signaling proteins SMAD2, SMAD3 and SMAD4 showed three different patterns. The receptor-regulated SMAD2 reached lower expression levels in AAA groups compared to controls. The expression of the second receptor-regulated SMAD (SMAD3) was increased significantly in eAAA samples ($p = 0.014$) and was elevated also in rAAA samples. The common partner SMAD (Co-SMAD) SMAD4 was found to be expressed at the same level in AAA samples and controls. The results are shown in Figure 21.

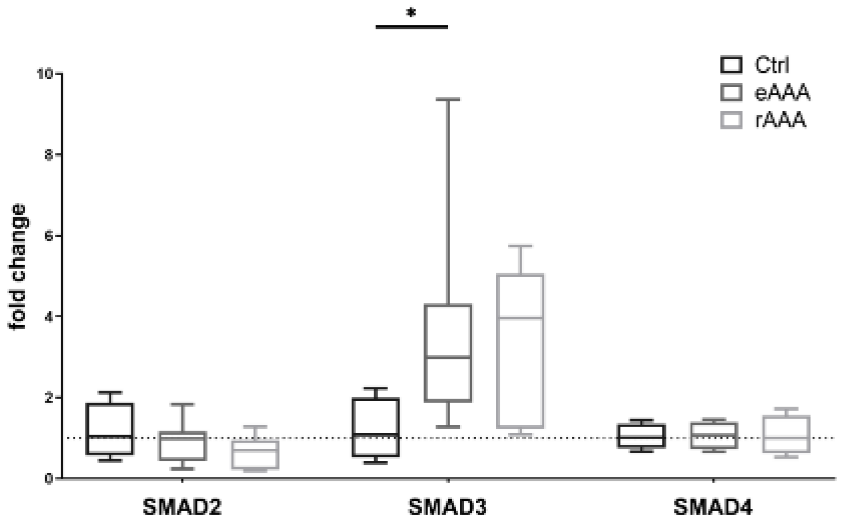

Figure 21: Relative mRNA expression of TGF-ß-related SMADs. Receptor-regulated SMADs (SMAD2 and SMAD3) and common partner SMAD (SMAD4). $p \leq 0.05$ summarized as *.

3.4. Histological evaluation of aortic tissue

3.4.1. Histological AAA morphology

3.4.1.1. HE and EvG staining*

Standard HE and EvG staining was used to evaluate the overall tissue morphology, focusing on the structural and cellular composition of the vessel wall as well inflammatory infiltration.

Both AAA groups showed typical characteristics of wall degeneration and inflammation compared to healthy aortic samples (Fig. 22 and Fig. 23).[38, 39] HE staining showed thickening of the intimal-medial layers and a disorganization of fibrous structures. While the fibers in healthy aortic samples showed a well-organized, parallel alignment without interruptions, the fiber structure in AAA samples appeared less aligned, irregular and interrupted by inflammatory infiltrates and hemorrhages. Inflammation was characterized by increased cellularity (purple-blue cell nuclei), increased occurrence of round-shaped inflammatory cells and neovessel formation. Atherosclerotic plaques were, among others, marked by the presence of foam cells, cholesterol crystals and calcified areas. These morphological characteristics were more advanced and more frequently observed in rAAA samples compared to eAAA (Fig. 22) [38, 39], reflecting progress of the AAA disease.

* The results in this section are included in the manuscripts: Metschl, S., et al., *Changes in Endocan and Dermatan Sulfate Are Associated with Biomechanical Properties of Abdominal Aortic Wall during Aneurysm Expansion and Rupture*. Thromb Haemost, 2022. 122(9): p. 1513-1523. and Reutersberg, B., et al., *CXCR4 - a possible serum marker for risk stratification of abdominal aortic aneurysms.* Vasa, 2022. Epub ahead of print.

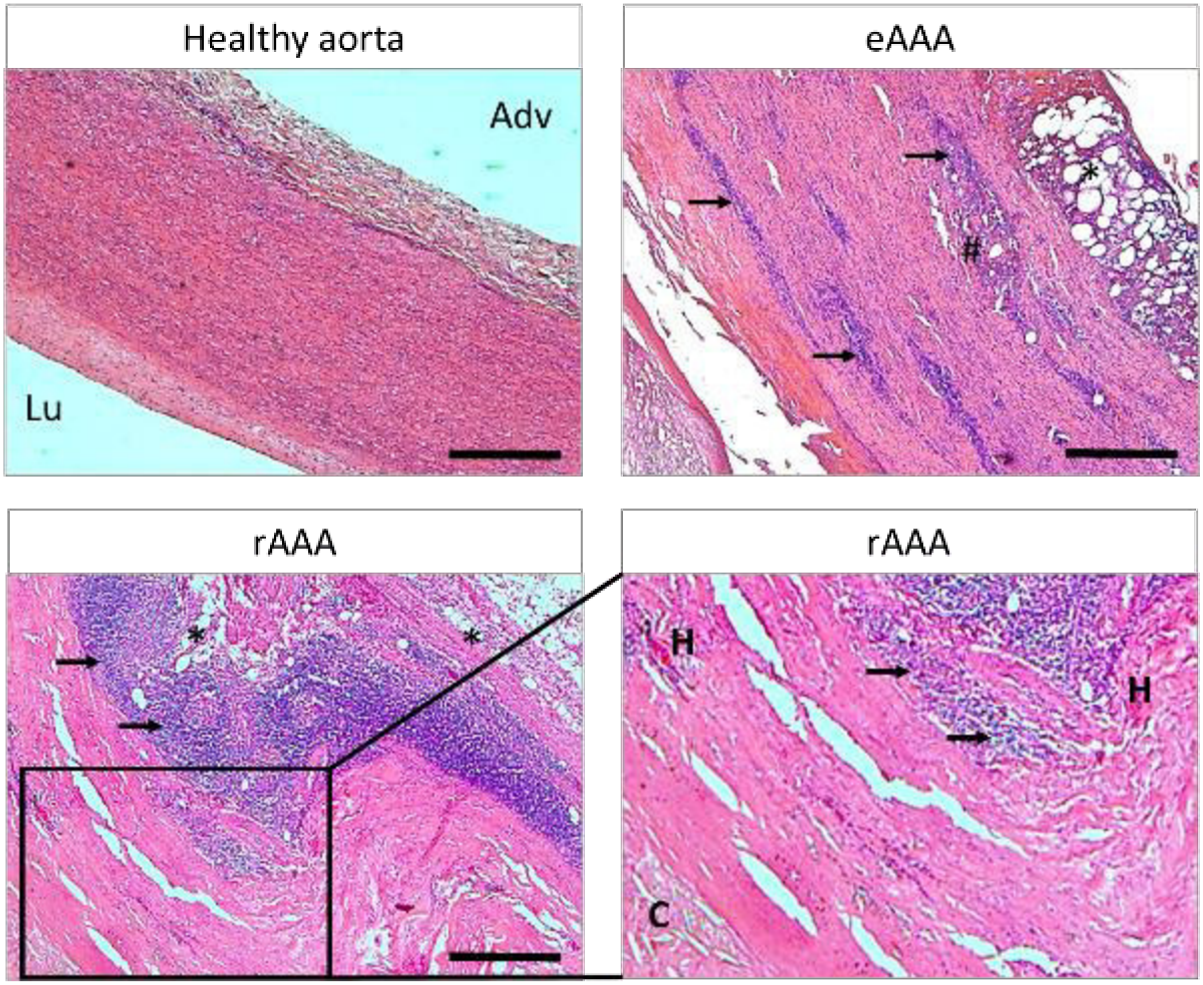

Figure 22: Representative HE staining of healthy, eAAA and rAAA samples. Healthy aorta: well-organized fiber structure with clear distinction of wall layers; eAAA: irregular structure with inflammatory infiltration; rAAA: disrupted vessel wall structure with advanced inflammatory infiltration; Lu = luminal side of the vessel wall, Adv = adventitial side of the vessel wall (same orientation in all images); inflammatory infiltrates marked by arrows (→), adipocytes marked by asterisk (*), neovessel formation marked by hash (#), cholesterol crystals marked by capital C, hemorrhage marked by capital H; scale bars representing 500 µm.

EvG staining confirmed a disorganized and interrupted fiber structure as well as rarefication of elastic fibers (dark blue to black) in AAA samples. Control samples showed a clear and regular alignment of both fibers, while especially the elastin fibers appeared disconnected and partly fragmented in the aneurysm samples. The amount of reddish collagen fibers, by contrast, appeared increased through the wall layers. Morphological characteristics were more pronounced in rAAA samples compared to eAAA (Fig. 23).[38]

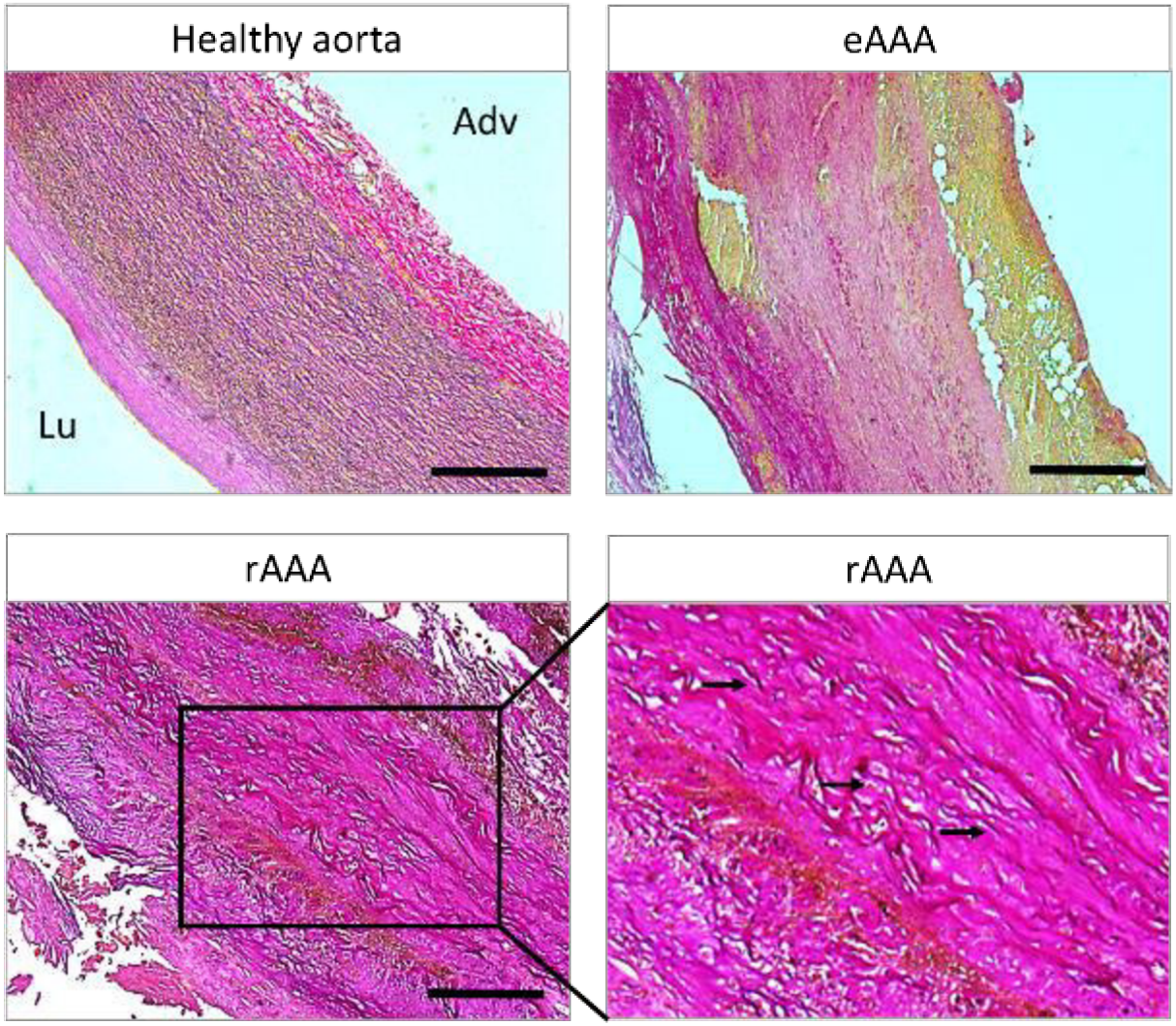

Figure 23: Representative EvG staining of healthy, eAAA and rAAA samples. Healthy aorta: regular alignment of collagen (reddish) and elastin (dark blue to black) fibers; eAAA: irregular structure with rarefication of elastin fibers; rAAA: fragmentation of elastin fibers and increased collagen content; Lu = luminal side of the vessel wall, Adv = adventitial side of the vessel wall (same orientation in all images); fragmented elastin fibers marked by arrows (→); scale bars representing 500 µm.

3.4.1.2. Alcian blue staining*

Alcian blue staining was used to evaluate the glycosaminoglycan content in relation to the vessel wall layers and overall vessel morphology. A high amount of glycosaminoglycans was found in both AAA and control samples while vascular degeneration and a disorganized fiber

* The results in this section are included in the manuscript: Metschl, S., et al., *Changes in Endocan and Dermatan Sulfate Are Associated with Biomechanical Properties of Abdominal Aortic Wall during Aneurysm Expansion and Rupture*. Thromb Haemost, 2022. 122(9): p. 1513-1523.

structure were typical characteristics of AAA samples. Increased cellularity in aneurysm samples was confirmed by increased occurrence of red cell nuclei. Healthy aortic samples showed a blue staining mainly in the medial layers, associated to both collagen and elastin fibers and in regular alignment. Glycosaminoglycans in AAA samples appeared to be more distributed over all layers, less aligned and less associated to the fibrous structures. Focal accumulations of intense blue staining ("hotspot" areas) were found more frequently in AAA samples and were advanced with disease progression (Fig. 24).[38]

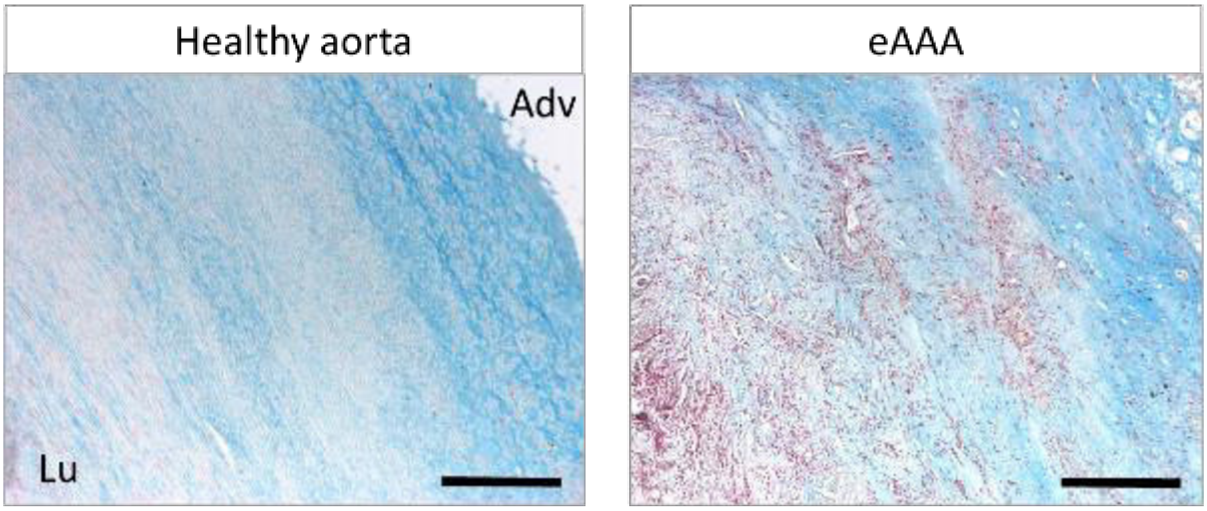

Figure 24: Representative alcian blue staining of healthy and eAAA samples. Healthy aorta: glycosaminoglycans (blue) associated to well-organized fibers; eAAA: disorganized fiber structure with glycosaminoglycan accumulations and increased cellularity (red); Lu = luminal side of the vessel wall, Adv = adventitial side of the vessel wall (same orientation in all images); scale bars representing 500 µm.

3.4.1.3. Immunohistochemical staining*

The abundance and localization of different immunohistochemical markers was evaluated for further characterization of the aortic samples. All immunohistochemical markers were stained mid- to dark-brown (Fig. 25-28).

* The results in this section are included in the manuscript: Reutersberg, B., et al., *CXCR4 - a possible serum marker for risk stratification of abdominal aortic aneurysms.* Vasa, 2022. Epub ahead of print.

SMA-positive cells (mainly VSMCs) are crucial for the vessel wall structure, as they synthesize ECM components and determine wall stability. Healthy aortic samples showed a high amount of closely packed SMA-positive cells through all layers of the vessel wall. A majority of cells exhibited the typical cobblestone-like shape. Decreased amounts of SMA-positive cells were found in AAA samples, with eAAA samples showing areas of higher SMA-density next to almost unstained areas. Ruptured samples, by contrast, were characterized by complete rarefication of VSMCs with only small areas of stained cells or individual positive cells remaining. Most of the SMA-positive cells in rAAA samples appeared to have a more longitudinal, spindle-like shape compared to those in healthy samples (Fig. 25).[39]

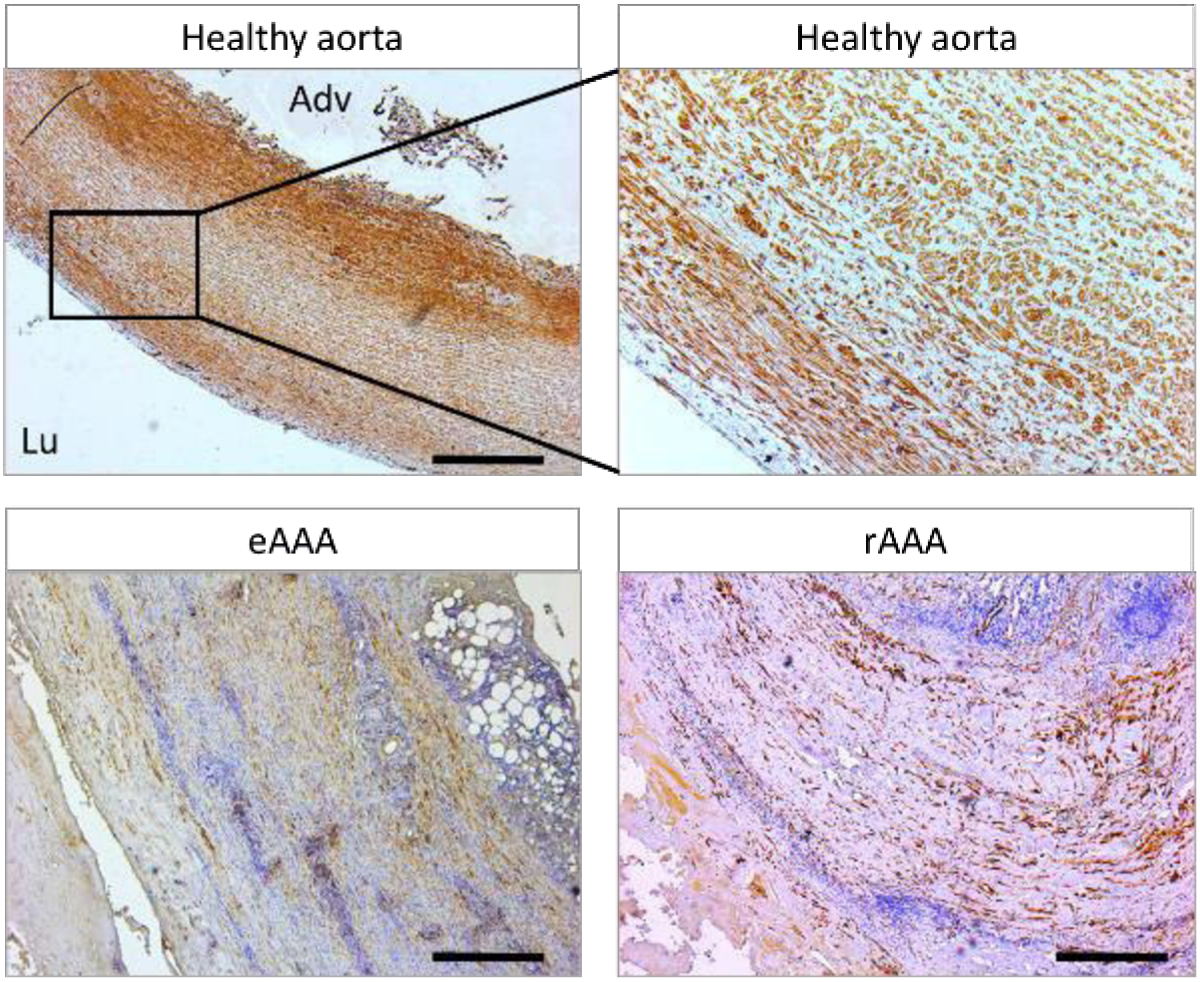

Figure 25: Representative SMA staining of healthy, eAAA and rAAA samples. Healthy aorta: dense, cobblestone-shaped SMA-positive cells (brown) in all vessel wall layers; eAAA: areas with varying SMA-density; rAAA: rarefication of SMA-positive cells; Lu = luminal side of the vessel wall, Adv = adventitial side of the vessel wall (same orientation in all images); scale bars representing 500 µm.

Inflammatory infiltration and the cellular context of inflammatory markers were evaluated via consecutive IHC staining. CD68-positive cells (representing a transmembrane protein expressed by macrophages and monocyte-lineage cells) as well as CD45-positive cells (representing the membrane-based leucocyte common antigen, described as pan-leucocyte marker for lymphoid cells) represent inflammatory processes within the aortic wall and are associated with degradation of ECM structures during AAA pathogenesis. Localization of CXCR4-positive cells was assessed in relation to these inflammatory cells and also in relation

to SMA-positive cells. CD68- as well as CD45-positive cells accumulated in areas of increased cellularity and were found in abundance in AAA samples. Ruptured samples showed more CD68- and CD45-positive cells and larger areas of accumulation than eAAA samples (Fig. 26 and Fig. 27).[39] CXCR4-positive cells co-localized strongly with CD45- and CD68-positive cells and were mainly observed in areas of inflammatory infiltration and neovessel formation. SMA-positive cells, by contrast, showed almost no co-localization with CXCR4-positive cells. CXCR4 was found mainly in the medial layers of AAA samples and in some cases also within the adventitia. The extent of CXCR4 staining was higher in rAAA compared to eAAA samples and positive cells were found in larger areas of the aortic wall (Fig. 26 and Fig. 27).[39]

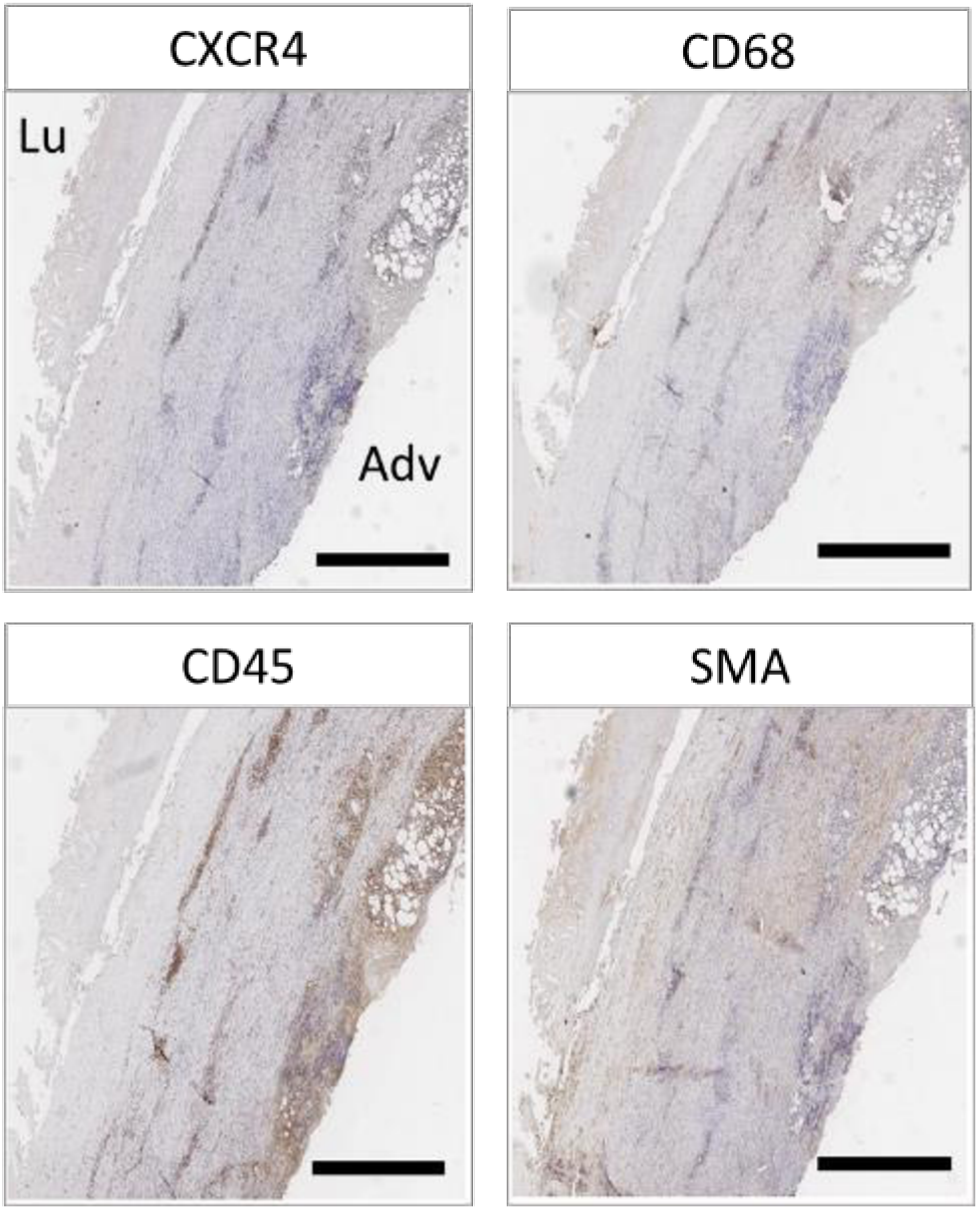

Figure 26: Representative consecutive IHC staining of an eAAA sample. Upper row: CXCR4 and CD68; lower row: CD45 and SMA; Lu = luminal side of the vessel wall, Adv = adventitial side of the vessel wall (same orientation in all images); scale bars representing 1000 µm.

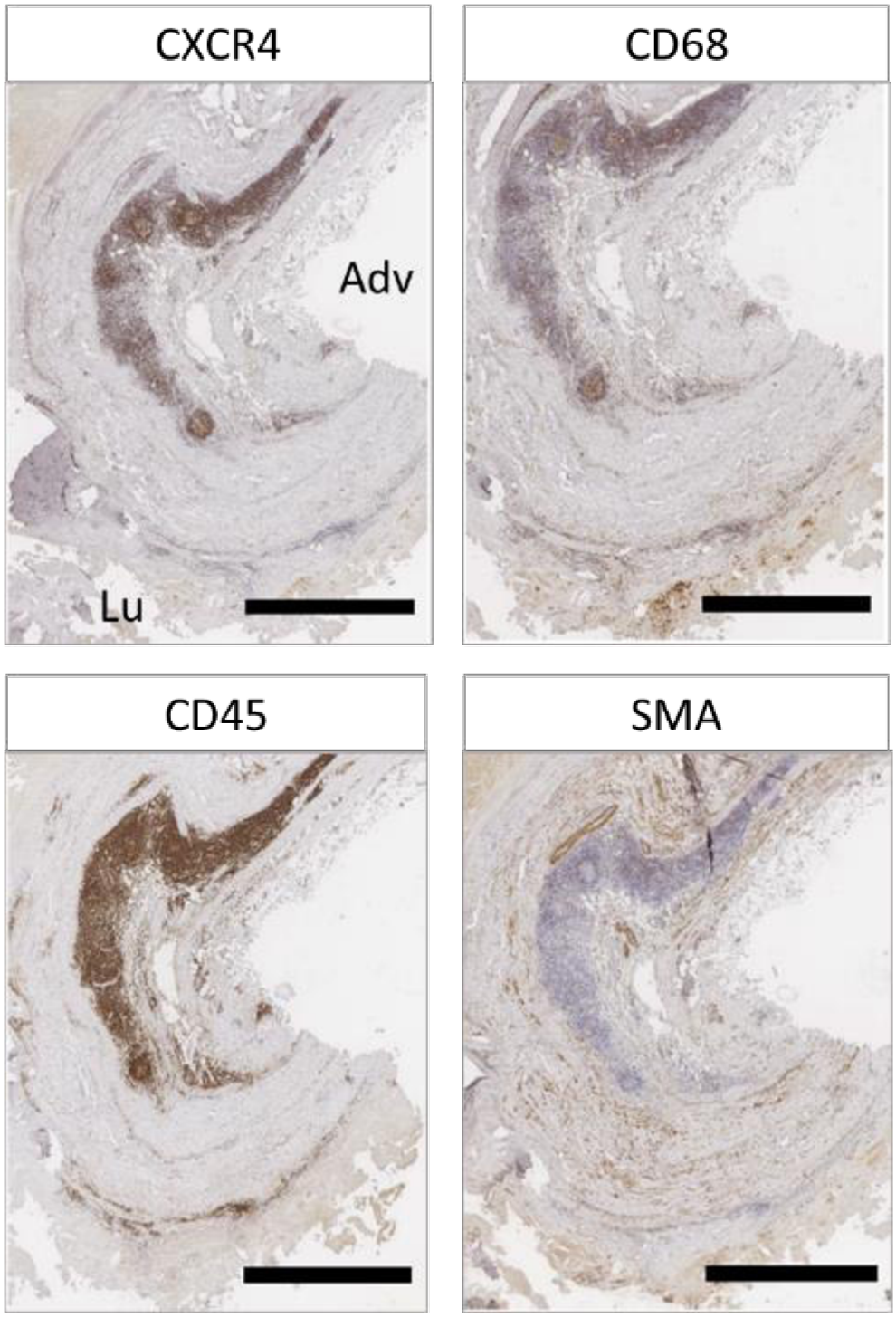

Figure 27: Representative consecutive IHC staining of a rAAA sample. Upper row: CXCR4 and CD68; lower row: CD45 and SMA; Lu = luminal side of the vessel wall, Adv = adventitial side of the vessel wall (same orientation in all images); scale bars representing 2000 µm.

In addition to the alcian blue staining, ESM1 staining was performed to specifically evaluate the content of endocan and its distribution within the vessel wall. In contrast to the glycosaminoglycan staining, large areas of ESM1-positive cells were observed in healthy aortic tissue while AAA samples showed much less ESM1-positive regions and a lower density of these positive cells. ESM1 was found mainly in areas of inflammatory infiltration and plaque formation in the aneurysmatic samples. In AAA samples, accumulations of ESM1 were observed in the adventitial layers while only small areas or individual positive cells were found in other wall layers. In the healthy samples, by contrast, the ESM1-positive cells were distributed through all wall layers (Fig. 28).

However, despite trying different antibody dilutions and modifications of the IHC protocol, the background signal in the ESM1 staining remained rather high and unspecific stains of e.g. thrombotic areas (see eAAA sample in Fig. 28) occurred frequently. The results of this particular staining should therefore be interpreted with caution.

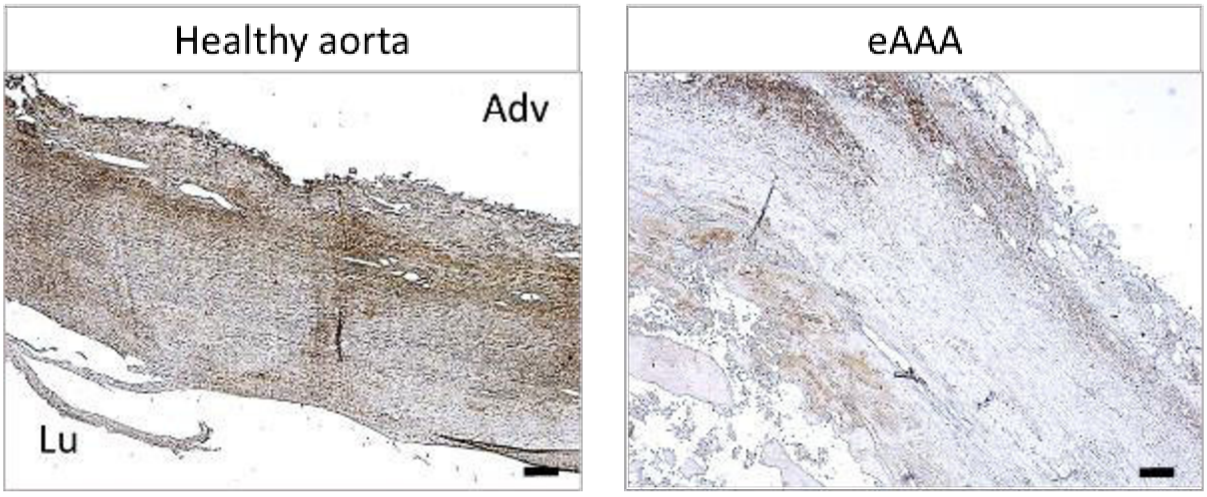

Figure 28: Representative ESM1 staining of healthy and eAAA samples. Healthy aorta: distribution of positive cells through all wall layers; eAAA: accumulation of positive cells in adventitial areas and unspecific staining of thrombotic region (light brown staining in luminal regions); Lu = luminal side of the vessel wall, Adv = adventitial side of the vessel wall (same orientation in all images); scale bars representing 100 µm.

3.4.2. Semiquantitative scoring*

Semiquantitative scoring of different histological staining (HE, EvG and alcian blue) was used to compare eAAA and rAAA samples based on histological tissue characteristics. Scoring data of eAAA and rAAA samples were evaluated using the Mann-Whitney test and the results are shown as violin plots (thicker dotted line representing the median; fine dotted lines representing the quartiles). As the scoring results were analyzed as ordinal data (scoring scale in steps of 0.5), violin plots were used for a better representation of data distribution (Fig. 29-31).

Tissue cellularity was scored on a similar level in eAAA and rAAA samples (median score 2.0 for eAAA and 2.0 for rAAA), with rAAA samples being scored on a slightly lower range (0.5 – 3.0) than eAAA samples (0.5 – 4.0). Inflammatory infiltration was scored higher on average in eAAA (median score 1.5 in eAAA and 1.25 in rAAA), while a majority of rAAA samples was scored between 0.5 and 2.0 and eAAA samples were scored on a wider range (0.0 – 4.0). The average distribution of neovessels was scored similarly in eAAA and rAAA (median score 1.5 for eAAA and 1.5 for rAAA) but rAAA samples were scored mainly between 1.0 and 2.0 while eAAA samples showed a wider range (0.0 – 3.0). Results are shown in Figure 29.

* The results in this section are included in the manuscript: Metschl, S., et al., *Changes in Endocan and Dermatan Sulfate Are Associated with Biomechanical Properties of Abdominal Aortic Wall during Aneurysm Expansion and Rupture*. Thromb Haemost, 2022. 122(9): p. 1513-1523.

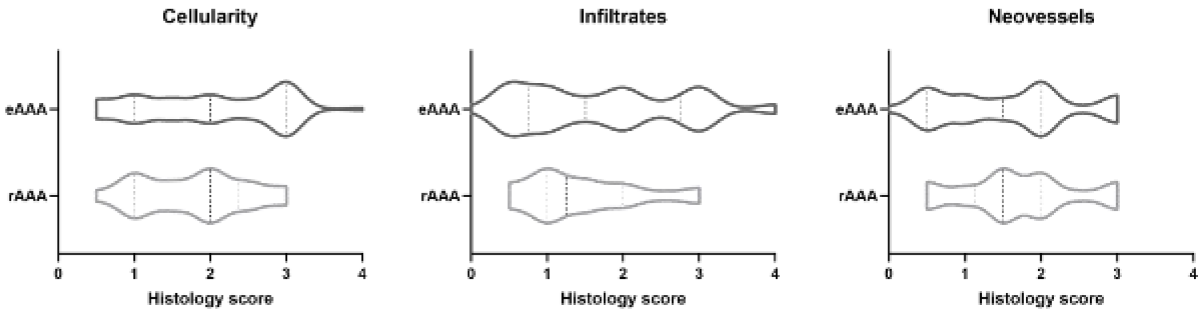

Figure 29: Semiquantitative scoring of histological characteristics in eAAA and rAAA samples. Tissue cellularity, inflammatory infiltration and extent of neovessels.

Tissue calcification was scored on a very low level in both study groups (median score 0.0 for eAAA and 0.0 for rAAA) and only a few individual samples were scored higher. Intramural hemorrhage was scored on a similar level in both groups (median score 1.0 for eAAA and 1.0 for rAAA) and also the scoring range was comparable (0.0 – 3.0). The average adventitial thickening was on the same level in both groups (median score 1.0 for eAAA and 1.0 for rAAA), while the scoring distribution was markedly different. While most of the eAAA samples were scored between 0.0 and 1.5, rAAA samples were scored mainly as 0.0 or 2.0. The overall extent of atherosclerosis (based on different individual characteristics) was scored similarly in eAAA and rAAA samples (median score 1.0 for eAAA and 1.0 for rAAA). The majority of samples was scored between 0.0 and 1.0 in both groups. The results are summarized in Figure 30.

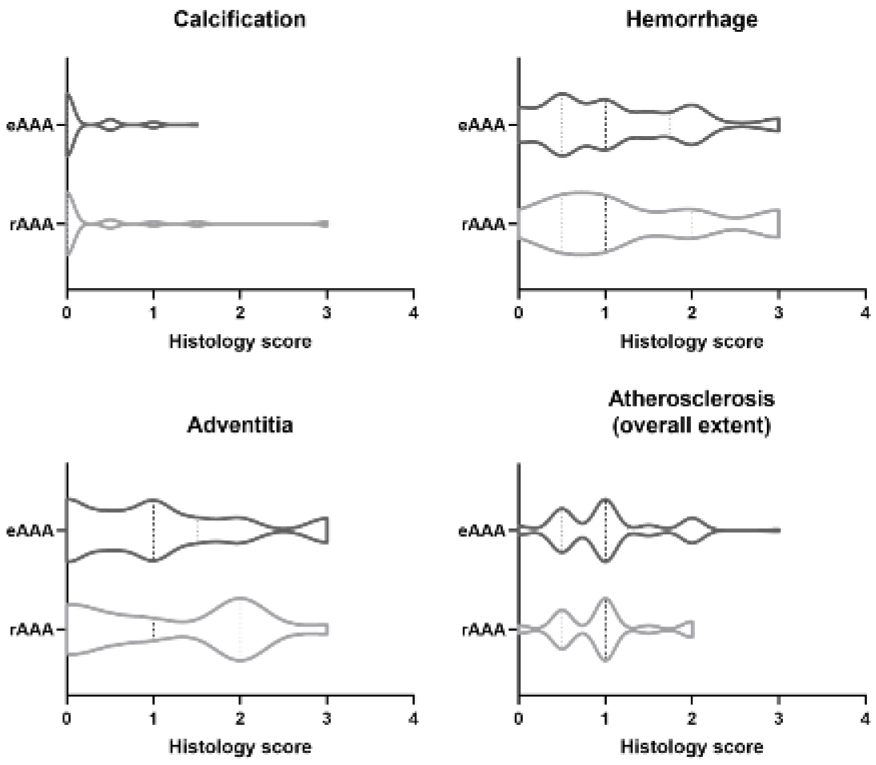

Figure 30: Semiquantitative scoring of histological characteristics in eAAA and rAAA samples. Upper row: tissue calcification and intramural hemorrhage; lower row: adventitial thickening and overall extent of atherosclerosis.

Regarding structural proteins and proteoglycans, the total extent of collagen fibers was scored higher on average in eAAA (median score 2.0 for eAAA and 1.75 in rAAA). Ruptured samples were scored mainly between 1.0 and 2.0. The average extent of elastin fibers was scored on the same level in both groups (median score 0.5 for eAAA and 0.5 for rAAA) and showed a relatively low overall scoring compared to other characteristics (most samples scored between 0.0 and 1.0). The total amount of proteoglycans was scored higher in rAAA samples (median score 1.5 for eAAA and 2.0 for rAAA). The majority of rAAA samples was scored between 2.0 and 2.5 while eAAA scoring was distributed more equally. Also focal accumulation of proteoglycans was scored higher in rAAA (median score 1.0 for eAAA and 1.25 for rAAA). Ruptured samples were mostly scored between 1.0 and 2.0 while eAAA samples were scored on a wider range again. The results are presented in Figure 31.[38]

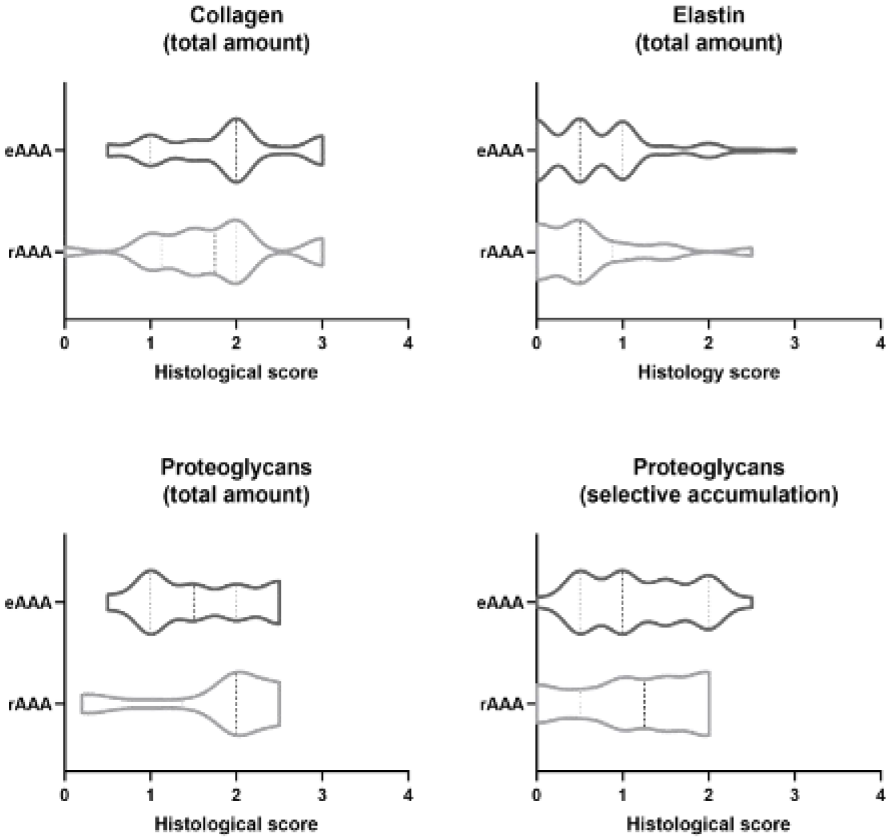

Figure 31: Semiquantitative scoring of histological characteristics in eAAA and rAAA samples. Upper row: total amounts of collagen and elastin; lower row: total amount and focal accumulation of proteoglycans.

None of the comparisons between eAAA and rAAA showed a statistically significant difference.

3.5. Mechanical properties of AAA tissue*

Mechanical parameters derived from tensile testing were compared between eAAA and rAAA samples to evaluate changes with disease progression and assess parameters of relevance for aneurysm rupture. Healthy aortic tissue could not be used for tensile testing due to deviating material properties, thus AAA parameters were not compared to healthy aortic parameters. Differences between the AAA groups were evaluated using the nonparametric Mann-Whitney

* The results in this section are included in the manuscript: Metschl, S., et al., *Changes in Endocan and Dermatan Sulfate Are Associated with Biomechanical Properties of Abdominal Aortic Wall during Aneurysm Expansion and Rupture*. Thromb Haemost, 2022. 122(9): p. 1513-1523.

test and results are presented as box plots (middle line representing the median; whiskers representing the 5 and 95 percentile). All results are summarized in Figure 32.[38]

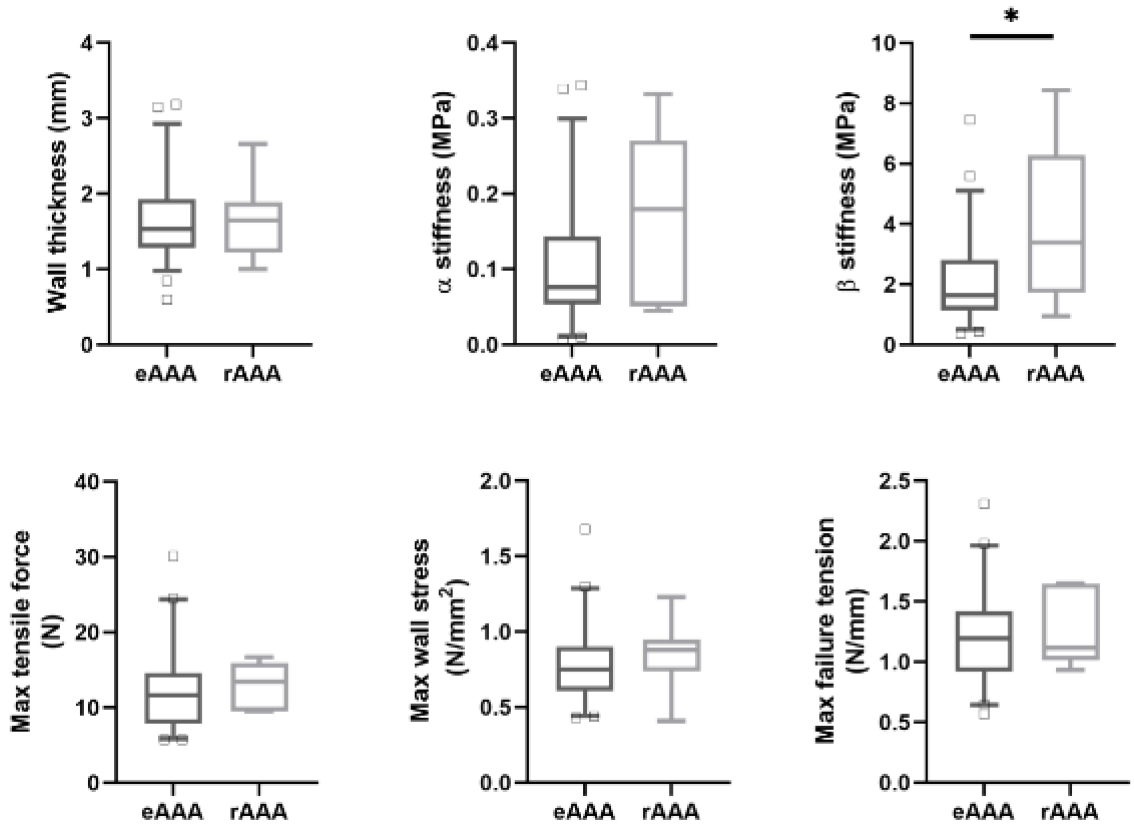

Figure 32: Mechanical parameters of eAAA and rAAA tissue. Upper row: wall thickness and elastic properties; lower row: maximum measured force and failure parameters. $p \leq 0.05$ summarized as *.

Specimen thickness, as measured prior to testing, did not differ between eAAA and rAAA (median thickness 1.5 mm for eAAA and 1.6 mm for rAAA). Tissue stiffness was higher in ruptured tissue for both α stiffness (median α stiffness 0.08 MPa for eAAA and 0.18 for rAAA) and β stiffness (median β stiffness 1.63 MPa for eAAA and 3.39 MPa for rAAA), with β stiffness showing a significant increase in rAAA tissue ($p = 0.022$). Both the maximum measured force and the calculated maximum stress (maximum force per cross-sectional specimen area) were higher in ruptured compared to elective tissue (median maximum force 11.6 N for eAAA and 13.5 N for rAAA; median maximum stress 0.75 N/mm^2 for eAAA and 0.88 N/mm^2 for rAAA). The calculated maximum failure tension (maximum force per specimen width), by contrast,

was higher in elective compared to ruptured tissue (median maximum failure tension 1.20 N/mm for eAAA and 1.12 N/mm for rAAA) (Fig. 32).

3.6. Correlation analyses

3.6.1. Correlation analysis of protein amounts in tissue and serum*

Correlation analysis was performed using protein amounts from tissue and serum measurements and focused particularly on correlations of endocan amounts with other parameters. The nonparametric Spearman correlation was used to determine r and p-values and all results are presented as scatter plots with regression lines (Fig. 33-34).

Tissue endocan correlated positively with both tissue CS and tissue DS ($r = 0.235$, $p = 0.04$ and $r = 0.291$, $p < 0.01$, respectively) and also with serum Col1 ($r = 0.388$, $p < 0.01$). Similar to tissue, serum endocan levels correlated positively with serum CS ($r = 0.327$, $p < 0.01$). Furthermore, serum endocan correlated with serum Col3 ($r = 0.268$, $p = 0.02$) and also serum CS showed a strong positive correlation with serum Col3 ($r = 0.635$, $p < 0.01$). The results are summarized in Figure 33.[38]

* The results in this section are included in the manuscript: Metschl, S., et al., *Changes in Endocan and Dermatan Sulfate Are Associated with Biomechanical Properties of Abdominal Aortic Wall during Aneurysm Expansion and Rupture*. Thromb Haemost, 2022. 122(9): p. 1513-1523.

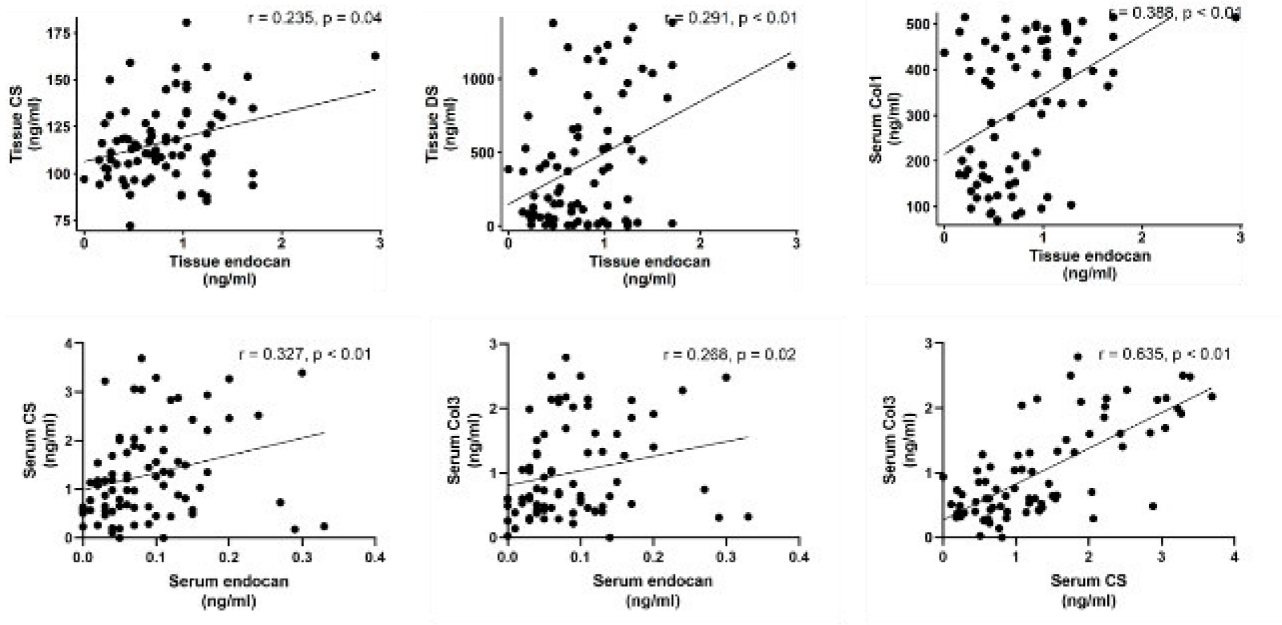

Figure 33: Correlation analysis of protein amounts in tissue and serum. Upper row: tissue endocan with tissue CS, tissue DS and serum Col1; lower row: serum endocan with serum CS and serum Col3, serum CS with serum Col3.

To gain closer insights into these correlations, corresponding subgroup correlation analyses were performed for eAAA and rAAA samples separately (Fig. 34). In general, the results from Fig. 33 could be confirmed only for eAAA samples when analyzed separately.[38] Tissue endocan in eAAA samples showed positive correlations with tissue CS, tissue DS and serum Col1 ($r = 0.231$, $p = 0.05$, $r = 0.274$, $p = 0.02$ and $r = 0.391$, $p < 0.01$, respectively). Also serum endocan in eAAA samples correlated positively with serum CS and serum Col3 ($r = 0.430$, $p < 0.01$ and $r = 0.291$, $p = 0.01$, respectively) and eAAA serum CS correlated strongly with serum Col3 ($r = 0.680$, $p < 0.01$). In contrast, correlations in rAAA samples alone were much weaker and did not reach statistical significance. Tissue endocan in rAAA samples correlated with tissue CS, tissue DS and serum Col1 ($r = 0.188$, $p = 0.61$, $r = 0.370$, $p = 0.30$ and $r = 0.152$, $p = 0.68$, respectively) and serum endocan in rAAA samples with serum CS and serum Col3 ($r = 0.027$, $p = 0.95$ and $r = 0.418$, $p = 0.20$, respectively). Serum CS in rAAA samples correlated with serum Col3 ($r = 0.188$, $p = 0.61$).

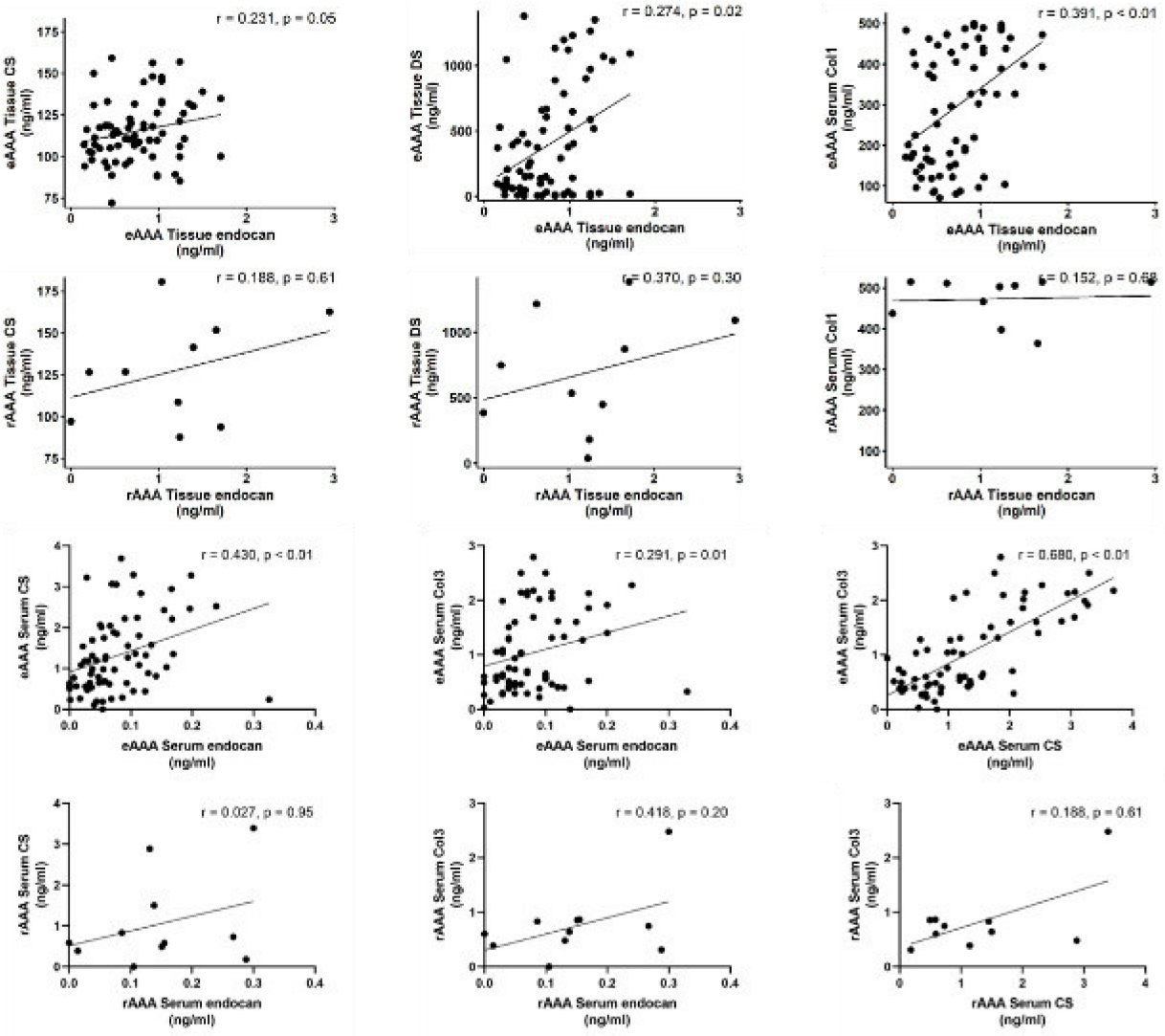

Figure 34: Correlation analysis of protein amounts in tissue and serum separately for eAAA and rAAA samples. Upper two rows: tissue endocan with tissue CS, tissue DS and serum Col1; lower two rows: serum endocan with serum CS and serum Col3, serum CS with serum Col3.

3.6.2. Correlation analysis of mechanical properties

Correlation analysis of material properties derived from tensile testing was performed to further characterize mechanical behavior of AAA tissue. The nonparametric Spearman correlation was used to determine r and p-values and all results are presented as scatter plots with regression lines (Fig. 35).

Specimen wall thickness correlated positively with both maximum tensile force (r = 0.505, p < 0.01) and maximum failure tension (r = 0.570, p < 0.01). Maximum tensile force and failure tension also showed a strong positive correlation with each other (r = 0.882, p < 0.01). The elastic properties α and β stiffness correlated positively with each other (r = 0.538, p < 0.01) (Fig. 35).

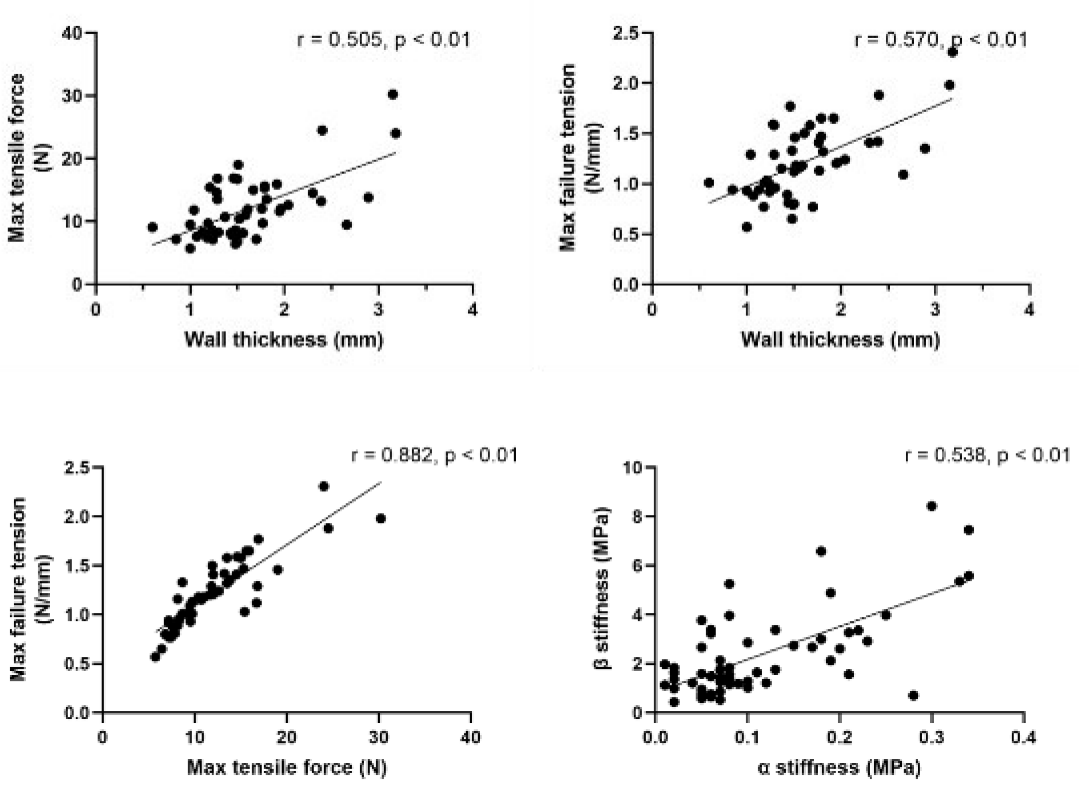

Figure 35: Correlation analysis of mechanical tissue properties. Upper row: wall thickness with maximum tensile force and failure tension; lower row: maximum tensile force with failure tension and α with β stiffness.

3.6.3. Correlation analysis of protein amounts and mechanical properties*

Protein amounts in tissue and serum were combined with mechanical properties for further correlation analysis and were used to determine possible mechano-biological relations. The

* The results in this section are included in the manuscript: Metschl, S., et al., *Changes in Endocan and Dermatan Sulfate Are Associated with Biomechanical Properties of Abdominal Aortic Wall during Aneurysm Expansion and Rupture*. Thromb Haemost, 2022. 122(9): p. 1513-1523.

nonparametric Spearman correlation was used to determine r and p-values and the results are presented as scatter plots with regression lines (Fig. 36).

Both serum Col1 and tissue endocan correlated positively with α stiffness ($r = 0.239$, $p = 0.07$ and $r = 0.311$, $p = 0.02$, respectively). Strong positive correlation was also observed between serum Col1 and the maximum tensile force ($r = 0.448$, $p < 0.01$). A similar correlation was found between tissue endocan and the maximum tensile force ($r = 0.274$, $p = 0.06$). Furthermore, serum Col1 correlated positively with the maximum failure tension ($r = 0.333$, $p = 0.02$) and tissue endocan with specimen wall thickness ($r = 0.242$, $p = 0.06$). All results are presented in Figure 36.[38]

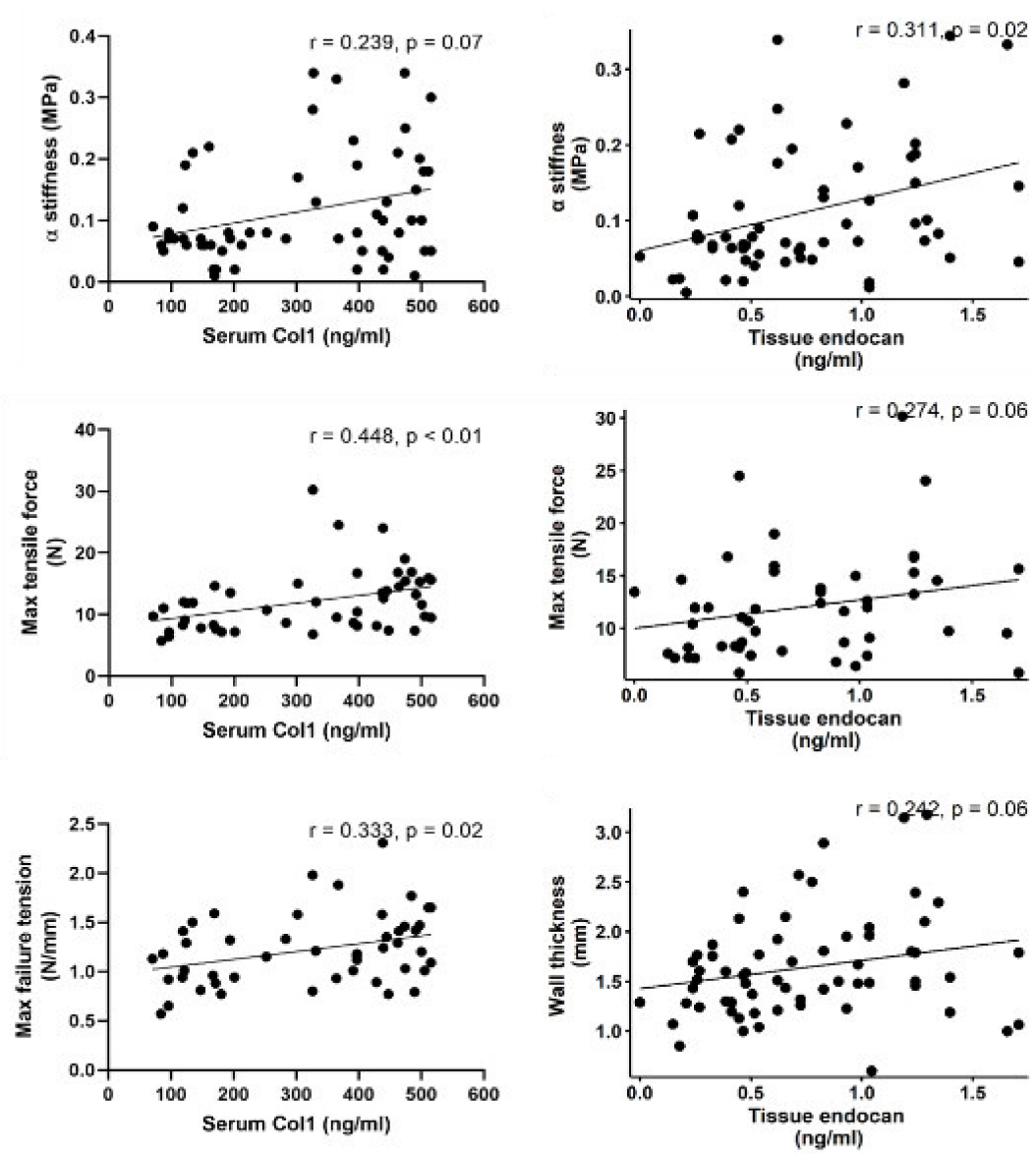

Figure 36: Correlation analysis of protein amounts and mechanical properties. Upper row: serum Col1 and tissue endocan with α stiffness; middle row: serum Col1 and tissue endocan with maximum tensile force; lower row: serum Col1 with maximum failure tension and tissue endocan with wall thickness.

3.6.4. Correlation analysis of protein amounts and clinical data

Correlation analysis between protein amounts and patient clinical data was applied to complement possible interactions with other parameters, focusing on blood parameters obtained from clinical chemistry. The nonparametric Spearman correlation was used to

determine r and p-values and the results are presented as scatter plots with regression lines (Fig. 37).

Tissue endocan showed a positive correlation with the total blood leucocyte count ($r = 0.360$, $p < 0.01$) while serum endocan correlated with blood urea ($r = 0.222$, $p = 0.04$). Results are summarized in Figure 37.

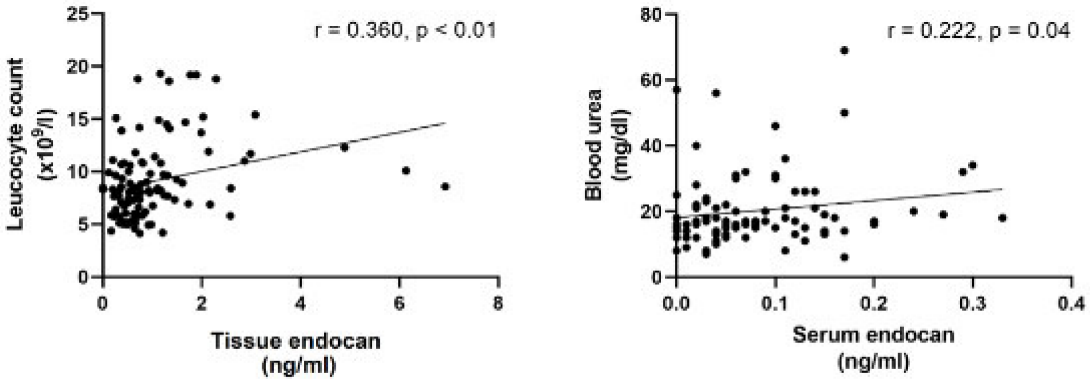

Figure 37: Correlation analysis of protein amounts and clinical data. Tissue endocan with blood leucocyte count and serum endocan with blood urea.

3.7. Protein kinase phosphorylation data*

Changes in phosphokinase activation during AAA development were evaluated using protein kinase phosphorylation data. To evaluate possible relations between mechanical loading and changes in protein amounts, the focus was placed on TGF-β related signaling. The relative activation levels of eAAA and rAAA samples were compared after normalization to healthy controls. The nonparametric Mann-Whitney test was used to determine differences between

* The results in this section are included in the manuscript: Metschl, S., et al., *Changes in Endocan and Dermatan Sulfate Are Associated with Biomechanical Properties of Abdominal Aortic Wall during Aneurysm Expansion and Rupture*. Thromb Haemost, 2022. 122(9): p. 1513-1523.

eAAA and rAAA activation levels and the results are shown as bar plots (whisker representing the standard error of the mean), separately for membrane parts A and B (Fig. 38).

The activation levels of almost all signaling proteins (except from mitogen- and stress-activated kinase 1/2 (MSK1/2)) on membrane part A were higher in eAAA compared to rAAA samples, with only the tyrosine-protein kinase Lyn being significantly elevated in eAAA ($p = 0.03$). Most of the signaling proteins (except from glycogen synthase kinase 3 (GSK-3a/b) and MSK1/2) showed also higher activation levels in eAAA relative to healthy controls. The activation levels in rAAA samples were elevated relative to healthy controls for CAMP response element-binding protein (CREB), epidermal growth factor receptor (EGFR), endothelial nitric oxide synthase (eNOS), Gardner-Rasheed feline sarcoma oncogene homolog (Fgr), JNK1/2/3, p38a, signal transducer and activator of transcription 2 (STAT2) and Yamaguchi sarcoma proto-oncogene tyrosine protein kinase (Yes).

On membrane part B, all activation levels (except from STAT3_S727 in rAAA samples) were higher relative to healthy controls. In contrast to membrane part A, the activation levels were higher in rAAA samples compared to eAAA in a majority of signaling proteins (without reaching statistical significance). Results from both membrane parts are summarized in Figure 38.[38]

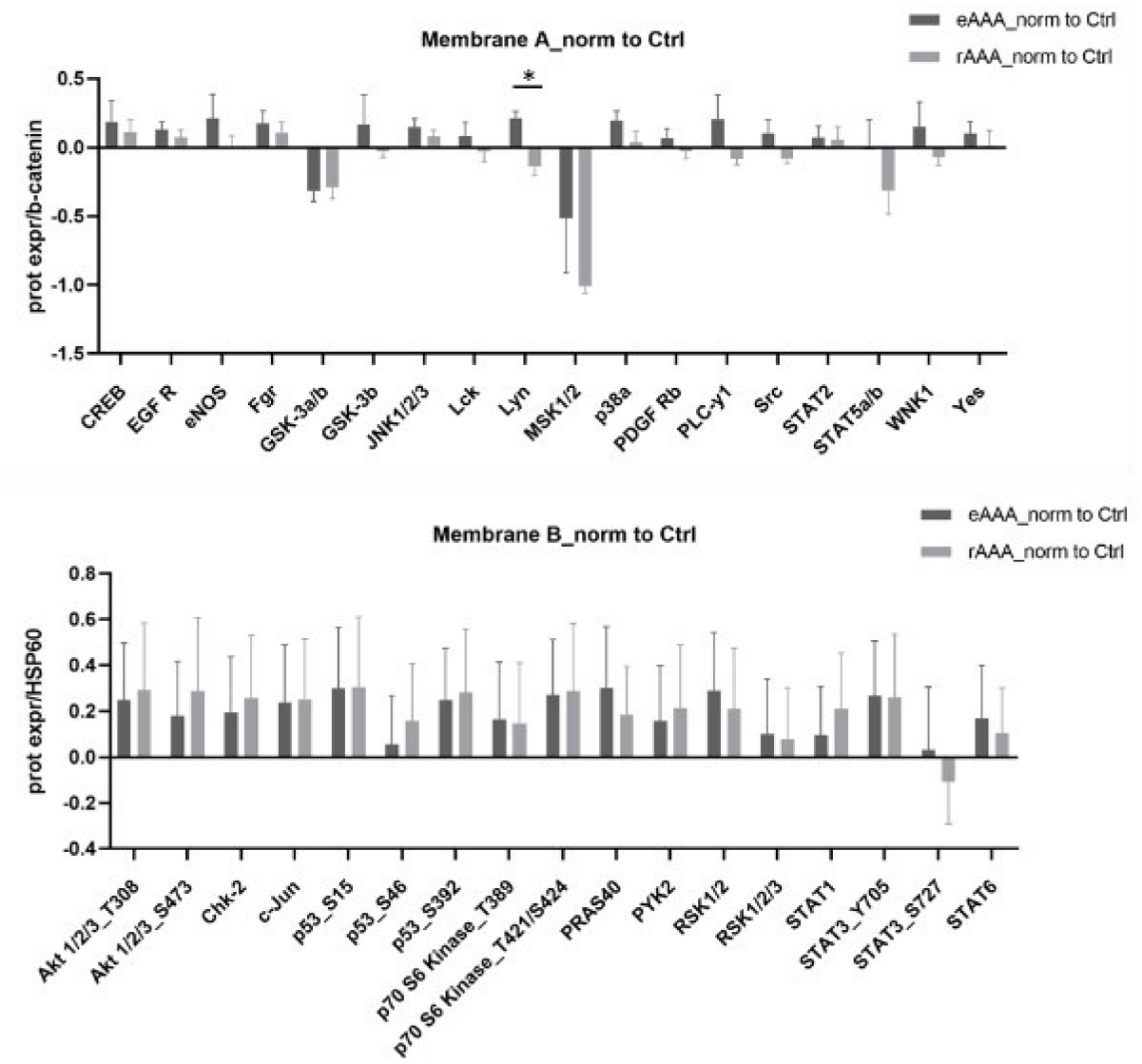

Figure 38: Relative protein kinase activation levels in eAAA and rAAA samples. Upper graph: membrane part A activation levels, normalized to b-catenin; lower graph: membrane part B activation levels, normalized to HSP60; eAAA and rAAA activation levels were also normalized to healthy controls. $p \leq 0.05$ summarized as *.

4. Discussion

It has been previously assumed that, in addition to collagenous and elastic fibers, proteoglycans might play a crucial role in the maintenance of the mechanical stability of a healthy aortic wall. However, few studies so far focused on the role of proteoglycans in an aneurysmatic vessel wall. Their functions within the biomechanical context as well as changes with disease progression are still largely unknown. This study aimed to evaluate the potential of load-bearing ECM proteins to serve as surrogate markers reflecting the biological integrity of an aortic wall and thus identify patients at increased risk of AAA rupture.

Patient characteristics, including demographic data and blood parameters, showed that the AAA study cohort reflected typical features of AAA patients. The vast majority of patients was male and all patients were of advanced age, both representing important risk factors of AAA disease.[2, 4] The fact that rAAA patients were older on average and had larger AAA diameters compared to eAAA patients confirms a continuous AAA growth over time and a higher risk of AAA rupture with larger diameters.[5] Patient comorbidities and medication showed that the majority of patients had already an elevated cardiovascular risk, being in line with what is known about typical AAA patients.[2] The fact that chronic kidney disease occurred more often in patients with ruptured AAAs could be attributed to the association of chronic kidney disease, AAA incidence and diameter.[40] It has been previously shown that signs of chronic kidney disease are associated to larger AAA diameters and a higher disease incidence.[40] Blood parameters also confirmed that the cohort of rAAA patients had a higher cardiovascular risk and a higher incidence of reduced renal function or renal diseases. Both groups of AAA patients showed clinical signs of reduced renal function when compared to the normal range. Protein amounts in aortic tissue suggest that both collagenous and proteoglycan ECM components respond to a certain extent to altered mechanical loads occurring during

aneurysm development. In a previous study [30], Tanios et al. showed associations between collagen and proteoglycans synthesis and mechanical conditions determined via immunohistological analysis. A distinction between already ruptured AAAs and electively treated ones, however, was not included into the study. Furthermore, the authors did not compare tissue and serum amounts of the involved ECM components.

In this study, both collagen types I and III showed increased amounts in aneurysmatic tissue as well as in the corresponding serum samples. These findings were supported also by the higher levels of mRNA expression in AAA tissue. N-terminal pro-peptide of procollagen type III (PIIINP), a peptide released from procollagen type III during collagen synthesis, has already been used as marker for collagen deposition in other organs [41, 42] and also to demonstrate increased collagen type III turnover in AAA disease.[43, 44] PIIINP has also been linked to AAA growth over time [45] and has been used to predict AAA rupture risk [46], supporting the role of increasing collagen type III levels during AAA progression. Regarding the amounts of collagen type I, conflicting roles have been described in earlier studies. Increased deposition of collagen type I in aneurysm samples was observed along with reduced levels of collagen type III [47], while another study showed contrary results with elevated collagen type III and decreased collagen type I.[48] In the present study, the role of both collagens being increased along with each other in advancing AAAs can be emphasized.

With regard to the analyzed tissue proteoglycan components, significantly increased amounts of both CS and DS were observed with AAA disease. These matrix-associated proteoglycans are known to be aggregating and collagen-binding, and to participate in and modulate collagenous fibril formation.[38, 49, 50] CS and DS proteoglycans have also been described as binding partners of other ECM components, like fibronectin and laminin.[51] Moreover, DS has been shown to have the capacity to bind to TGFβ and EGFR and could therefore not only

contribute to aortic wall stability but also serve as a regulatory factor of fibrosis itself.[38, 52] Associations between the mRNA expression of proteoglycans and collagens as well as increased mRNA levels of collagen-related proteoglycans in AAA tissue were already found in preliminary, unpublished studies. The role of collagen-proteoglycan interactions in AAA tissue could then be further strengthened in this study.

Another aspect of increased proteoglycan levels in AAA disease could be their key function in the context of wound healing. Especially DS proteoglycans are released in high concentrations during wound healing processes and are the most abundant soluble proteoglycans found in wounds.[52] Despite being primarily described in skin injuries and skin repair, similar patterns could also play a role in the compensatory tissue-healing mechanisms that occur during aneurysm development [53] and could be involved in the aortic repair processes.

In contrast to CS and DS proteoglycans, HS amounts did not change between the study groups in tissue samples.[38] HS proteoglycans are found predominantly on cell surfaces and in basement membranes and are less associated with the ECM.[23] These proteoglycans seem to be less involved in the binding of collagenous fibers and in providing mechanical strength, and might therefore be less affected during AAA development.[38] Moreover, HS was able to modify in vitro elastin aggregation and assembly [54] and was also shown to interact with tropoelastin, the soluble precursor of elastin.[55] These possible associations with elastic fibers could explain the constant quantities of HS in the aortic tissue. Compared to other ECM components, elastic fibers have a relatively long biological half-life and are therefore not dependent on continuous replacement or adjustment of quantities.[56] Taken together, different biological functions of the respective proteoglycan groups seem to be reflected in their tissue amounts during AAA progression.[38]

The findings in corresponding serum samples suggest that aneurysm-induced changes of the ECM are reflected to a certain extent also in blood. Especially collagen type I and endocan levels were increased in AAA serum and could represent processes of ECM turnover and adjustment in response to AAA growth.[38] Increased collagen turnover, measured again via PIIINP, has been described in serum of AAA patients compared to control subjects [43] but could not be validated as reliable marker for AAA in a later study.[57] Regarding proteoglycan amounts in serum, pro-inflammatory processes within the aneurysm wall seem to constitute an important aspect. Preliminary unpublished studies showed that different types of proteoglycans have different mRNA expression patterns during AAA progression and that increased amounts of smaller proteoglycans were associated especially with inflammatory processes. Among these smaller proteoglycans, endocan (50 kDa) appears to have a special role in the context of vascular inflammation and cardiovascular disease. Endocan, formerly named endothelial cell-specific molecule 1 (ESM1), was characterized as a soluble DS proteoglycan with a large proportion circulating in the bloodstream.[25] Initially, endocan was shown to be mediator of cell proliferation in human kidney cells [25] and increased serum endocan levels in chronic kidney patients were associated with an increase in cardiovascular events.[58] This would also be consistent with the present observation that AAA patients had a high incidence of chronic kidney disease and clinical signs of reduced renal functions along with elevated serum endocan levels. Next to chronic kidney patients, endocan levels were found to be elevated in septic patients and were also described as a marker of endothelial dysfunction.[59] Moreover, endocan-integrin interactions implicate a regulatory role in the initial leucocyte extravasation at inflammatory sites.[60] Increased tissue and serum levels of endocan were also related to neovascularization and were proposed as biomarkers of inflammatory processes.[61] Taken together, the current findings suggest a role of endocan in

the activation of vascular inflammation and endothelial cell-dependent diseases and could provide a basis for further investigations of its biomarker potential.

Another important aspect of circulating biomarkers is their method of secretion and the question of where serum proteoglycans could be derived from. It is well-described that proteoglycans can be secreted directly within the ECM and can also be stored in intracellular secretory granules.[21] Moreover, recent studies showed that the proteoglycan composition of secretory granules is regulated through MAPK signaling.[62] Detectable serum levels of proteoglycans in AAA patients could therefore be explained either by release from granules or by release from the matrix itself following degradation processes. Especially in advanced AAAs aortic endothelial layers are increasingly damaged and thus the transfer of ECM components into the bloodstream could be enabled.[38]

The secretion of specifically DS proteoglycans plays an important role also in the context of anticoagulant activity. Both DS and its derivatives have early been identified as antithrombotic factors with a certain therapeutic potential [63] and were described to enhance antithrombin activity.[64] In a later study, aneurysmatic tissue has been shown to have a higher anticoagulant activity than a healthy aorta [65], which could be attributed to an increased DS content. This would also be in line with the current findings in AAA tissue.[38] In contrast to that, the strongly decreased levels of DS in AAA serum could be caused by anticoagulant activation, resulting in DS consumption in advanced AAAs.[38] Possible reasons for this activation of anticoagulation could be the formation of intraluminal thrombus or intraabdominal bleeding due to full or partial tearing of the aneurysm wall. Compared to serum endocan, serum DS seems to reflect different biological functions and might also play a different role in the context of rupture-prone AAAs.

Besides ECM components of the aortic wall, the amounts of inflammatory factors in tissue and serum samples were measured to evaluate possible associations between inflammatory degradation and AAA progression. The receptor-ligand-complex CXCR4/CXCL12 has already been described as a potential inflammatory marker in the context of AAA development [29], but was only analyzed in AAA tissue and in electively removed AAAs. In the present study, CXCR4 and CXCL12 amounts in tissue did not change between AAA groups and healthy tissue. The previous findings in AAA tissue could therefore not be confirmed. Elevated amounts of both CXCR4 and CXCL12 could, however, be detected in serum samples. While CXCL12 was elevated in both AAA groups compared to controls, CXCR4 was increased only in rAAA compared to eAAA samples. Given the fact that tissue amounts of CXCR4 and CXCL12 were unaltered, the detected serum amounts might have a different biological origin and could thus reflect other underlying disease conditions. The CXCR4/CXCL12 axis has been shown to be involved in the regulation of atherosclerosis and CXCL12 has been proposed as a pro-atherogenic biomarker.[66] The generally higher atherosclerotic burden of AAA patients could be a reason for the increased amounts in serum. In addition, this axis has been described in the context of autoimmune diseases and different types of cancer.[67] Compared to collagens and PGs, the role of CXCR4/CXCL12 in aortic wall degeneration seems to be less clear and less suitable for associations with the underlying AAA status. The further focus of this study was therefore placed on the ECM components.

The histological findings of this study are in accordance with several well-described morphological hallmarks of aneurysm formation. Increasing disruption of the vessel wall morphology along with a loss of elastic fibers, enhanced collagen deposition and inflammatory infiltration define the pathohistology of aortic aneurysms.[68, 69] Collagen deposition in EvG staining of AAA samples confirms the findings of protein and gene expression analysis.

Moreover, the lower content of elastic fibers in AAA tissue along with the enhanced amount of collagen fibers seems to be reflected in the increased wall stiffness of rAAA samples determined by mechanical testing. Accumulations of PGs in the alcian blue staining strengthens the results from protein measurements and could also be validated by semiquantitative scoring. Regarding the amounts of proteoglycans in aneurysm tissue compared to control aortas, conflicting data were reported so far. Earlier studies described reduced total proteoglycan contents as well as alterations in the amounts of different proteoglycan subgroups.[30, 70] Other studies showed accumulating CS proteoglycans in thoracic aneurysm samples [71] and a relative enrichment of DS proteoglycans in AAA tissue.[65] The current histological findings suggest an increase in total proteoglycan amounts and in focal proteoglycan-rich regions. Close structural and functional connections between collagen fibers and proteoglycans could explain the increasing amounts of both ECM components along with each other. IHC staining showed an accumulation of inflammatory cells (CD68-, CD45- and CXCR4-positive cells) with AAA progression [39], which could partly be confirmed by semiquantitative scoring of tissue cellularity and neovessel formation. Inflammatory infiltration was more advanced in rAAA compared to eAAA samples, being in line with the progression of morphological hallmarks in advancing AAAs.[68] The rarefication of ECM-producing SMCs in AAA samples is in accordance with earlier findings [68], and could be one reason for a reduced wall stability in aneurysmatic samples. The relatively long half-life of ECM proteins might be the cause for the increased amounts of ECM components along with diminished SMCs in AAA tissue. Structural proteins could still be present in the vessel wall while their synthesizing SMCs have already decreased.

Correlation analysis of protein amounts showed strong associations between PG and collagen levels in tissue and corresponding serum. Correlations between tissue endocan and the overall

tissue CS and DS content could be explained by its structural composition.[38] Endocan has been described as DS proteoglycan and also as being composed of CS/DS chains [25, 72], linking the endocan content to its individual components. The same applies to the association between serum endocan and serum CS. The correlating quantities of tissue and serum endocan with serum collagens could be based on the interrelated synthesis of both components as well as on the aforementioned binding capacities.[30, 49] The ability of CS and DS to aggregate collagens seems to be reflected also in serum amounts and might be of special importance in the context of serum biomarkers.[38] Connections between endocan levels and patient leucocyte counts might be attributed to its pro-inflammatory role and contribution to leucocyte activation.[59, 60] These findings underline the role of endocan in the inflammatory processes involved in AAA expansion. A possible association to kidney-dependent processes could be shown by the correlation between serum endocan and urea levels. This is in line with previous findings of serum endocan in kidney patients [58] and needs to be further evaluated with respect to AAA development.

Combined correlation analysis of protein amounts and mechanical properties of the diseased aortic wall demonstrated that serum Col1 and tissue endocan are associated with similar material properties. Both parameters showed strong correlations with wall strength and wall stiffness and were significantly increased in AAA, especially in rAAA samples.[38] It has been previously shown that AAA tissue has a diminished mechanical compliance compared to healthy aortic segments and wall strength in aneurysmal tissue was found to be reduced by 50%. Moreover, growing aneurysms were characterized by elevated mechanical stress upon the vessel wall while ruptured tissue was found to be weaker and often thicker than tissue from elective AAAs .[15, 73] These differences in mechanical properties could not be clearly confirmed in the present study, as only wall stiffness was significantly elevated in rAAA

samples. Increased vessel wall stiffness in AAA samples has already been described in earlier studies utilizing biaxial testing.[74]

The aforementioned gain in tissue Col1 and endocan could constitute a response to continuous wall weakening and an attempt to stabilize the aortic wall.[38] A serum marker of collagen turnover has earlier been related to AAA growth and rupture risk, emphasizing the potential of collagen as marker of AAA progression.[45] By specifically upregulating those ECM components that contribute to mechanical stability and rupture resistance, a loss of wall stability could be counteracted.[38] As those AAAs with high levels of Col1 and endocan are still the ones that ruptured in the end, mechanisms of wall weakening must, however, outweigh this increase in stabilizing proteins. Inflammatory processes, proteolytic degradation, immune response and other factors contribute to progressive destabilization and might play a crucial role for the final aneurysm rupture. A previous study demonstrated that enhanced collagen neo-synthesis is related to increasing beta stiffness and reduced AAA distensibility, suggesting that newly synthesized collagen has altered material properties.[75] Above all, the diseased aortic wall is less elastic and elastin fibers replaced by collagens or proteoglycans may significantly contribute to changes in the overall mechanical properties These altered mechanical features could be one reason why stabilizing measures eventually fail to prevent aneurysm rupture.

Analysis of protein kinase phosphorylation showed higher levels of activation in AAA compared to healthy samples especially for proteins related to ECM regulation and VSMC proliferation. This mainly comprises Src family kinases (SFKs) as well as proteins related to the platelet-derived growth factor (PDGF) and epidermal growth factor (EGF).[38] The central role of TGF-β in the regulation of cell differentiation and proliferation is well-described and the effects of TGF-β activation were shown to be mediated through Src-activation.[76] TGF-β has

also been shown to specifically induce the expression of genes related to ECM components via Src activation.[77] This crucial role of TGF-β could partly be confirmed by the present mRNA expression data. TGF-β (B1 and B2) expression levels as well as the expression of downstream SMAD3 were elevated in AAA tissue along with the increased expression of ECM collagens (Col1A1 and Col3A1).

Src, Lyn and Lck belong to the group of SFKs and share a regulatory role in cell growth and survival as well as in ECM-degrading processes.[78] Lyn was found to be expressed in VSMCs and to function as an upstream kinase of proliferative activity [79]. In renal fibroblasts, inhibition of Src resulted in diminished expression of collagen type I and α-smooth muscle actin, emphasizing its role as mediator of fibrotic responses.[80] Collagen type I, inversely, was described to increase VSMC proliferation through Src-dependent signaling, which could also be related to the increased levels of collagen found in AAA.[81] The lower activation of SFK-related factors (Src, Lyn, Lck) in rAAAs could be interpreted as deactivation of ECM synthesis and a resulting weaker aortic wall. In contrast to Src, the roles of Lyn and Lck in AAA are almost unknown and need to be further elucidated.

Both PDGF and its downstream signaling molecule phospholipase C (PLC) were demonstrated to stimulate the proliferation of VSMCs through ECM proteins.[82] It has also been shown that STAT3, downstream of PDGF, exerts a regulatory role on proliferation and migration of pulmonary artery SMCs.[83] This again indicates a potential deregulation of PDGF and its downstream signaling factors in rAAA, together with an altered pattern of SMC proliferation.[38]

Other pathways that could be involved in ECM regulation are the EGFR-induced PLC and STAT3 signaling [84] as well as the Src/EGFR/PI3K/Akt/JNK1/2 axis that was shown to be present in tracheal SMCs.[85] Moreover, EGFR/Src activation appears to be crucial for TGF-β induced

translational regulation in primary cultures of VSMCs.[86] Taken together, decreased activation of associated factors in rAAA suggests a lower potential for VSMCs to migrate and proliferate in order to counteract vascular strain.

The regulatory role of STAT proteins in inflammatory processes, such as a chronically inflamed vessel wall in AAA, indicates that activation of STATs promotes the weakening of ECM structures. An increased activation of STAT3 and STAT5 was found in AAA tissue compared to normal aortic samples.[87] The present findings of reduced STAT activation in rAAA compared to eAAA could imply counter-regulatory processes in order to limit aneurysmal inflammation and further vessel wall degradation.

Regarding associations between proteoglycans and the involved signaling pathways, biglycan, consisting of CS and DS, was shown to be present in aortic tissue and to have regulatory effects on TGF-β signaling.[88] TGF-β was also found to increase biglycan expression, suggesting interactions between ECM composition and its regulating pathways.[89]

Despite different levels of activation in eAAA and rAAA, the present findings show that the overall increase of ECM components in the aneurysmatic aorta is associated to a certain extent with the activation of various proliferative pathways. With regard to the increasing VSMC apoptosis during aneurysm development [90], an upregulated proliferation could contribute to ECM maintenance and might counteract increasing mechanical loads. This proliferative activity could help keeping eAAAs in a stable state to a certain degree.[38]

VSMC proliferation in mature and healthy arteries is limited to relatively low levels, but upon vascular injury VSMCs can switch to a proliferative state again.[91] Both TGF-β and PDGF are described as phenotypic modulators of VSMCs in the context of vascular injury models.[92] Overexpression of TGF-β promotes VSMC proliferation and ECM deposition while PDGF stimulates proliferation with downregulation of SMC-specific markers.[92]

Taken together, the present study showed that various pathways known to be related to VSMC proliferation and ECM synthesis appear to be activated to a greater extent in eAAA compared to rAAA. In contrast to pathway activation data, the protein levels of most target ECM components in tissue and serum were higher in rAAA samples. Given the relatively long half-life of structural proteins, the measured protein levels in aortic tissue may reflect an earlier state of matrix regulation than at the time of sample collection. Lower activation of proliferative pathways could have a closer temporal association to AAA rupture than protein levels itself, or could even act as trigger for the final, decisive decrease in aortic wall strength. It might also be possible that other regulatory mechanisms, such as cross-activation of the involved pathways, compensate rAAA de-activation and keep the levels of structural proteins high. Such regulatory mechanisms remain to be further evaluated in order to fully understand the underlying interplay of VSMCs and matrix components in AAA.

5. Study limitations

Firstly, the unequal number of patients included in the eAAA and rAAA study groups constitutes one important limitation. The number of patients with a ruptured AAA was smaller due to the disease pattern itself and the comparatively rare cases of aneurysm rupture admitted to the hospital. The operative procedure of an open AAA repair is another factor in this context, as the open repair has a steadily decreasing caseload compared to EVAR procedures. Moreover, open AAA surgery always represents an emergency procedure where sample collection (of both tissue and blood) is not always possible.

Due to the limited availability of samples from kidney transplants, the number of healthy control samples was relatively small. It was not possible to match these samples to the AAA groups regarding patient gender and age. Patient characteristics and clinical data from the healthy controls were not available due to the respective study protocols and data protection guidelines.

Regarding mechanical testing, one important limitation was the absence of tissue properties from healthy control samples. Deviating material properties are presumed for healthy aortas and a direct comparison to aneurysmatic aortas was therefore not possible with this type of testing. For a more comprehensive comparison of material properties, additional testing procedures or a correction for material differences would need to be applied.

Moreover, all correlation analyses between biological and mechanical data are limited to the description of possible associations. All statements on underlying mechanisms and causalities remain speculative and would need to be confirmed by further analyses.

With regard to the role of potential circulating biomarkers, further limiting factors need to be addressed. Firstly, to gain a better insight into the biomarker potential of ECM components, serum measurements would need to be compared to the actual AAA development and

medical outcome of the respective patients. Follow-up data on AAA development (such as imaging data over time and repeated blood sampling) as well as follow-up patient records are required for an in-depth evaluation and were not available for this study. Moreover, the diagnostic value of a biomarker measurement in blood must be carefully considered in the context of well-established diagnostic tools. A potential biomarker needs to add medical value and ideally provide better information than e.g. the routine ultrasound measurements or other imaging techniques applied in clinical practice. Additional time and expenditure for biomarker measurements need to be well-justified and important biomarker characteristics, such as sensitivity and specificity, need to be considered to evaluate their clinical potential.

Reference list

1. Sakalihasan, N., et al., *Aneurysm: Epidemiology Aetiology and Pathophysiology*, in *Biomechanics and Mechanobiology of Aneurysms*, T. McGloughlin, Editor. 2011, Springer Berlin Heidelberg: Berlin, Heidelberg. p. 1-33.
2. Sakalihasan, N., et al., *Abdominal aortic aneurysms.* Nat Rev Dis Primers, 2018. **4**(1): p. 34.
3. Nordon, I.M., et al., *Pathophysiology and epidemiology of abdominal aortic aneurysms.* Nat Rev Cardiol, 2011. **8**(2): p. 92-102.
4. Lederle, F.A., *In the clinic. Abdominal aortic aneurysm.* Ann Intern Med, 2009. **150**(9): p. ITC5-1-15; quiz ITC5-16.
5. Ockert, S., et al., *Rupturiertes abdominelles Aortenaneurysma.* Gefässchirurgie, 2007. **12**(5): p. 379-391.
6. Chaikof, E.L., et al., *The Society for Vascular Surgery practice guidelines on the care of patients with an abdominal aortic aneurysm.* J Vasc Surg, 2018. **67**(1): p. 2-77.e2.
7. Polzer, S., et al., *Biomechanical indices are more sensitive than diameter in predicting rupture of asymptomatic abdominal aortic aneurysms.* J Vasc Surg, 2020. **71**(2): p. 617-626.e6.
8. Kontopodis, N., et al., *The - Not So - Solid 5.5 cm Threshold for Abdominal Aortic Aneurysm Repair: Facts, Misinterpretations, and Future Directions.* Front Surg, 2016. **3**: p. 1.
9. Torres-Fonseca, M., et al., *Pathophisiology of abdominal aortic aneurysm: biomarkers and novel therapeutic targets.* Clin Investig Arterioscler, 2019. **31**(4): p. 166-177.
10. Wanhainen, A., K. Mani, and J. Golledge, *Surrogate Markers of Abdominal Aortic Aneurysm Progression.* Arterioscler Thromb Vasc Biol, 2016. **36**(2): p. 236-44.
11. Wagenseil, J.E. and R.P. Mecham, *Vascular extracellular matrix and arterial mechanics.* Physiol Rev, 2009. **89**(3): p. 957-89.
12. Humphrey, J.D., et al., *Role of mechanotransduction in vascular biology: focus on thoracic aortic aneurysms and dissections.* Circ Res, 2015. **116**(8): p. 1448-61.
13. Daugherty, A. and L.A. Cassis, *Mechanisms of abdominal aortic aneurysm formation.* Curr Atheroscler Rep, 2002. **4**(3): p. 222-7.
14. Davis, F.M., A. Daugherty, and H.S. Lu, *Updates of Recent Aortic Aneurysm Research.* Arterioscler Thromb Vasc Biol, 2019. **39**(3): p. e83-e90.
15. Vorp, D.A., *Biomechanics of abdominal aortic aneurysm.* J Biomech, 2007. **40**(9): p. 1887-902.
16. Sugita, S. and T. Matsumoto, *Multiphoton microscopy observations of 3D elastin and collagen fiber microstructure changes during pressurization in aortic media.* Biomech Model Mechanobiol, 2017. **16**(3): p. 763-773.

17. Davis, E.C., *Smooth muscle cell to elastic lamina connections in developing mouse aorta. Role in aortic medial organization.* Lab Invest, 1993. **68**(1): p. 89-99.
18. Pope, F.M., et al., *Patients with Ehlers-Danlos syndrome type IV lack type III collagen.* Proc Natl Acad Sci U S A, 1975. **72**(4): p. 1314-6.
19. Schwarze, U., et al., *Haploinsufficiency for one COL3A1 allele of type III procollagen results in a phenotype similar to the vascular form of Ehlers-Danlos syndrome, Ehlers-Danlos syndrome type IV.* Am J Hum Genet, 2001. **69**(5): p. 989-1001.
20. Tonar, Z., et al., *Vasa vasorum in the tunica media and tunica adventitia of the porcine aorta.* Ann Anat, 2016. **205**: p. 22-36.
21. Lindahl, U., et al., *Proteoglycans and Sulfated Glycosaminoglycans*, in *Essentials of Glycobiology*, A. Varki, et al., Editors. 2015, Cold Spring Harbor Laboratory Press

: Cold Spring Harbor (NY). p. 207-21.
22. Figueroa, J.E., J. Oubre, and P. Vijayagopal, *Modulation of vascular smooth muscle cells proteoglycan synthesis by the extracellular matrix.* J Cell Physiol, 2004. **198**(2): p. 302-9.
23. Iozzo, R.V. and L. Schaefer, *Proteoglycan form and function: A comprehensive nomenclature of proteoglycans.* Matrix Biol, 2015. **42**: p. 11-55.
24. Scott, J.E., *Proteoglycan-fibrillar collagen interactions.* Biochem J, 1988. **252**(2): p. 313-23.
25. Béchard, D., et al., *Endocan is a novel chondroitin sulfate/dermatan sulfate proteoglycan that promotes hepatocyte growth factor/scatter factor mitogenic activity.* J Biol Chem, 2001. **276**(51): p. 48341-9.
26. Michineau, S., et al., *Chemokine (C-X-C Motif) Receptor 4 Blockade by AMD3100 Inhibits Experimental Abdominal Aortic Aneurysm Expansion Through Anti-Inflammatory Effects.* Arteriosclerosis, Thrombosis, and Vascular Biology, 2014. **34**(8): p. 1747-1755.
27. Wilson, W.R.W., et al., *Elevated Plasma MMP1 and MMP9 are Associated with Abdominal Aortic Aneurysm Rupture.* European Journal of Vascular and Endovascular Surgery, 2008. **35**(5): p. 580-584.
28. Reeps, C., et al., *Glucose Metabolism in the Vessel Wall Correlates With Mechanical Instability and Inflammatory Changes in a Patient With a Growing Aneurysm of the Abdominal Aorta.* Circulation: Cardiovascular Imaging, 2009. **2**(6): p. 507-509.
29. Tanios, F., et al., *CXCR4: A Potential Marker for Inflammatory Activity in Abdominal Aortic Aneurysm Wall.* European Journal of Vascular and Endovascular Surgery, 2015. **50**(6): p. 745-753.
30. Tanios, F., et al., *Interaction of biomechanics with extracellular matrix components in abdominal aortic aneurysm wall.* Eur J Vasc Endovasc Surg, 2015. **50**(2): p. 167-74.

31. Reeps, C., et al., *Measuring and modeling patient-specific distributions of material properties in abdominal aortic aneurysm wall.* Biomech Model Mechanobiol, 2013. **12**(4): p. 717-33.
32. Leung, D.Y., S. Glagov, and M.B. Mathews, *Cyclic stretching stimulates synthesis of matrix components by arterial smooth muscle cells in vitro.* Science, 1976. **191**(4226): p. 475-7.
33. Angelov, S.N., et al., *TGF-β (Transforming Growth Factor-β) Signaling Protects the Thoracic and Abdominal Aorta From Angiotensin II-Induced Pathology by Distinct Mechanisms.* Arterioscler Thromb Vasc Biol, 2017. **37**(11): p. 2102-2113.
34. Wang, Y., et al., *Transforming growth factor-β and abdominal aortic aneurysms.* Cardiovasc Pathol, 2013. **22**(2): p. 126-32.
35. Raghavan, M.L. and D.A. Vorp, *Toward a biomechanical tool to evaluate rupture potential of abdominal aortic aneurysm: identification of a finite strain constitutive model and evaluation of its applicability.* J Biomech, 2000. **33**(4): p. 475-82.
36. Rausch, S.M., et al., *Material model of lung parenchyma based on living precision-cut lung slice testing.* J Mech Behav Biomed Mater, 2011. **4**(4): p. 583-92.
37. Schindelin, J., et al., *Fiji: an open-source platform for biological-image analysis.* Nat Methods, 2012. **9**(7): p. 676-82.
38. Metschl, S., et al., *Changes in Endocan and Dermatan Sulfate Are Associated with Biomechanical Properties of Abdominal Aortic Wall during Aneurysm Expansion and Rupture.* Thromb Haemost, 2022. **122**(9): p. 1513-1523.
39. Reutersberg, B., et al., *CXCR4 - a possible serum marker for risk stratification of abdominal aortic aneurysms.* Vasa, 2022. **Epub ahead of print**.
40. Matsushita, K., et al., *Chronic kidney disease measures and the risk of abdominal aortic aneurysm.* Atherosclerosis, 2018. **279**: p. 107-113.
41. Berry, S.D., et al., *Procollagen type III N-terminal peptide (P3NP) and lean mass: a cross-sectional study.* J Frailty Aging, 2013. **2**(3): p. 129-34.
42. Lotfy, N., et al., *Procollagen III amino terminal propeptide (PIIINP): A marker of MTX induced liver fibrosis in rheumatoid arthritis patients?* QJM: An International Journal of Medicine, 2019. **14**: p. 182-189.
43. Satta, J., et al., *Increased turnover of collagen in abdominal aortic aneurysms, demonstrated by measuring the concentration of the aminoterminal propeptide of type III procollagen in peripheral and aortal blood samples.* Journal of Vascular Surgery, 1995. **22**(2): p. 155-160.
44. Treska, V. and O. Topolcan, *Plasma and tissue levels of collagen types I and III markers in patients with abdominal aortic aneurysms.* Int Angiol, 2000. **19**(1): p. 64-8.
45. Satta, J., et al., *Aminoterminal propeptide of type III procollagen in the follow-up of patients with abdominal aortic aneurysms.* Journal of Vascular Surgery, 1997. **25**(5): p. 909-915.

46. Lindholt, J.S., et al., *Five-year results of elastin and collagen markers as predictive tools in the management of small abdominal aortic aneurysms.* Eur J Vasc Endovasc Surg, 2001. **21**(3): p. 235-40.
47. Rodella, L.F., et al., *Abdominal aortic aneurysm and histological, clinical, radiological correlation.* Acta Histochem, 2016. **118**(3): p. 256-62.
48. Klaus, V., et al., *Association of Matrix Metalloproteinase Levels with Collagen Degradation in the Context of Abdominal Aortic Aneurysm.* Eur J Vasc Endovasc Surg, 2017. **53**(4): p. 549-558.
49. Tatara, Y., et al., *Chondroitin sulfate cluster of epiphycan from salmon nasal cartilage defines binding specificity to collagens.* Glycobiology, 2015. **25**(5): p. 557-69.
50. Kvist, A.J., et al., *Chondroitin sulfate perlecan enhances collagen fibril formation. Implications for perlecan chondrodysplasias.* J Biol Chem, 2006. **281**(44): p. 33127-39.
51. Joladarashi, D., P.V. Salimath, and N.D. Chilkunda, *Diabetes results in structural alteration of chondroitin sulfate/dermatan sulfate in the rat kidney: effects on the binding to extracellular matrix components.* Glycobiology, 2011. **21**(7): p. 960-72.
52. Trowbridge, J.M. and R.L. Gallo, *Dermatan sulfate: new functions from an old glycosaminoglycan.* Glycobiology, 2002. **12**(9): p. 117r-25r.
53. Raffort, J., et al., *Monocytes and macrophages in abdominal aortic aneurysm.* Nat Rev Cardiol, 2017. **14**(8): p. 457-471.
54. Annovi, G., et al., *Heparan sulfate affects elastin deposition in fibroblasts cultured from donors of different ages.* Rejuvenation Res, 2012. **15**(1): p. 22-31.
55. Hayes, A.J., et al., *Colocalization in vivo and association in vitro of perlecan and elastin.* Histochem Cell Biol, 2011. **136**(4): p. 437-54.
56. Uitto, J., Q. Li, and Z. Urban, *The complexity of elastic fibre biogenesis in the skin--a perspective to the clinical heterogeneity of cutis laxa.* Exp Dermatol, 2013. **22**(2): p. 88-92.
57. Eugster, T., et al., *Aminoterminal propeptide of type III procollagen and matrix metalloproteinases-2 and -9 failed to serve as serum markers for abdominal aortic aneurysm.* Eur J Vasc Endovasc Surg, 2005. **29**(4): p. 378-82.
58. Yilmaz, M.I., et al., *Plasma endocan levels associate with inflammation, vascular abnormalities, cardiovascular events, and survival in chronic kidney disease.* Kidney Int, 2014. **86**(6): p. 1213-20.
59. Scherpereel, A., et al., *Endocan, a new endothelial marker in human sepsis.* Crit Care Med, 2006. **34**(2): p. 532-7.

60. Béchard, D., et al., *Human endothelial-cell specific molecule-1 binds directly to the integrin CD11a/CD18 (LFA-1) and blocks binding to intercellular adhesion molecule-1.* J Immunol, 2001. **167**(6): p. 3099-106.
61. Kali, A. and K.S. Shetty, *Endocan: a novel circulating proteoglycan.* Indian J Pharmacol, 2014. **46**(6): p. 579-83.
62. Hu Frisk, J.M., et al., *Mitogen-Activated Protein Kinase Signaling Regulates Proteoglycan Composition of Mast Cell Secretory Granules.* Front Immunol, 2018. **9**: p. 1670.
63. Linhardt, R.J. and R.E. Hileman, *Dermatan sulfate as a potential therapeutic agent.* Gen Pharmacol, 1995. **26**(3): p. 443-51.
64. Casu, B., M. Guerrini, and G. Torri, *Structural and conformational aspects of the anticoagulant and anti-thrombotic activity of heparin and dermatan sulfate.* Curr Pharm Des, 2004. **10**(9): p. 939-49.
65. Tovar, A.M., et al., *The dermatan sulfate-dependent anticoagulant pathway is mostly preserved in aneurysm and in severe atherosclerotic lesions while the heparan sulfate pathway is disrupted.* Clin Chim Acta, 2011. **412**(11-12): p. 906-13.
66. Murad, H.A.S., M.M. Rafeeq, and T.M.A. Alqurashi, *Role and implications of the CXCL12/CXCR4/CXCR7 axis in atherosclerosis: still a debate.* Annals of Medicine, 2021. **53**(1): p. 1598-1612.
67. Mousavi, A., *CXCL12/CXCR4 signal transduction in diseases and its molecular approaches in targeted-therapy.* Immunol Lett, 2020. **217**: p. 91-115.
68. Jones, G.T., *The pathohistology of abdominal aortic aneurysm.* Diagnosis, Screening and Treatment of Abdominal, Thoracoabdominal and Thoracic Aortic Aneurysms, 2011: p. 414.
69. Busch, A., et al., *Vessel wall morphology is equivalent for different artery types and localizations of advanced human aneurysms.* Histochem Cell Biol, 2017. **148**(4): p. 425-433.
70. Theocharis, A.D., et al., *Human abdominal aortic aneurysm is closely associated with compositional and specific structural modifications at the glycosaminoglycan level.* Atherosclerosis, 1999. **145**(2): p. 359-68.
71. Cikach, F.S., et al., *Massive aggrecan and versican accumulation in thoracic aortic aneurysm and dissection.* JCI Insight, 2018. **3**(5).
72. Sarrazin, S., et al., *Characterization and binding activity of the chondroitin/dermatan sulfate chain from Endocan, a soluble endothelial proteoglycan.* Glycobiology, 2010. **20**(11): p. 1380-8.
73. Di Martino, E.S., et al., *Biomechanical properties of ruptured versus electively repaired abdominal aortic aneurysm wall tissue.* J Vasc Surg, 2006. **43**(3): p. 570-6; discussion 576.

74. Vande Geest, J.P., M.S. Sacks, and D.A. Vorp, *The effects of aneurysm on the biaxial mechanical behavior of human abdominal aorta.* J Biomech, 2006. **39**(7): p. 1324-34.
75. Wilson, K.A., et al., *The relationship between abdominal aortic aneurysm distensibility and serum markers of elastin and collagen metabolism.* Eur J Vasc Endovasc Surg, 2001. **21**(2): p. 175-8.
76. Zhang, H., K.J. Davies, and H.J. Forman, *TGFβ1 rapidly activates Src through a non-canonical redox signaling mechanism.* Arch Biochem Biophys, 2015. **568**: p. 1-7.
77. Sato, M., et al., *c-Src and hydrogen peroxide mediate transforming growth factor-beta1-induced smooth muscle cell-gene expression in 10T1/2 cells.* Arterioscler Thromb Vasc Biol, 2005. **25**(2): p. 341-7.
78. Te Boekhorst, V. and P. Friedl, *Plasticity of Cancer Cell Invasion-Mechanisms and Implications for Therapy.* Adv Cancer Res, 2016. **132**: p. 209-64.
79. Huhtinen, A., et al., *Gene expression profiles and signaling mechanisms in α(2B)-adrenoceptor-evoked proliferation of vascular smooth muscle cells.* BMC Syst Biol, 2017. **11**(1): p. 65.
80. Yan, Y., et al., *Src inhibition blocks renal interstitial fibroblast activation and ameliorates renal fibrosis.* Kidney Int, 2016. **89**(1): p. 68-81.
81. Hollenbeck, S.T., et al., *Type I collagen synergistically enhances PDGF-induced smooth muscle cell proliferation through pp60src-dependent crosstalk between the alpha2beta1 integrin and PDGFbeta receptor.* Biochem Biophys Res Commun, 2004. **325**(1): p. 328-37.
82. Liu, B., et al., *The role of phospholipase C and phosphatidylinositol 3-kinase in vascular smooth muscle cell migration and proliferation.* J Surg Res, 2004. **120**(2): p. 256-65.
83. Qian, Z., et al., *PDGFBB promotes proliferation and migration via regulating miR-1181/STAT3 axis in human pulmonary arterial smooth muscle cells.* Am J Physiol Lung Cell Mol Physiol, 2018. **315**(6): p. L965-l976.
84. Ou, Y., et al., *Migfilin protein promotes migration and invasion in human glioma through epidermal growth factor receptor-mediated phospholipase C-γ and STAT3 protein signaling pathways.* J Biol Chem, 2012. **287**(39): p. 32394-405.
85. Yang, C.M., et al., *c-Src-dependent transactivation of EGFR mediates CORM-2-induced HO-1 expression in human tracheal smooth muscle cells.* J Cell Physiol, 2015. **230**(10): p. 2351-61.
86. Samarakoon, R., et al., *TGF-beta1-induced plasminogen activator inhibitor-1 expression in vascular smooth muscle cells requires pp60(c-src)/EGFR(Y845) and Rho/ROCK signaling.* J Mol Cell Cardiol, 2008. **44**(3): p. 527-38.

87. Liao, M., et al., *Local and systemic alterations in signal transducers and activators of transcription (STAT) associated with human abdominal aortic aneurysms.* J Surg Res, 2012. **176**(1): p. 321-8.
88. Hara, T., et al., *Biglycan Intensifies ALK5-Smad2/3 Signaling by TGF-β(1) and Downregulates Syndecan-4 in Cultured Vascular Endothelial Cells.* J Cell Biochem, 2017. **118**(5): p. 1087-1096.
89. Burch, M.L., et al., *TGF-beta stimulates biglycan synthesis via p38 and ERK phosphorylation of the linker region of Smad2.* Cell Mol Life Sci, 2010. **67**(12): p. 2077-90.
90. Henderson, E.L., et al., *Death of smooth muscle cells and expression of mediators of apoptosis by T lymphocytes in human abdominal aortic aneurysms.* Circulation, 1999. **99**(1): p. 96-104.
91. Roostalu, U. and J.K. Wong, *Arterial smooth muscle dynamics in development and repair.* Dev Biol, 2018. **435**(2): p. 109-121.
92. Owens, G.K., M.S. Kumar, and B.R. Wamhoff, *Molecular regulation of vascular smooth muscle cell differentiation in development and disease.* Physiol Rev, 2004. **84**(3): p. 767-801.

LMU LUDWIG-MAXIMILIANS-UNIVERSITÄT MÜNCHEN

Dean's Office
Medical Faculty

MMRS MUNICH MEDICAL RESEARCH SCHOOL

Affidavit

Metschl Susanne

Surname, first name

Biedersteiner Str. 29

Street

80802 München

Zip code, town

Germany

Country

I hereby declare, that the submitted thesis entitled

Individualized rupture risk assessment and analysis of mechanotransduction in the abdominal aortic aneurysm

is my own work. I have only used the sources indicated and have not made unauthorised use of services of a third party. Where the work of others has been quoted or reproduced, the source is always given.

I further declare that the dissertation presented here has not been submitted in the same or similar form to any other institution for the purpose of obtaining an academic degree.

München, 06.02.2023

Place, date

Susanne Metschl

Signature doctoral candidate

LMU LUDWIG-MAXIMILIANS-UNIVERSITÄT MÜNCHEN

Dean's Office
Medical Faculty

MMRS MUNICH MEDICAL RESEARCH SCHOOL

Confirmation of congruency between printed and electronic version of the doctoral thesis

Metschl Susanne

Surname, first name

Biedersteiner Str. 29

Street

80802 München

Zip code, town

Germany

Country

I hereby declare that the electronic version of the submitted thesis, entitled

Individualized rupture risk assessment and analysis of mechanotransduction in the abdominal aortic aneurysm

is congruent with the printed version both in content and format.

München, 06.02.2023

Place, date

Susanne Metschl

Signature doctoral candidate

List of publications

CXCR4 - a possible serum marker for risk stratification of abdominal aortic aneurysms. Reutersberg B, Metschl S, Salvermoser M, Eckstein HH, Knappich C, Maegdefessel L, Pelisek J, Busch A (2022). Vasa, Epub ahead of print. https://doi.org/10.1024/0301-1526/a001049

Changes in endocan and dermatan sulfate are associated with biomechanical properties of abdominal aortic wall during aneurysm expansion and rupture. Metschl S, Bruder L, Paloschi V, Jakob K, Reutersberg B, Reeps C, Maegdefessel L, Gee M, Eckstein HH, Pelisek J (2022). Thrombosis and Haemostasis, 122(9), 1513-1523. https://doi.org/10.1055/a-1772-0574

Long non-coding RNA MIAT controls advanced atherosclerotic lesion formation and plaque destabilization. Fasolo F, Jin H, Winski G, Chernogubova E, Pauli J, Winter H, Li D, Glukha N, Bauer S, Metschl S, Wu Z, Koschinsky M, Reilly M, Pelisek J, Kempf W, Eckstein HH, Soehnlein O, Matic L, Hedin U, Bäcklund A, Bergmark C, Paloschi V, Maegdefessel L (2021). Circulation, 144(19), 1567-1583. https://doi.org/10.1161/CIRCULATIONAHA.120.052023

Lenvatinib halts aortic aneurysm growth by restoring smooth muscle cell contractility. Busch A, Pauli J, Winski G, Bleichert S, Chernogubova E, Metschl S, Winter H, Trenner M, Wiegering A, Otto C, Fischer J, Reiser J, Werner J, Roy J, Brostjan C, Knappich C, Eckstein HH, Paloschi V, Maegdefessel L (2021). JCI Insight, 6(15), e140364. https://doi.org/10.1172/jci.insight.140364

Biobanking: Objectives, Requirements, and Future Challenges-Experiences from the Munich Vascular Biobank. Pelisek J, Hegenloh R, Bauer S, Metschl S, Pauli J, Glukha N, Busch A, Reutersberg B, Kallmayer M, Trenner M, Wendorff H, Tsantilas P, Schmid S, Knappich C, Schaeffer C, Stadlbauer T, Biro G, Wertern U, Meisner F, Stoklasa K, Menges AL, Radu O, Dallmann-Sieber S, Karlas A, Knipfer E, Reeps C, Zimmermann A, Maegdefessel L, Eckstein HH (2019). Journal of Clinical Medicine, 8(2), 251. https://doi.org/10.3390/jcm8020251